Konya Mühendislik Bilimleri Dergisi
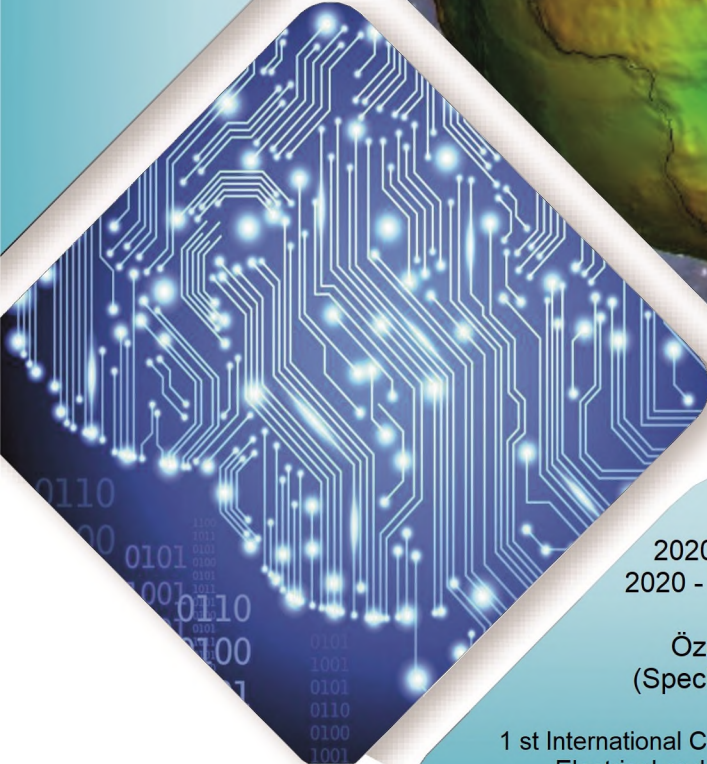# Konya Journal of Engineering Sciences

2020 - Cilt : 8
2020 - Volume : 8

Özel Sayı
(Special Issue)

1 st International Conference on Computer,
Electrical and Electronic Sciences
(ICCEES 2020)

Editorial Board/Yayın Kurulu

İÇİNDEKİLER (CONTENTS)

Özel Sayı Makalesi (Special Issue Article)

RESHAPING HUMAN INTENTION ON HUMAN-MACHINE INTERACTION BY USING HOLOGRAMS

[1]Kemal ERDOĞAN iD **, [2]Akif DURDU** iD **, [3]Rahime CEYLAN** iD
[1]kerdogan@ktun.edu.tr, [2]adurdu@ktun.edu.tr, [3]rceylan@ktun.edu.tr

[1,2,3]*Konya Technical University, Department of Electrical and Electronics Engineering, Konya, TURKEY*

ABSTRACT: Decision making could be critically important for people in some situations. People have intentions to choose a side if it is time to make decision. These intentions are strongly related to the knowledge and experience. But sometimes outer effects could reshape their intentions easily. In this paper, an experimental work is studied for Human-Machine Interaction in which if holograms could change or affect the human intention. And also the question which asks whether people trust on a hologram agent while making decision or not is researched. To study this research, a memory game application is developed and this application is run on Microsoft Hololens device. Hololens is used to maintain the Augmented Reality (AR) environment with holograms. An algorithm with a Finite State Machines (FSM) is developed to manage the response of hologram agent while giving hint to the confused users. The accuracy of the hints changes nonlinearly. 3 different game stages are trained on users to see how they are affected by both virtual and real world noises. According to the results, intention of majority of users was affected by the hologram while making the decisions. Also it is observed that some users who were concentrated too much to memorize the order of objects did not realize the hologram, and some few could not understand the actions of hologram.

Key Words: *Augmented Reality, Decision Making, Finite State Machines, Human-Machine Interaction, Intention Reshaping.*

İnsan - Makine Etkileşiminde Hologram Kullanılarak İnsan Niyetinin Yönlendirilmesi

ÖZ: Karar verme, bazı durumlarda insanlar için kritik derecede önemli olabilir. İnsanların karar verme zamanı geldiğinde taraf seçme niyetleri vardır. Bu niyetler, bilgi ve geçmiş deneyimlerle ilişkilidir. Ancak bazen dış etkiler insan niyetini kolayca yeniden şekillendirebilir. Bu makalede, İnsan-Makine Etkileşimi için deneysel bir çalışma gerçekleştirilmiştir. Burada hologramların insan niyetini değiştirip değiştiremeyeceği araştırılmıştır. Ayrıca insanların karar verirken hologram etmene güvenip güvenmediği de araştırılmıştır. Bu araştırmayı incelemek için bir hafıza oyunu uygulaması geliştirilmiş ve bu uygulama Microsoft Hololens cihazında koşturulmuştur. Hololens, Hologramlarla Artırılmış Gerçeklik (AG) ortamını sağlamak için kullanılmıştır. Sonlu Durum Makineleri (SDM) içeren bir algoritma, kafası karışan kullanıcılara ipucu verirken hologram etmenin tepkilerini yönetmek için geliştirilmiştir. İpuçlarının doğruluğu doğrusal olmayan bir şekilde değişmektedir. Kullanıcıların hem sanal hem de gerçek dünya seslerinden nasıl etkilendiklerini görmek için 3 farklı oyun aşaması tasarlanmıştır. Çalışmadan elde edilen sonuçlara göre, kullanıcıların çoğunluğunun niyeti karar verirken hologramdan etkilenmiştir. Ayrıca nesnelerin sırasını ezberlemek için konsantre olan bazı kullanıcıların hologramın farkına varamadığı, bazılarının da hologramın eylemlerini anlayamadığı görülmüştür.

Anahtar Kelimeler: *Artırılmış Gerçeklik, Karar Verme, Sonlu Durum Makineleri, İnsan-Makine Etkileşimi, Niyeti Yeniden Şekillendirme.*

1. INTRODUCTION

People make decisions when they are facing up to a fork in situations. These situations are composed of three parts; firstly there has to be more than one option in front of the person. As an example situation is that coming to a fork while going on an unknown road. Will you take the right or the left path? Additionally the person could have expectations about these options. These expectations are formed according to beliefs and probabilities. Degree of beliefs and as the third part, experiences have important roles while making decisions. People make estimations using past assessments. These all 3 parts form the structure of decision making (Hastie *et al.*, 2010).

It was studied before that if a person's intention while making decision could be reshaped or changed by using robots (Durdu *et al.*, 2012). Using holograms for this mission instead of robots is a novel idea as the Human Machine Interaction (HMI). According to our knowledge this type of research had not been tried before this.

Besides, several researches have been made to see the degree of trust of users on robots and factors affecting the interaction between robot and human but nothing have been studied on holograms (Hancock *et al.*, 2011; Freedy *et al.*, 2007). In this work, the degree of trust was not experienced but it was simply practiced if the user trusts on a hologram agent while making decision or not.

Microsoft's Hololens device is used to maintain the holographic environment for this study (Microsoft, 2019). An Augmented Reality (AR) application is developed for Hololens. This AR application is the experimental setup for the study. A screenshot of Hololens device is given in Figure 1.

Importance of AR is considerably increasing because today holograms are getting much more place in our life than yesterday. AR devices and applications are developing. Microsoft has an application store for Hololens. Head Mounted Displays (HMDs) like Hololens are very popular in AR and this is a very competitive market.

Figure 1. A screenshot while a user was playing the developed game app

2. RELATED WORKS

2.1. Intention Reshaping or Affecting Decision Making

Some researches on Human Intention Reshaping or Changing Human Intentions by using robots are studied before. Mobile robots were used to change previously estimated human intentions (Durdu *et al.*, 2012). Experiments were practiced in a specially designed real human robot environment. In the experimental scenario of the study, a human walks in a room, where a set of autonomous robots and other objects are placed in. These robots are formed like mobile chair and mobile stairs. Other elements in the room are bookshelf, coffee table, computer and cameras. Computer observes motions, positions and postures of the human with the connected cameras. Interactions are processed by computer with the use of Observable Operator Models method to estimate human intentions. According to these intention estimations, robots are controlled to change the intention of the human in the room.

2.2. Intention Reshaping or Affecting Decision Making

AR systems are defined as they have three characteristics in a survey in 1997. These systems should combine virtual and real environment. Also it is added as; they are interactive systems in real time and registered in 3D (Azuma, 1997). Taxonomy was declared for AR, VR and Mixed Reality (MR) in 1994 and stated as MR contains AR but today it is common AR and MR definitions could be used as substitute for another (Milgram and Kishino, 1994). Wearable technologies for AR and VR are developing but Hololens is a very new wearable device which was released in 2016 and according to our knowledge it has not used to link any interaction between human and machines with the aim of reshaping human intention or affecting decision making.

There is a study aiming to enhance the interaction between Hololens and user (Funk *et al.*, 2017). Authors used Kinect sensor to allow users interacting naturally with holograms in AR environment on Hololens. They also prepared and gave five different examples of gestures that could be used for a natural interaction for Hololens.

There are also different interaction models developed which offers interaction between users in AR environment. These users could be connected to the AR environment with HMDs, tablets or PCs (Chen *et al.*, 2015).

3. MATERIALS AND METHOD

The experimental setup is designed to be like a game. A person user is wanted to play a memory game in this setup. The idea of this game is that user is being wanted to make decisions, in other words user would face up to a fork and has to make decision to choose a side.

To achieve this target, a kind of difficult memory game application for Hololens was prepared. In this memory game 9 different shaped and colored objects are present. When user starts the game, lights are blinking under these objects in a particular and randomized order (Figure 2).

User is wanted to memorize this order, and he/she is wanted to select the objects in this order. As user selects the objects with the order in his/her memory, objects are getting lined up on the tables closer to him/her. User would be counted successful, when right object is chosen in every movement. If user fails to select the right object, a hologram appears in the scene. Hologram tries to give hint to the user. This hologram is a butterfly. When the hologram appears butterfly is flying around the scene and game objects. And finally it perches on an object.
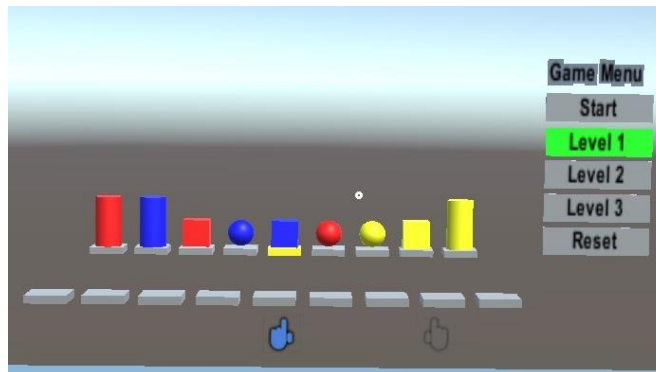
Figure 2. Tables under objects blink to show the desired order

A Finite State Machine (FSM) structure has built to control the hologram which gives right hint or wrong hint to the user according to user's movements. It is prepared to prove that a hologram can reshape human's intention or affect it while making decisions. The FSM mechanism was formed by two main structures. First FSM algorithm has a very simple structure to hide or show the hint (Figure 3).

The other part of the FSM structure which is deciding to give right or wrong hint to the user was designed to work with a more complex algorithm. It is observing user's movements and collecting data about user's successful movements, number of total movements, number of fails, when the true hint or wrong hint shown to the user (Figure 4).

It does not give right hint or wrong hint to the user every time. If the hint was given without a complex algorithm or if it was always given right or wrong hint repeatedly, user would easily solve and understand that. Then user would make decisions quickly without thinking, as the hint shows or opposite of the hint shows.

With that result there would not be any interaction between human and hologram. For example in the experiments, at the beginning stages of developing the application, hint was showing true hint at first but then it was always showing the wrong hint. At this point it was observed that user never choose the object that the hint shows, because user learned that hint always gives the wrong hint.

The aim is testing that, if user completely minds the hologram's movements or has the hologram any effects on human's intention while making the decision. To prove this the memory game was designed a little harder. It has 9 objects in total and user needs to memorize the order of these objects nearly in 5 seconds.

Experiments showed that most of people could not memorize after 4th or 5th object. At this time user comes to a fork and hint becomes very useful for the user. When the hologram shows the right hint at this point, user could think he was already inclined to choose that right object like he was remembering something around that object. But if the hologram gives the wrong hint and the user also obey both wrong and right hints, this situation will obviously prove that human user's intention is changed by hologram.
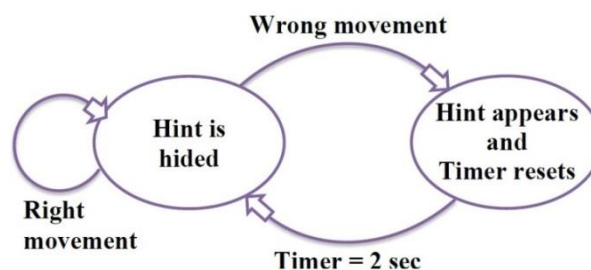
Figure 3. FSM Structure manages the hologram hint's behaviour. It appears for 2 seconds, when user made a wrong movement
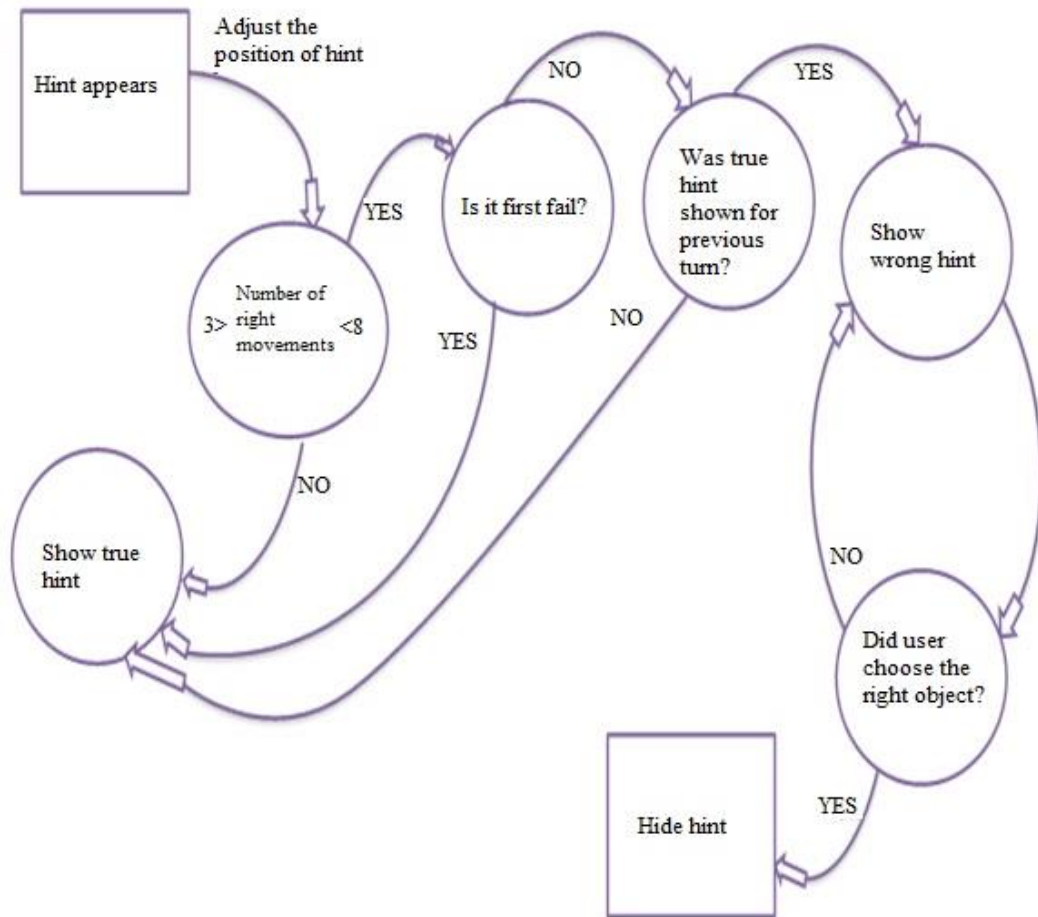
Figure 4. FSM Structure which is deciding to give right or wrong hint to the user

Additionally, with the aim of making the game harder and mind confusing, three different levels are prepared for the game application. Some outer physical actions and virtual scene effects are added on the basic game environment in 2nd and 3rd levels. Also answers of the users are recorded and success rates are measured for every level to compare how accuracy of the user is affected with the noises.

1st level is the basic level and users are getting used to the game and environment. In 1st level user does not face up with an unordinary situation. Only goal for the user is to memorize the order of the blinking lights for the elements in this level. In 2nd level a virtual noise is applied; a big size bouncy video suddenly starts in about 5th second of the game to confuse the user while he was trying to memorize the order of the objects (Figure 5). And lastly in 3rd level user is disturbed with a real world action. User is wanted to walk forward or backwards to observe that if user both minds the real world and virtual world together and if real world movements confuses his motivation on focusing to the virtual world or not. Also in 3rd level the plane where the gaming objects settle on is waving with a period of time to make it harder.

Experiments were done in Ohio State University PCVLAB with 10 different people. Before doing experiments they are all educated about how to use Hololens device with the application named as "Learn Gestures" that was already prepared by Microsoft for this purpose.

Figure 5. A large scale video which is recorded with a POV cam suddenly appears behind game scene.

4. RESULTS AND DISCUSSION

Participating users are all asked if they realized a butterfly hologram appears when they make mistake. Some of them were very well concentrated on memorizing the order of objects, these type users replied this question they did not realized anything. Majority of users declared that they saw the butterfly hologram was trying to give hint when they go wrong. And some of the users replied there were something in background but they did not consider it was a hint (Table.1).

According to the results, 90% of users recognize the butterfly hologram during the game but 33% of these users could not recognize that the butterfly hologram was giving hint to them about next possibly true movements. 83% of the remaining users, who recognized the hologram butterfly, trusted in the butterfly's hints. They have followed the hint and declared that they had changed their mind according to the hints given by the hologram. One of the participants also stated as he recognized that the hints of the hologram butterfly are doubtful and he added he did not follow the hints as the levels of game progressed.

Table 1.a) Statistics for Level 1

Level1				
	# of Movements	# of Mistakess	# of Right Movements	# of Resets
User1	15	6	9	2
User2	7 (Gave Up)	6	1	3
User3	11	2	9	0
User4	14	5	9	0
User5	20	11	9	0
User6	15	6	9	8
User7	14	5	9	2
User8	15	6	9	0
User9	10	1	9	2
User10	16	7	9	2

Table 1.b) Statistics for Level 2

Level2				
	# of Movements	# of Mistakes	# of Right Movements	# of Resets
User1	6 (Gave Up)	4	2	1
User2	Did not Try	-	-	-
User3	17	8	9	3
User4	10	1	9	0
User5	13	4	9	0
User6	21	12	9	0
User7	16	7	9	1
User8	14	5	9	0
User9	19	10	9	0
User10	12	3	9	0

Table 1.c) Statistics for Level 3

Level3				
	# of Movements	# of Mistakes	# of Right Movements	# of Resets
User1	5 (Gave Up)	4	1	0
User2	Did not Try	-	-	-
User3	17	8	9	
User4	11	2	9	0
User5	16	7	9	0
User6	19	10	9	0
User7	14	5	9	0
User8	13	4	9	0
User9	10	1	9	1
User10	11	2	9	0

Table 1.d) Questions Replied by Each User in the End of the Experiment

	Recognition of butterfly	Recognition of butterfly as a hint	Trust of user to the hint	Recognition of that hologram shows the wrong hint sometimes	Negatively affected of the attention of user	Did user walk during 3rd level?
U1	√	√	X	√	√	-
U2	√	X	-	-	-	-
U3	X	-	-	-	NC[a]	X
U4	√	X	-	-	√	SOME
U5	√	√	√	√	NC	X
U6	√	√	√	√	NC	X
U7	√	√	√	√	√	X
U8	√	X	-	-	√	√
U9	√	√	√	√	NC	X
U10	√	√	√	√	√	X

The 33% of the users who did not recognize the butterfly or the butterfly was giving hint, were the highest scored users. This shows that these users were highly concentrated on memorizing the order of the blinking lights. So they did fewer mistakes and they did not recognize the butterfly hologram was giving hint. They declared there was a butterfly in the background but it was only a background animation or something like that.

Also all users were wanted to walk forward or backwards while playing the game level 3 but only 20% of the users practiced it. But even these users could not practice walking as it should be. They only took a few steps forward.

5. CONCLUSION

In this paper an AR application was developed for an AR environment with the use of Hololens. The application prepares a gaming environment which uses holograms instead of robots with the aim of interaction between Human and Hologram as HMI. Users were wanted to memorize the order of the blinking objects in the beginning of the game then users were wanted to put them in a right order. While users were trying to do this successfully, a hologram tried to give hints nonlinearly. Sometimes hologram tried to misdirect the user. At this point human intention reshaping or affecting the decision making of human was realized. This study shows that holograms are able to reshape the intention of the user. With this result, target of the study was accomplished successfully.

On the other hand this study showed that it is very difficult to handle real world and virtual world movements together. None of the users made it successfully.

This study would be enhanced by using real time live holograms. Also AI techniques could be used to develop algorithms to control hologram. Another idea could be that real world noises could be changed.

It is planned to build the similar memory game environment with a robotic arm and effects of holograms and robots would be compared in Human Machine Interactions.

6. ACKNOWLEDGEMENT

REFERENCES

Azuma, R. T., "A Survey of Augmented Reality", Teleoperators and Virtual Environments 6, 4 (August 1997), 355-385

Chen, H., Lee, A. S., Swift, M. and Tang, J. C., 2015. "3D Collaboration Method over HoloLens™ and Skype™ End Points", In Proceedings of the 3rd International Workshop on Immersive Media Experiences (ImmersiveME '15). ACM, New York, NY, USA, 27-30.

Durdu, A., Erkmen, I. and Erkmen, A. M., "Observable operator models for reshaping estimated human intention by robot moves in human-robot interactions", 2012 International Symposium on Innovations in Intelligent Systems and Applications, Trabzon, 2012, pp. 1-5.

Freedy, A., DeVisser, E., Weltman, G. and Coeyman, N., "Measurement of trust in human-robot collaboration," 2007 International Symposium on Collaborative Technologies and Systems, Orlando, FL, 2007, pp. 106-114.

Funk, M., Kritzler, M. and Michahelles. F., 2017. "HoloLens is more than air Tap: natural and intuitive interaction with holograms", In Proceedings of the Seventh International Conference on the Internet of Things (IoT '17). ACM, New York, NY, USA, Article 31, 2 pages.

Hancock PA, Billings DR, Schaefer KE, Chen JY, de Visser EJ, Parasuraman R., "A Meta-Analysis of Factors Affecting Trust in Human-Robot Interaction", Hum Factors.2011 Oct;53(5):517-27.

Hastie, R., Dawes, R., Rational Choice in an Uncertain World: The Psychology of Judgment and Decision Making, Second Edition, Pittsburgh, USA, 2010, SAGE pubs, Ch-2 What is decision making? Pp. 23-43

Microsoft Hololens Development Edition https://www.microsoft.com/en-us/hololens/hardware

Milgram, P. and Kishino, F., "A Taxonomy of Mixed Reality Visual Displays", IEICE Transactions on Information Systems, Vol E77-D, No.12 December 1994.

DÜŞÜK MALİYETLİ SÜREKLİ DALGA DOPPLER RADARI İLE TEMASSIZ YAŞAMSAL BELİRTİ ÖLÇÜMÜ

[1]İbrahim ŞEFLEK ⬤ , [2]Ercan YALDIZ ⬤

[1,2]Konya Teknik Üniversitesi, Mühendislik ve Doğa Bilimleri Fakültesi, Elektrik-Elektronik Mühendisliği Bölümü, Konya, TÜRKİYE
[1] iseflek@ktun.edu.tr, [2]eyaldiz@ktun.edu.tr

ÖZ: Hayati sinyallerin temassız olarak uzaktan algılanması birçok uygulama açısından önem arz etmektedir. Bu algılamayı gerçekleştiren radarlar biyoradar olarak adlandırılmaktadır. Biyoradar kişinin solunum ve kalp atışından kaynaklanan göğüs duvarı hareketinin değişimiyle Doppler prensibini kullanarak hayati sinyallerin doğru bir şekilde ölçülmesini sağlamaktadır. Bu çalışmada, 24 GHz çalışma frekansına sahip düşük maliyetli sürekli dalga (CW) Doppler radarı kullanılarak insan denekten temassız bir şekilde yaşamsal belirti (solunum, kalp atış hızı) ölçümleri gerçekleştirilmiştir. Ölçümlerden elde edilen sinyallerin işlenmesinde iki farklı yöntem kullanılmıştır. İlk yöntem Hızlı Fourier Dönüşümünü (FFT) esas alırken ikinci yöntemde Dalgacık yöntemine dayalı Çoklu Çözünürlük Analizi (MRA) yöntemi kullanılmaktadır. Solunum hızında birinci ve ikinci yöntem için elde edilen sonuçlar %3.75 ve %0' hata oranlıdır. Kalp atışı için sırasıyla %9.35 ve %8.45 hata oranlı değerler elde edilmiştir. Bu sonuçlar özellikle radarların tıbbi uygulamalar için başarıyla kullanılabileceğini göstermektedir.

Anahtar Kelimeler: *Doppler radar, Radar sinyal işleme, Hayati sinyal tespiti, Temassız ölçüm, Biyoradar*

Contactless Vital Signs Measurement with Low Cost Continuous Wave Doppler Radar

ABSTRACT: Remote sensing of vital signals without contact is important for many applications. Radars that perform this detection are called bio-radar. Bio-radar provides accurate measurement of vital signals using the Doppler principle with the change of chest wall movement caused by a person's breathing and heartbeat. In this study, non-contact vital signs (respiration, heart rate) measurements for human subject were performed using a low cost continuous wave (CW) Doppler radar with a 24 GHz operating frequency. Two different methods have been used to process the signals obtained from the measurements. While the first method is based on the Fast Fourier Transform (FFT), the second method uses the Multi-Resolution Analysis (MRA) method based on the Wavelet method. The results obtained by the first and second methods for respiration are 3.75% and 0% error rates, respectively. These values for heartbeat are 9.35% and 8.45%. These results show that radars can be used successfully for medical applications.

Key Words: *Doppler radar, Radar signal processing, Vital signs detection, Non-contact measurement, bio-radar*

GİRİŞ (INTRODUCTION)

Nesnelerin uzaktan temassız algılanması yirminci yüzyılda özellikle savaşların seyrini değiştirecek öneme sahip olmuş ve radarların ne kadar önemli birer donanım olduğunu ortaya koymuştur. Askeri kullanım amacıyla ortaya çıktığı ilk dönemlerinin aksine radarlar bugün hemen hemen hayatın her alanında karşımıza çıkmaktadır. Elektronik devre üretim teknolojisinin gelişimi bu sonucu ortaya

çıkarmış ve radar boyutları oldukça küçülmüştür (Azevedo ve McEwan 1997; Andersen ve diğ., 2017). Özellikle iç ortam kullanımları için uygun hale gelen radarlar, daha önce kablolu olarak gerçekleştirilen uygulamaların temassız olarak gerçekleştirme fikrini gündeme getirmiştir (Amin ve diğ. 2017). Bu durum tıp alanında da kendine yer bulmuştur. Farklı radar tipleriyle; yaşlı ve hasta gözetimi, yanık ve yeni doğan vakalarının yaşamsal belirti takibi ve uyku apnesi gibi durumlarda radarların kullanılabileceği öne sürülmüştür (Hu ve diğ., 2013; Anishchenko ve diğ., 2019; Lin ve diğ., 2016; Adib ve diğ.,2015; Qi ve diğ.,2016). Çalışmaların temelini insanın solunum ve kalp atışından kaynaklı göğüs kafesi hareketinin tespiti oluşturmaktadır. Böylece yaşamsal belirti sinyalleri elde edilebilmektedir (Islam ve diğ., 2020; Seflek ve diğ., 2020; Abdul-Atty ve diğ., 2020; Acar ve diğ., 2021). Radarlar sağlık çalışanlarının işini kolaylaştırmanın yanı sıra, salgın hastalık vb. durumlarda onların korunması için de oldukça önemlidir. Ayrıca kablo ve prob gibi hastayı rahatsız eden, hatta yanık vakalarında ekstra yaralanmalara sebep olan durumlardan da hastayı kurtarabilecektir. Bu çalışmada sağlıklı bir gönüllü insan denekten düşük maliyetli bir CW Doppler radar kullanılarak, uygun sinyal işleme yöntemleri ile yaşamsal sinyaller elde edilmiştir.

MATERYAL VE YÖNTEM (MATERIAL AND METHOD)

Bir CW Doppler radarı sabit frekansta ürettiği sinyali verici antenle hedefe gönderir. Gönderilen sinyal ifadesi,

$$S_{TX}(t) = A_T \cos(2\pi f_c t + \phi(t)) \qquad (1)$$

şeklinde gösterilir. Burada A_T gönderilen sinyalin genliğini, f_c gönderilen sinyalin frekansını ve $\phi(t)$ ise faz gürültüsünü göstermektedir. Hedeften yansıyan sinyal, hedef hareketi kaynaklı faz gecikmesiyle birlikte alıcı anten vasıtasıyla alınır. Alınan sinyal ifadesi,

$$S_{RX}(t) = A_R \cos(2\pi f_c t - \frac{4\pi d_0}{\lambda} - \frac{4\pi x(t)}{\lambda} - \phi(t - \frac{2d(t)}{c})) \qquad (2)$$

şeklinde olur. Elde edilen sinyalde A_R alınan sinyalin genliği, d_0 hedefin radardan olan uzaklığı ve $x(t)$ hedefin hareketidir. $\phi(t - \frac{2d(t)}{c})$ ifadesi gecikmiş faz gürültüsünü, $d(t)$; d_0 ve $x(t)$ uzaklıkları toplamını ve $\frac{2d(t)}{c}$ ise radar ile hedef arasındaki uçuş süresini göstermektedir. Alınan sinyal bir karıştırıcı vasıtasıyla gönderilen sinyalle temel bant seviyesine indirgenir. Temel bant sinyali,

$$B(t) = \cos(\frac{4\pi d_0}{\lambda} + \frac{4\pi x(t)}{\lambda} + \Delta\phi(t)) \qquad (3)$$

olarak elde edilir. $\Delta\phi(t) = \phi(t) - \phi(t - \frac{2d(t)}{c})$ ifadesi rezidual faz gürültüsüdür. Eşitlik (3)'te görüleceği gibi, sinyal çıkışı radarın hedeften olan uzaklığına bağlıdır. $(4\pi d_0)/\lambda$ terimi faz sinyalinde DC ofsete sebep olmaktadır ve faz kayması sonucu algılama sonucunu etkilemektedir. $(4\pi d_0)/\lambda$ teriminin $\pi/2$'nin tek ve çift katlarına bağlı olarak, ideal sonuç yani hedef hareketi ile uyumlu çıkış ve boş nokta (null point) hedef hareketi ile uyumsuz çıkış ürettiği görülmektedir. Bu sorunu ortadan kaldırmak ve daima ideal bir sonuç elde edilebilmesi için dördün (quadrature) alıcılı CW radar kullanılmıştır. Dördün alıcıda birbirinden 90° faz farklı iki çıkış üretilmesi bu sorunu gidermektedir. Çıkışta kanalın biri daima ideal sonucu üretmektedir. Eşitlik (4) dördün alıcılı CW radarın temel bant çıkışlarını göstermektedir.

$$B_I(t) = A_I \cos(\frac{4\pi d_0}{\lambda} + \frac{4\pi x(t)}{\lambda} + \Delta\phi(t))$$
$$B_Q(t) = A_Q \sin(\frac{4\pi d_0}{\lambda} + \frac{4\pi x(t)}{\lambda} + \Delta\phi(t)) \qquad (4)$$

Kanalların arktanjant demodülasyonu ile birleştirilmesi, kanal seçimi işlemini ortadan kaldırmakta ve yüksek doğrulukta daha hızlı sonuçlar vermektedir. Arktanjant demodülasyonu sonucu,

$$\phi(t) = \arctan\left(\frac{B_Q(t)}{B_I(t)}\right) = \frac{4\pi d_0}{\lambda} + \frac{4\pi x(t)}{\lambda} + \Delta\phi(t)) \quad (5)$$

ifadesi elde edilir. Böylece faz sinyali, hedef hareketi ile doğrudan orantılı hale gelmektedir. Yaşamsal belirti sinyalleri elde edilen bu faz sinyalinden ortaya çıkarılmaktadır.

Ölçüm Düzeneği ve Ölçümlerin Gerçekleştirilmesi (Measurement Setup and Performing Measurements)

Yaşamsal belirti ölçümlerinin gerçekleştirilmesinde RF-Beam firmasının ürettiği K-LC6 radar modülü kullanılmaktadır. Radar 24 GHz çalışma frekansı ve dördün alıcı yapısına sahiptir. Şekil-1 K-LC6'nın blok diyagramını göstermektedir.
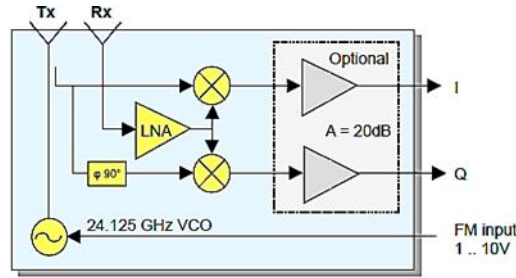
Şekil 1. K-LC6 blok diyagramı
Figure 1. Block diagram of K-LC6

Temel bant çıkış sinyalleri I ve Q, AD-620 mikrovolt sinyal modülü ile kuvvetlendirilmektedir. Solunum ve kalp atış sinyallerinin frekansı sırası ile 0.1-0.5 ve 0.8-2 Hz arasında değişmektedir. Kuvvetlendirilen sinyaller hem bu frekans bant aralıklarını kapsayacak şekilde hem de örtüşmeyi (aliasing) önlemek amacıyla gerçekleştirilen 30 Hz kesim frekanslı aktif alçak geçiren filtre ile filtrelenmektedir. Sinyaller işlenmesi için VTK 1050 veri toplama cihazı ile 200 Hz örnekleme frekansında sayısallaştırılarak bilgisayara kaydedilmektedir. Ölçüm için sağlıklı bir gönüllü denek radarın 1 m karşısına oturtulmaktadır. Sabit bir şekilde oturan denekten 60 saniye boyunca ölçümler alınmaktadır. Şekil-2 ölçüm ortamını göstermektedir.

Şekil 2. Ölçüm ortamı
Figure 2. Measurement environment

BULGULAR (RESULTS)

Elde edilen radar sinyallerini işlemek için iki farklı yöntem kullanılmaktadır. Birinci yöntemde I ve Q temel bant sinyallerine normalizasyon uygulanmaktadır. Ardından arktanjant demodülasyonu ile birleştirilen I ve Q sinyallerinin faz bilgisine ulaşılmaktadır. Faz bilgisinin doğru bir şekilde elde edilmesi

için, arktanjant demodüleli sinyale faz açma (unwrapping) işlemi uygulanır. Arktanjant fonksiyonu $(\pi/2, -\pi/2)$ aralığında değerler almaktadır. Hedef hareketi büyük olursa bu değerler aşılmakta ve faz sinyalinde süreksizlik meydana gelmektedir. Bu süreksizliklerin ortadan kaldırılabilmesi için sinyal işlemede π'nin tamsayı katları ile çarpılarak faz açma işlemi gerçekleştirilir. Faz sinyali, solunum sinyalini elde etmek için 0.1-0.5 Hz frekans aralığında bant geçiren filtre ile filtrelenmektedir. Benzer şekilde 0.8-2 Hz aralığında bant geçiren filtre kalp atış sinyalini elde etmek amacıyla faz sinyaline uygulanmaktadır. Sinyal periyodikliğini artırma amacıyla otokorelasyon gerçekleştirilmektedir. Son olarak sinyale Hızlı Fourier Dönüşümü (FFT) uygulanmaktadır. Solunum ve kalp atış hızı tespit edilmektedir. Şekil-3 sinyalin işlenmesi için kullanılan birinci yöntemin blok diyagramını göstermektedir.

Sinyallerin işlenmesi için kullanılan ikinci yöntemde ise sinyaller ilk yönteme benzer şekilde normalizasyona, arktanjant demodülasyonuna ve faz açma işlemine tabi tutulmaktadır. Demodüle edilmiş sinyale çoklu çözünürlük analizi (MRA) uygulanmaktadır (Mallat, 1989). MRA, sinyali yaklaşım (CA) ve detay katsayılarına (CD) ayırarak, sinyalin değişken çözünürlükteki ikili frekans bantlarında incelenmesini sağlamaktadır. İkili frekans bantları kullanılarak sinyal ayrışımı ve ilgilenilen fizyolojik sinyallerin çıkarılması sağlanmaktadır. MRA için ana dalgacık fonksiyonu olarak Symlet 7 kullanılmaktadır. Şekil-4 sinyalin işlenmesi için kullanılan ikinci yöntemin blok diyagramını göstermektedir.
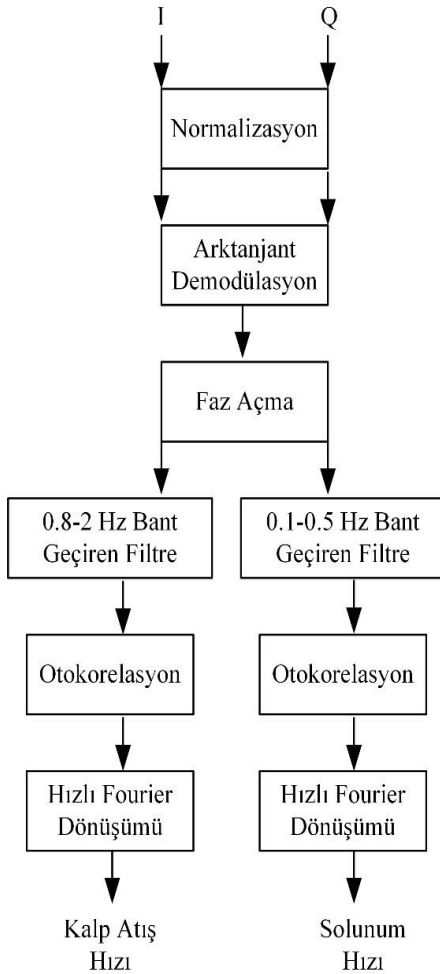
Şekil 3. Kullanılan birinci yöntemin blok diyagramı **Şekil 4.** Kullanılan ikinci yöntemin blok diyagramı
Figure 3. Block diagram of the first method used   *Figure 4. Block diagram of the second method used*

Birinci yöntem kullanılarak gerçekleştirilen bir ölçümün sonuçları Şekil-5'te gösterilmektedir. Şekil-6'da aynı ölçüm için ikinci yöntem kullanarak elde edilen sonuçlar gösterilmektedir. Ölçüm sonuçlarının

doğruluğunun karşılaştırılması amacıyla referans olarak Veron 501 pulse oksimetresi kullanılır. Ayrıca solunum referansı için ölçüm sırasında nefes alış-verişi denek tarafından sayılmaktadır.

(a)

(b)

(c)
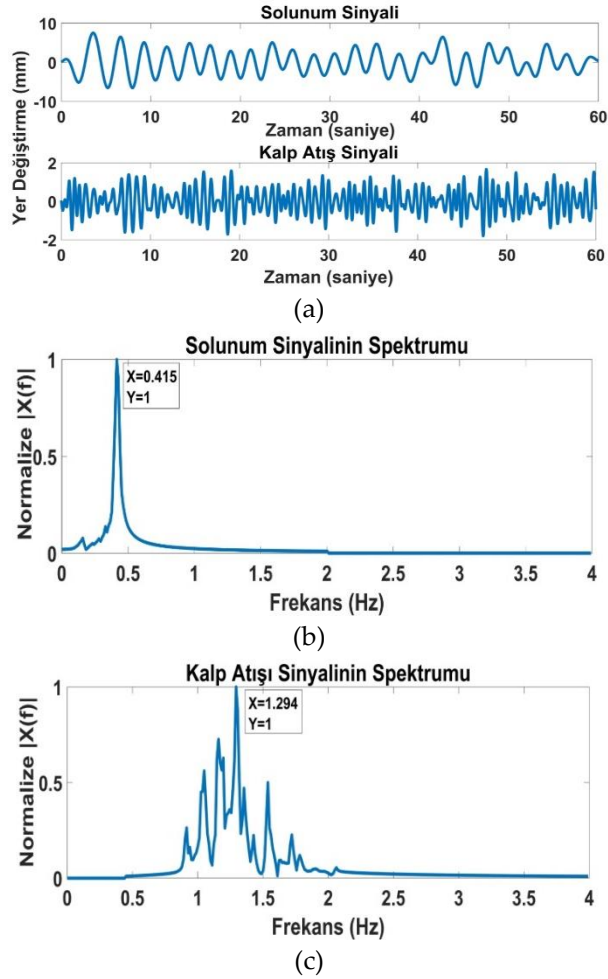
Şekil 5. Birinci yöntem kullanılarak elde edilen ölçüm sonuçları (a) Solunum ve kalp atış sinyali (b) Solunum sinyalinin frekans spektrumu (c) Kalp atışı sinyalinin frekans spektrumu

Figure 5. Measurement results obtained using the first method (a) Respiration and heartbeat signal (b) Frequency spectrum of respiration signal (c) Frequency spectrum of heartbeat signal

(a)   (b)
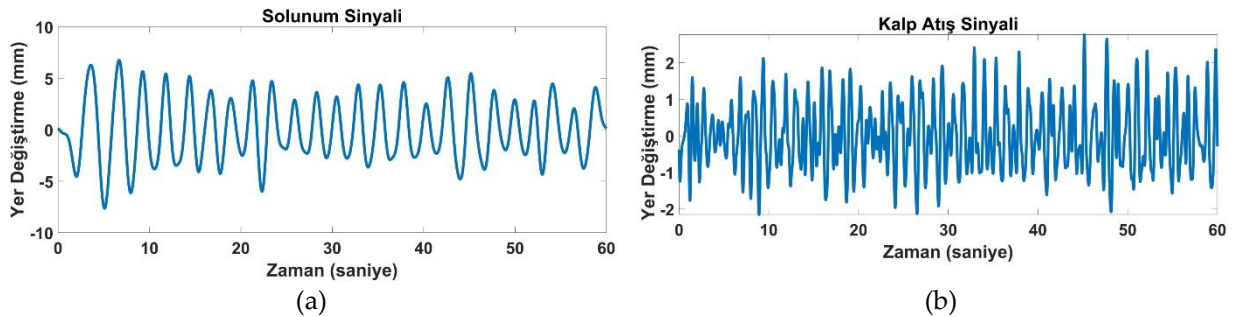
Şekil 6. İkinci yöntem kullanılarak elde edilen ölçüm sonuçları (a) Solunum sinyali (b) Kalp atış sinyali

Figure 6. Measurement results obtained using the second method (a) Respiration signal (b) Heartbeat signal

İki yönteme ait ölçüm sonuçları, referans değerlerle karşılaştırılarak yüzde hata oranları ile sunulmaktadır. Solunum için referans değeri 24 tür. Birinci yöntemde bu değer %3.75 hata ile 24.9 olarak hesaplanmıştır. İkinci yöntemde %0 hata ile 24 solunum sayısı hesaplanmıştır. Kalp atış ölçümlerinde referans 71 atımdır. İki farklı yöntem için sırasıyla %9.35 hata ile 77.64 ve %8.45 hata ile 65 değerleri

bulunmuştur. Sonuçlar incelendiğinde çoklu çözünürlük analizinin (MRA) kullanıldığı yöntemin daha başarılı olduğu görülmektedir.

SONUÇLAR (CONCLUSIONS**)**

Düşük maliyetli 24 GHz çalışma frekansında çalışan bir CW Doppler radarı kullanılarak sağlıklı bir bireyin temassız yaşamsal belirti ölçümleri gerçekleştirilmiştir. Ölçüm sonucu elde edilen sinyallerin işlenmesinde iki farklı sinyal işleme yöntemi kullanılmıştır. Kullanılan yöntemlerin hata oranı solunum sinyali tespiti için %3.75 ve %0 olmuştur. Kalp atış sinyali için bu oranlar %9.35 ve %8.45'tür. Sonuçlardan MRA yönteminin daha başarılı olduğu görülmektedir. Kalp atış sinyalinin hata oranının yüksek olması kalbin çok küçük yer değiştirme hareketinden kaynaklandığı değerlendirilmektedir. Bu sonuçlar radarların temassız ölçümlerde sağlık çalışanı ve hastalara sağladığı avantajlarla tıp alanında gelecekte yoğun bir şekilde kullanılabileceğini göstermektedir.

KAYNAKLAR (REFERENCES**)**

Abdul-Atty, M.M., Amar, A.S.I. ve Mabrouk, M., 2020, "C-Band FMCW Radar Design and Implementation for Breathing Rate Estimation", *Advances in Science, Technology and Engineering Systems Journal*, cilt. 5, no. 5, ss. 1299-1307.

Acar, Y. E., Saritas, I. ve Yaldiz, E., 2021, "An Experimental Study: Detecting the Respiration Rates of Multiple Stationary Human Targets by Stepped Frequency Continuous Wave Radar", *Measurement*, cilt.167,108268.

Adib, F., Mao, H., Kabelac, Z., Katabi, D. ve Miller, R. C. "Smart homes that monitor breathing and heart rate", *Proceedings of the 33rd Annual ACM Conference on Human Factors in Computing Systems*, ss.837-846, 2015.

Amin, M., 2017, Radar for indoor monitoring: detection, classification, and assessment, CRC Press.

Andersen N., Granhaug, K., Michaelsen, J. A., Bagga, S., Hjortland, H. A., Knutsen, M. R., ve Wisland, D. T., 2017, "A 118-mW pulse-based radar SoC in 55-nm CMOS for non-contact human vital signs detection*", IEEE Journal of Solid-State Circuits*, cilt.52, no.12, ss.3421-3433.

Anishchenko, L., Zhuravlev, A. ve Chizh, M., 2019, "Fall detection using multiple bioradars and convolutional neural networks", *Sensors*, cilt.19 no.24, ss.5569.

Azevedo, S. ve McEwan, T. E., 1997,"Micropower impulse radar", *IEEE Potentials*, cilt.16 no.2, ss.15-20.

Hu, W., Zhao, Z., Wang, Y., Zhang, H. ve Lin, F., 2013, "Noncontact accurate measurement of cardiopulmonary activity using a compact quadrature Doppler radar sensor", *IEEE Transactions on Biomedical Engineering*, cilt.61 no.3, ss.725-735.

Islam, Shekh MM, Motoyama, N., Pacheco, S. ve Lubecke, V. M.. "Non-Contact Vital Signs Monitoring for Multiple Subjects Using a Millimeter Wave FMCW Automotive Radar ", *IEEE/MTT-S International Microwave Symposium (IMS),ss.783-786, 2020.*

K-LC6 Radar Modülü. https://www.rfbeam.ch/product?id=12, ziyaret tarihi: 14.08.2020.

Lin, F., Zhuang, Y., Song, C., Wang, A., Li, Y., Gu, C. ve Xu, W., 2016, "SleepSense: A noncontact and cost-effective sleep monitoring system", *IEEE Transactions on Biomedical Circuits and Systems*, cilt.11 no.1, ss.189-202.

Mallat, SG., 1989, "A theory for multiresolution signal decomposition: the wavelet representation", *IEEE Trans Pattern Anal Mach Intell*, cilt.11 no.7 s.674–693.

Qi, F., Li, C., Wang, S., Zhang, H., Wang, J. ve Lu, G., 2016, "Contact-free detection of obstructive sleep apnea based on wavelet information entropy spectrum using bio-radar", *Entropy*, cilt.18 no.8, ss.306.

Seflek, I., Acar, Y. E. ve Yaldiz, E., 2020, "Small Motion Detection and Non-Contact Vital Signs Monitoring with Continuous Wave Doppler Radars", *Elektronika ir Elektrotechnika*, cilt.26 no.3, ss.54-60.

FUSED DEEP FEATURES BASED CLASSIFICATION FRAMEWORK FOR COVID-19 CLASSIFICATION WITH OPTIMIZED MLP

¹Şaban ÖZTÜRK iD **, ²Enes YİĞİT** iD **, ³Umut ÖZKAYA** iD

¹Amasya Üniversitesi, Teknoloji Fakültesi, Elektrik-Elektronik Mühendisliği Bölümü, Amasya, TÜRKİYE
²Karamanoğlu Mehmetbey Üniversitesi, Mühendislik ve Mimarlık Fakültesi, Elektrik-Elektronik Mühendisliği Bölümü, Karaman, TÜRKİYE
³ Konya Teknik Üniversitesi, Mühendislik ve Doğa Bilimleri Fakültesi, Elektrik-Elektronik Mühendisliği Bölümü, Konya, TÜRKİYE
¹msaban.ozturk@amasya.edu.tr, ²enesyigit@kmu.edu.tr, ³uozkaya@ktun.edu.tr

ABSTRACT: The new type of Coronavirus disease called COVID-19 continues to spread quite rapidly. Although it shows some specific symptoms, this disease, which can show different symptoms in almost every individual, has caused hundreds of thousands of patients to die. Although healthcare professionals work hard to prevent further loss of life, the rate of disease spread is very high. For this reason, the help of computer aided diagnosis (CAD) and artificial intelligence (AI) algorithms is vital. In this study, a method based on optimization of convolutional neural network (CNN) architecture, which is the most effective image analysis method of today, is proposed to fulfill the mentioned COVID-19 detection needs. First, COVID-19 images are trained using ResNet-50 and VGG-16 architectures. Then, features in the last layer of these two architectures are combined with feature fusion. These new image features matrices obtained with feature fusion are classified for COVID detection. A multi-layer perceptron (MLP) structure optimized by the whale optimization algorithm is used for the classification process. The obtained results show that the performance of the proposed framework is almost 4.5% higher than VGG-16 performance and almost 3.5% higher than ResNet-50 performance.

Key Words: COVID-19, Coronavirus, Classification, MLP, Feature Fusion.

Optimize Edilmiş ÇKA ile Covıd-19 Sınıflandırması için Kaynaştırılmış Derin Özelliklere Dayalı Sınıflandırma Çerçevesi

ÖZ: COVID-19 adı verilen yeni tip Koronavirüs hastalığı oldukça hızlı yayılmaya devam etmektedir. Bazı spesifik semptomlar gösterse de hemen her bireyde farklı semptomlar gösterebilen bu hastalık yüzbinlerce hastanın hayatını kaybetmesine neden olmuştur. Sağlık uzmanları, daha fazla yaşam kaybını önlemek için çok çalışsalar da, hastalık yayılma oranı çok yüksektir. Bu nedenle Bilgisayar Destekli Teşhis (BDT) ve Yapay Zeka (YZ) algoritmalarının desteği hayati önem taşımaktadır. Bu çalışmada, belirtilen COVID-19 algılama ihtiyaçlarını karşılamak için günümüzün en etkili görüntü analiz yöntemi olan Evrişimli Sinir Ağı (ESA) mimarisinin optimizasyonuna dayalı bir yöntem önerilmiştir. İlk olarak, COVID-19 görüntüleri ResNet-50 ve VGG-16 mimarileri kullanılarak eğitilir. Ardından, bu iki mimarinin son katmanındaki özellikler füzyon işlemi uygulanmıştır. Füzyon işlemi ile elde edilen bu yeni görüntü özellikleri matrisleri, COVID-19 tespiti için sınıflandırılır. Sınıflandırma işlemi için Balina Optimizasyon Algoritması (BOA) ile optimize edilmiş Çok Katmanlı Bir Algılayıcı (ÇKA) yapısı kullanılır. Elde edilen sonuçlar, önerilen çerçevenin performansının VGG-16 performansından neredeyse % 4,5 ve ResNet-50 performansından neredeyse % 3,5 daha yüksek olduğunu göstermektedir.

1. INTRODUCTION

The new type of coronavirus, called COVID-19 by the world health organization (WHO), spread rapidly among people and turned into a severe epidemic. First seen in Wuhan, China, COVID-19 spread all over the world in a short time. This virus, which seriously threatens human health, has caused the death of many people (Jaiswal *et al.*, 2020). Among the most common symptoms of this disease are fever, cough, and breathing problems. However, these symptoms and their severity differ from person to person (Öztürk *et al.*, 2020a). An effective and approved vaccine for COVID-19, which can spread quite quickly through airborne droplets, has yet to be found. In addition, there is still no consensus on a definitive treatment method. As a result of all these facts, governments are trying to mitigate the epidemic by introducing serious measures and various rules. Although these measures are different from the usual social order, they begin to be accepted as new normal. In order to return to the old social order and end the COVID-19 pandemic, researchers are doing everything. Especially, researchers in the medical field carry out very devoted studies in terms of vaccines, medicines, and medical applications.

Considering the workload on medical professionals, it is clear that it is necessary to leverage technological developments to find a solution to COVID-19. Today, developments such as the widespread use of technological devices and the integration of artificial intelligence algorithms in almost every field are very promising (Vaishya *et al.*, 2020). Many AI researchers focus their full concentration on this area to help combat COVID-19 by shifting these advances in technology to the medical domain. For this purpose, researchers are working on an automatic analysis of chest X-ray and CT images. Because the Real-Time Reverse Transcription Polymerase Chain Reaction (RT-PCR) method is time-consuming and has error-prone results (Zu *et al.*, 2019).

CNN, the most powerful image processing method of today, is frequently used for processing X-ray and CT images related to COVID-19. In some studies for COVID-19 detection, hand-crafted features or more straightforward techniques are used. These methods are often preferred when there is not enough dataset to train a CNN architecture. When the COVID-19 epidemic started, some studies used hand-crafted methods because there were not enough COVID-19 datasets containing enough samples in the literature. Datasets containing insufficient samples cause overfitting problems in a deep CNN network. The most striking works performed without using any deep learning architecture are briefly summarized below. Barstugan *et al.* (2020) used Grey Level Co-occurrence Matrix (GLCM), Local Directional Pattern (LDP), Grey Level Run Length Matrix (GLRLM), Grey-Level Size Zone Matrix (GLSZM), and Discrete Wavelet Transform (DWT) algorithms to extract image features. Randhawa *et al.* (2020) proposed supervised machine learning with digital signal processing (MLDSP) for genome analyses of COVID-19. Öztürk *et al.* (2020) proposed a hybrid method that includes image augmentation and data oversampling with hand-crafted features. Elaziz *et al.* (2020) presented a machine learning method for the chest x-ray images using new Fractional Multichannel Exponent Moments (FrMEMs). Shi *et al.* (2020) proposed an infection Size Aware Random Forest method (iSARF) in order to automatically categorize images into groups. Sun *et al.* (2020) proposed an Adaptive Feature Selection guided Deep Forest (AFS-DF) for COVID-19 classification based on chest CT images. The results produced by hand-crafted methods are inspiring. However, as the number and variety of images related to COVID-19 increased, the performance of many of these methods did not meet the expectation. With the emergence of datasets containing a sufficient number and variety of samples to train CNN architectures, studies containing CNN have started to emerge rapidly.

It is almost impossible to examine all of the CNN-guided COVID-19 detection studies available in the literature. Currently, the number of COVID-19 classification, segmentation, detection, etc. studies is more than 50,000. For this reason, some of the most interesting and groundbreaking studies are summarized below. Hemdan *et al.* (2020) proposed a deep learning framework namely COVIDX-net. It consists seven different CNN architectures such as VGG19, MobileNet, and etc. Ozturk *et al.* (2020b) proposed a linear CNN model both binary and multi-class COVID-19 image classification. Afshar *et al.* (2020) presented

capsule network approach, referred to as the COVID-CAPS, being capable of handling small datasets. Their methods are based on the capsule network approach. Sahlol *et al.* (2020) combined CNN and a swarm-based feature selection algorithm to classify COVID-19 X-ray images. They facilitated the feature extraction strength of CNN and Marine Predators Algorithm to select the most relevant features. Nour *et al.* (2020) used CNN architecture to extract robust features from COVID-19 images. They feed machine learning algorithms using these deep features (k-nearest neighbor, support vector machine, and decision tree). Singh *et al.* (2020) presented a deep CNN method to classify chest X-ray-based COVID-19 images. Also, they tuned the parameters of CNN using Multi-objective Adaptive Differential Evolution (MADE). Ucar and Korkmaz (2020) proposed a type of SqueezeNet architecture for the classification of COVID-19 related chest X-ray images (named as COVIDiagnosis-Net). Their architecture is tuned for the COVID-19 diagnosis with a Bayesian optimization additive. Fan *et al.* (2020) proposed COVID-19 Lung Infection Segmentation Deep Network (Inf-Net) for the segmentation of CT slices. Wang *et al.* (2020) proposed a method based on a weakly-supervised to classify and localize COVID-19 lesions from CT images. Pham (2020) implemented a comprehensive study that includes pre-trained CNN models to classify COVID-19. Albahri *et al.* (2020) applied taxonomy analysis on binary and multi-class COVID-19 classification problems. Pereira *et al.* (2020) proposed a CNN method with early and late fusion to analyze COVID-19 infected X-ray images.

In this study, a highly efficient AI method that takes advantage of the feature representation power of different CNN architectures is presented. VGG-16 and ResNet-50 methods, which are the two most powerful CNN methods used as backbones in the literature, are used to extract features from images. There are studies that classify the feature vectors obtained by these two architectures separately. But the thought that combining the feature representation ability of the two architectures will improve performance is quite exciting. For this purpose, feature vectors in the previous layer of the softmax layer are taken in both architectures. These feature vectors need to be combined into a single feature vector. An MLP structure is used to handle this step in an end-to-end manner. Two feature vectors are applied to the MLP input. MLP parameters are updated with the whale optimization algorithm. The most important contributions of the proposed method can be summarized as follows:

- An approach is proposed that combines the power of two different CNN architectures with powerful feature extraction capabilities.
- A robust combination of feature vectors in an end-to-end fashion using the whale optimization algorithm
- The proposed method, which is very easy to apply, significantly reduces the rate of misdiagnosis.

The rest of this study is organized as follows: Section 2 includes dataset details, methodological background, and details of the proposed method. Experimental settings and performance indicators of the proposed method are presented in Section 3. The conclusion is given in Section 4.

2. MATERIAL AND METHODS

SARS-CoV-2 CT scan dataset is used to test the performance of the proposed method (Soares *et al.*, 2020). It is also possible to access this data on the Kaggle (https://www.kaggle.com/plameneduardo/sarscov2-ctscan-dataset). The dataset consists of 2482 CT images in total. 1252 of these images belong to patients infected by SARS-CoV-2. In 1230 CT images, it contains CT images of patients not infected with SARS-CoV-2. However, these 1230 images show CT images of other pulmonary diseases patients. For this reason, the dataset is relatively challenging. We did not apply any pre-processing or augmentation to the original images in the data. This is because the performance of the proposed method can be fairly compared with the performance of other state-of-the-art methods. Some of the sample images of the dataset are shown in Figure 1. Figure 1 (a) shows images of patients infected by SARS-CoV-2, Figure 1 (b) shows other images.
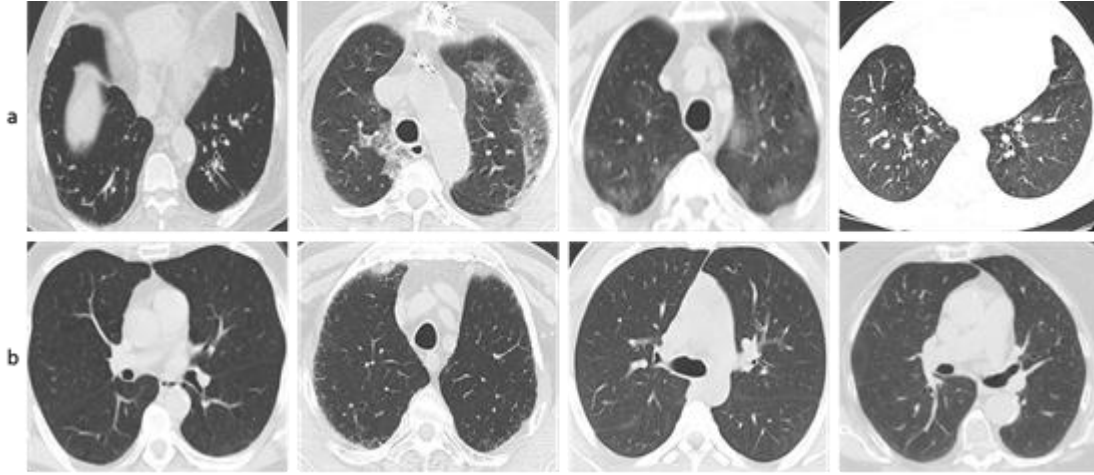
Figure 1. Sample images from SARS-CoV-2 CT scan dataset, a) infected by SARS-CoV-2 CT scan dataset, b) non-infected by SARS-CoV-2 CT scan dataset

CNN architectures have achieved significant success since the day it was first proposed. By solving many image processing problems, it has become a milestone in image analysis. Of course, It did not realize all these with just one architecture. New CNN architectures have been suggested frequently since its inception. For this reason, it is possible to find many different CNN architectures in the literature. Some of these architectures are very popular, while others are almost never used. In this study, VGG-16 and ResNet-50 architectures, which are accepted by artificial intelligence researchers and used as backbones in many studies, are used. Before going into the details of these architectures, brief information about the main CNN layers will be useful. CNN architectures generally consist of specific layers and various connection types. The convolution layer is the layer where learned properties are stored. It can be said that this layer, which contains a single kernel consisting of two-dimensional matrices, is the most critical layer of a CNN architecture. The kernels in this layer are scrolled on the image. This enables weight sharing and spatial information features. The other basic layer is the pooling layer. The pooling layer reduces the image dimensions while preserving the important features in the image. Thus, the number of parameters that need to be trained in the CNN architecture is greatly reduced. It has types such as max-pooling, average-pooling, sum-pooling. ReLU is the activation function. It is a very fast and simple function used to break the linearity in the network. The fully connected layer (FCL) is actually a kind of ANN structure. In this section, matrices are transformed into vectors and processed with the help of neurons. Softmax layer is preferred for classifying the vectors at the output according to their ratios. Finally, if a residual architecture is to be used (e.g., ResNet), the concatenate layer is required. This layer combines different layer outputs (Öztürk and Özkaya, 2020). After this quick and basic introduction to CNN layers, it will be useful to calculate a CNN output consisting of convolution, pooling, and ReLU layer. Equation 1 is used for this operation.

$$f\left(l_{next}\right) = pool_{nxn}\left(\sigma\left(w \otimes \left[D_{in}\right] + b\right)\right) \tag{1}$$

in which, f represents CNN, l_{next} is the input of the next layer of the output of the current layer, $pool$ represents pooling layer (max-pooling, average-pooling, or sum-pooling), nxn represents pooling window, σ is ReLU function, w represents convolution layer, D_{in} is the input of the current layer, b is the bias value.

VGG-16 architecture (Simonyan and Zisserman, 2014). includes 16 weight layers. So it contains 13 convolution layers and 3 FCL layers. Parameters in these layers are updateable. All convolution layers are 3x3 pixels with the stride of 1. All pooling layers consist of 2x2 windows with the stride of 2. Two FCLs

consist of 4,096 nodes, while the last FCL consists of 1000 nodes. It includes nearly 138 million trainable parameters.

ResNet-50 architecture (He *et al.*, 2016) is a very striking structure consisting of residual modules. It includes 50 weight layers. Although it is deeper than the VGG-16 model, it takes up less space. It consists of five stages each with a convolution and identity block. Each convolution block has three convolution layers and each identity block also has 3 convolution layers. It has nearly 23 million trainable parameters.

An MLP structure is a type of feedforward ANN architecture. A basic MLP structure consists of at least three layers: an input layer, a hidden layer, and an output layer. It is possible to increase the depth of MLP architecture. For this, the number of hidden layers in the MLP structure is increased. A nonlinear activation function generally follows neurons in the MLP structure. It is possible to train MLP architecture with backpropagation methods. Although it is a type of ANN, in some cases the name MLP is used in structures consisting of multiple layers of perceptrons. The selection of activation functions is one of the most important steps in solving a problem. In addition, it is very important in algorithms used for updating trainable parameters. Stochastic gradient descent (SGD) is widely used for the optimization of parameters (Wu *et al.*, 2020). In the optimization process performed with SGD, it may take time to reach global minima, and problems with the vanishing of gradients or explosion of gradients may be encountered. In some cases, it remains stuck in the local minima. Many optimization techniques have been proposed to overcome these problems. In this study, MLP parameters are updated with the whale optimization algorithm (WOA) (Mirjalili and Lewis, 2016). WOA is a meta-heuristic optimization algorithm. It is based on the hunting strategy of humpback whales. For brief information about the WOA algorithm, the encircling prey, spiral bubble-net feeding maneuver, and search for prey stages are mathematically examined. In the encircling prey stage, humpback whales determine the location of the prey and surround the prey. The WOA algorithm tries to determine the optimum position for the hunt. After the best search agent is determined, other search agents update their positions. The purpose of this update process is to move towards the best location. Equations 2 and 3 define this process.

$$D = \left| C.X^{*}(t) - X(t) \right| \tag{2}$$

$$X(t+1) = X^{*}(t) - A.D \tag{3}$$

where t represents the current iteration, C and A indicate coefficient vectors, X^{*} represents the best solution position vector, X indicates the current position vector, and '.' represents element-by-element multiplication. Also, other terms are calculated; $A=2a.r-a$ and $C=2.r$.

Two different approaches named as 'shrinking encircling mechanism' and 'spiral updating position' are used to better define the bubble-net behavior. In the shrinking encircling mechanism, the area is narrowed by decreasing the value of the a parameter. In this case the A is a random value in the interval [$-a$, a]. In the spiral updating position stage, the distance between the whale's location and the prey location is calculated. A spiral equation is defined between these two locations. With this equality, the whale updates its position with a helix-shaped movement. In Equation 4 this movement is defined.

$$X(t+1) = \left| X^{*}(t) - X(t) \right|.e^{bl}.\cos(2\pi l) + X^{*}(t) \tag{4}$$

in which, b defines shape of the logarithmic spiral, l represents random number in the interval [-1, 1]. In the search for prey (exploration) phase, humpback whales take positions at random according to each other's positions in search of prey. Therefore, in this step the value of A takes values either greater than 1 or less than -1. In this step, the location of the search agents is determined randomly. The mathematical model of this situation is as in Equation 5 and Equation 6.

$$D = \left| C.X_{rand} - X \right| \tag{5}$$

$$X\left(t+1\right) = X_{rand} - A.D$$

(6)

High-level features obtained from pre-trained networks are used in the framework of the proposed method. VGG-16 and ResNet-50 models were used as pre-trained networks. These models are trained with the transfer learning method. For training and test data, the features obtained from pre-trained CNN networks were given as input to the designed ANN structure after the fusion process. The parameter update process in the ANN model was performed with the Whale Optimization Algorithm (WOA) instead of the stochastic gradient descent algorithm. Weight and bias values have been updated more successfully than conventional ANN models. The block diagram of the proposed approach is given in Figure 2.
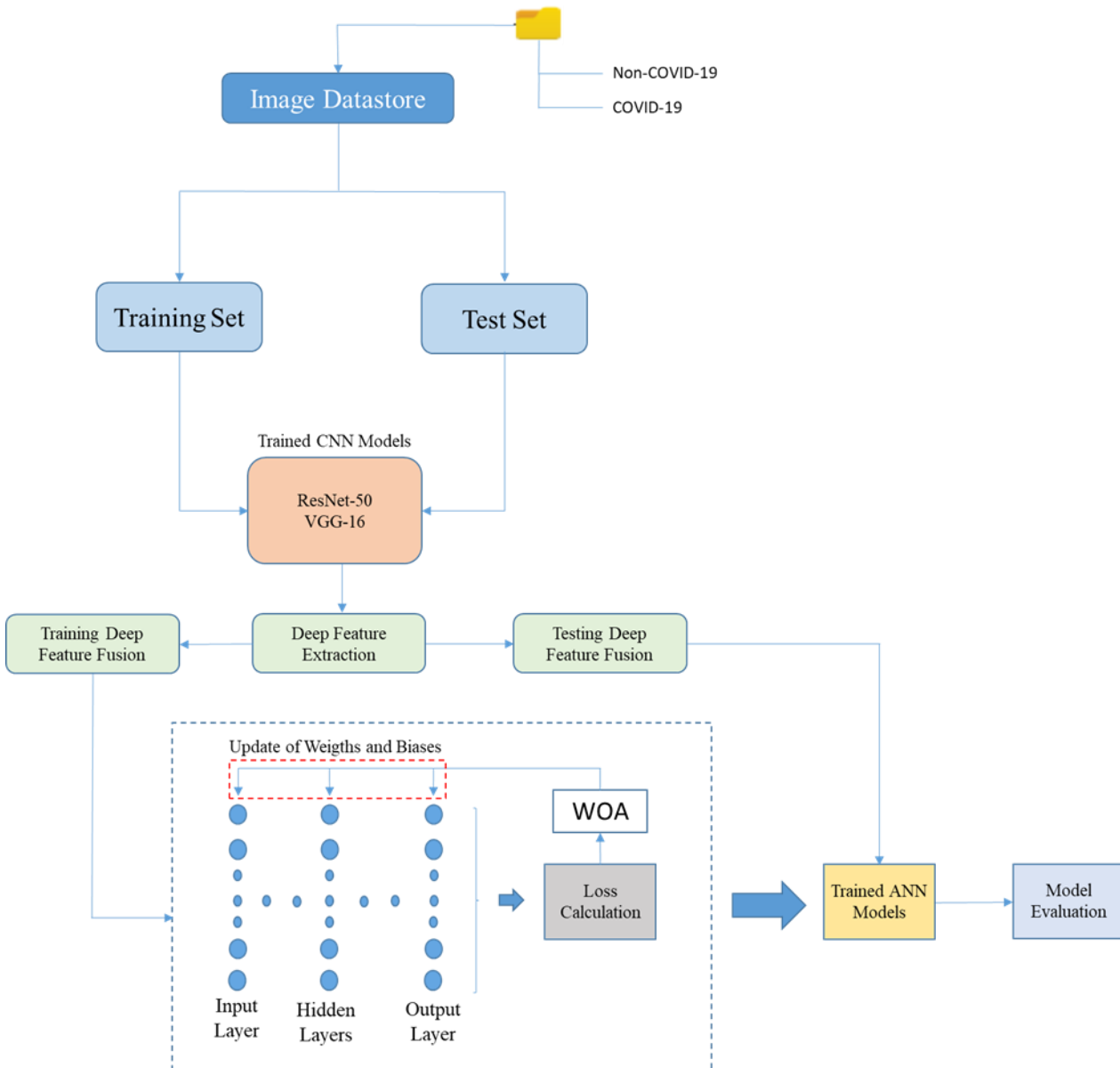
Figure 2. The block diagram of the proposed model

3. RESULTS AND DISCUSSION

As part of the study, the experiments were carried out on a workstation with Intel Core i7-7700 HQ CPU at 2.8 GHz, 16 GB RAM, and NVIDIA GTX 1080 GPU. Matlab 2020a was preferred as a simulation environment.

Some performance metrics obtained from the confusion matrix, which are Accuracy (ACC), Sensitivity (SEN), Specificity (SPE), F1-Score, Precision (PRE), Matthews Correlation Coefficient (MCC) and Kappa, were used to evaluate the models proposed in the study. These performance metrics are calculated by means of True Positive (TP), True Negative (TN), False Positive (FP) and False Negative (FN) indices as follows:

$$Accuracy = (TP + TN) / (TP + FN + TN + FP) \tag{7}$$

$$Sensitivity = TP / (TP + FN) \tag{8}$$

$$Specificity = TN / (TN + FP) \tag{9}$$

$$Precision = TP / (TP + FP) \tag{10}$$

$$F1 - Score = (2 \times TP) / (2 \times TP + FN + FP) \tag{11}$$

$$MCC = \frac{TP \times TN - FP \times FN}{\sqrt{(TP + FP)(TP + FN)(TN + FP)(TN + FN)}} \tag{12}$$

$$Kappa = \left(total\ accuracy - random\ accuracy \right) / \left(1 - random\ accuracy \right) \tag{13}$$

By using transfer learning, training of GoogleNet, ResNet-50, DenseNet-201 and VGG-16 structures was carried out within pre-trained CNN models. During the training phase, the mini-batch size was determined as 10, and the training was completed in 30 epochs. The training process finished with 5580 iterations in total. Each epoch was completed after 186 iterations. The initial learning rate is 0.1. The learning drop factor and period are chosen as 0.1 and 10 epochs, respectively. Test data were used instead of validation data, and it was performed in each 1000 iterations. In this way, the optimization process can be carried out quickly and accurately. Stochastic Gradient Descent with Momentum (SGDM) method was preferred in the optimization process. Training and test charts of pre-trained CNN networks used in the study are available in Figure 3-6.
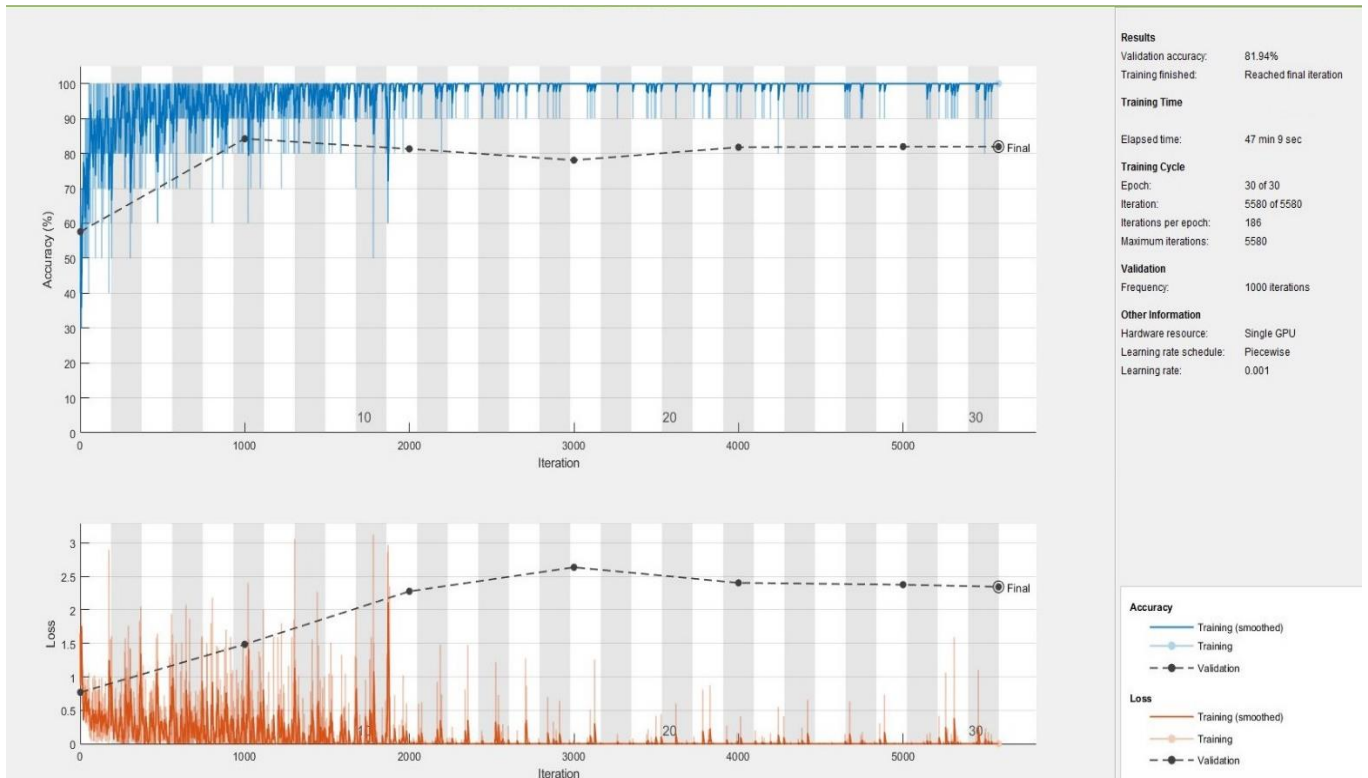
Figure 3. Training and Testing Process of GoogleNet
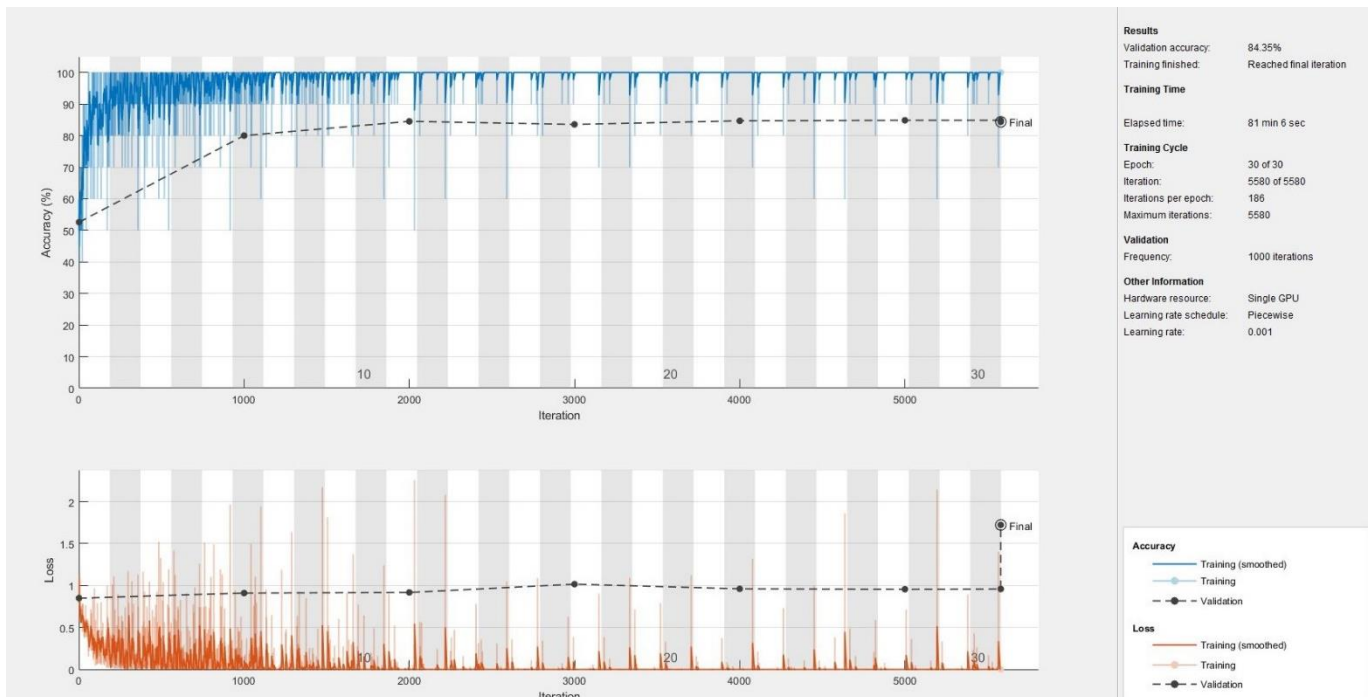
Figure 4. Training and Testing Process of ResNet-50
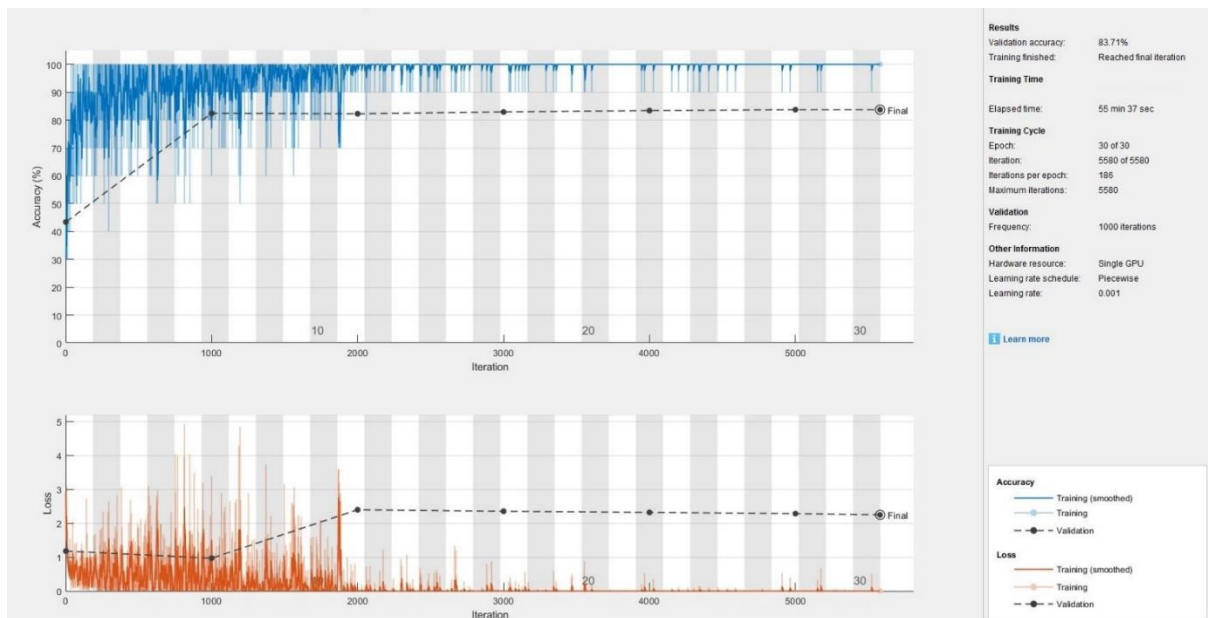
Figure 5. Training and Testing Process of VGG-16
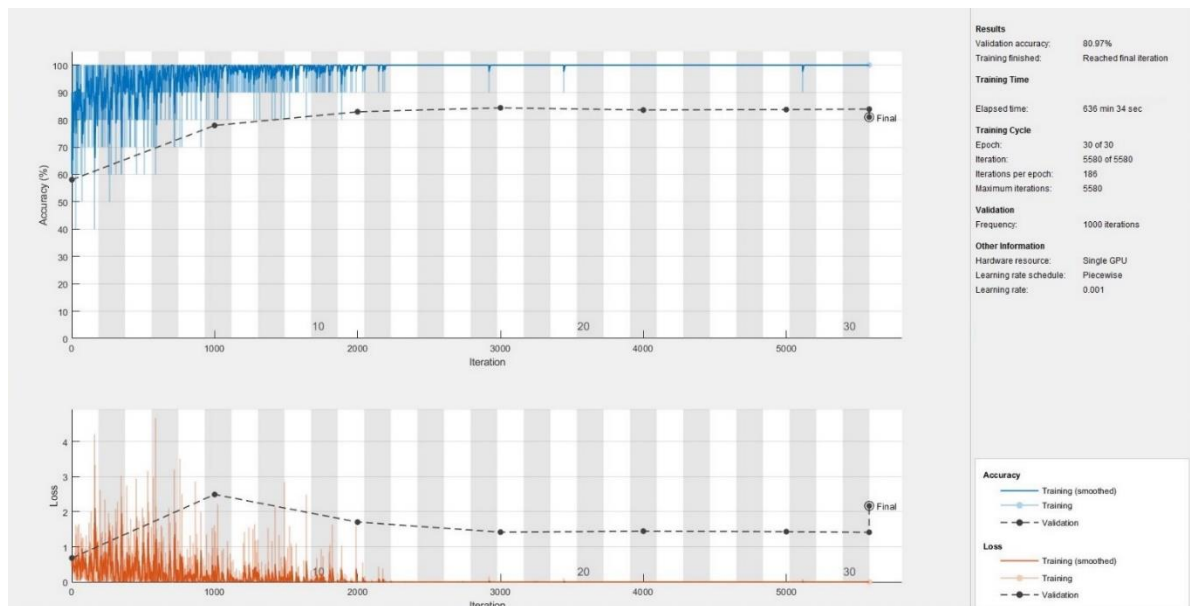
Figure 6. Training and Testing Process of DenseNet-201

There are two graphs in the figures, namely accuracy, and loss. The blue curves on the accuracy graph represent the accuracy of the training data, while the black curves show the accuracy of the test data. The red curves in the loss graph represent the loss of training data, while the black curves represent the loss of test data. Since the number of parameters included in the pre-trained CNN models are different from each other, the training durations are also different from each other. The pre-trained CNN network with the shortest training period is GoogleNet and the training process was completed in 47 min 9 seconds. Then, the VGG-16 model completed training with 55 min 37 seconds. There are two pre-trained CNN network models with the longest training period. One of them is the ResNet-50 model and it completed the training process in 81 min 6 sec. DenseNet-201 is the model that has by far more training time than the training of other pre-trained CNN models. This model completed the training process in 636 min 34 sec. Achieving high classification accuracy in such short training times depends on transfer learning. In addition to the accuracy metric, other classification metrics are given in Table 1.

Table 1. Comparison of Metric Performance

Methods	Evaluation Metrics (%)						
	ACC	SEN	SPE	PRE	F1-score	MCC	Kappa
VGG-16	83.71	68.05	99.67	99.53	80.83	71.22	67.52
ResNet-50	84.35	69.01	**100**	**100**	81.66	72.42	68.80
GoogleNet	81.94	65.81	98.37	97.63	78.63	67.73	63.98
DenseNet-201	80.97	62.62	99.67	99.49	76.86	66.89	62.07
Proposed Method	**88.06**	**81.47**	94.79	94.10	**87.33**	**76.87**	**76.16**

Table 1 includes the classification performance of four pre-trained CNN models and the proposed method. When evaluated in terms of performance, the DenseNet-201 model showed the lowest performance. The performance of this model is 80.91% ACC, 62.62% SEN, 99.67% SPE, 99.49% PRE, 76.86% F1-Score, 66.89% MCC and 62.07% Kappa. ResNet-50 model showed the highest performance in pre-trained CNN models. The performance of the VGG-16 model is also very close to that of the ResNet-50 model. The classification metrics obtained with ResNet-50 were 84.35% ACC, 69.01% SEN, 100.00% SPE, 100.00% PRE, 81.66% F1-Score, 72.42% MCC and 68.80% Kappa. The proposed method has achieved higher performance than pre-trained CNN models. The performance of the proposed method is 88.06% ACC, 81.47% SEN, 94.79% SPE, 94.10% PRE, 87.33% F1-Score, 76.87% MCC and 76.16% Kappa. The proposed method stands out in all classification metrics except specificity and precision metrics. In Figure 7, the confusion matrix of pre-trained CNN models is given.

(a)

(b)

(c)

(d)
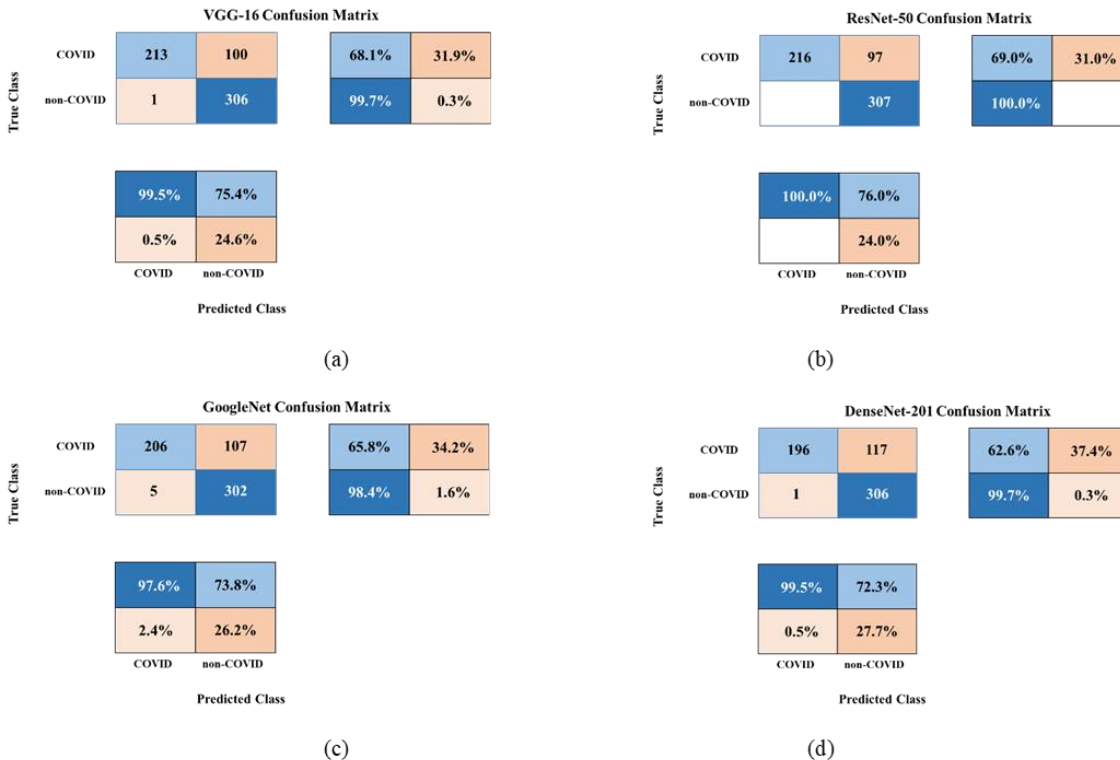
Figure 7. Confusion Matrix of pre-trained CNNs (a) VGG-16 (b) ResNet-50 (c) GoogleNet (d) DenseNet-201

Class accuracy and error rates can be seen in the confusion matrices obtained for test data. In the confusion matrix of the ResNet-50 model, 100% classification accuracy has been achieved in the non-COVID class. In the COVID class, this accuracy is 69.0%. In the DenseNet-201 model with the lowest performance, the classification accuracy achieved in the COVID class is 62.6%. In the non-COVID class,

the classification accuracy is 99.7%. The highest error rate for the COVID class belongs to the DenseNet-201 model, with 37.4%. Figure 8 contains the confusion matrix of the proposed method.

Figure 8. Confusion Matrix of Proposed Method

In the concept of class accuracies of the proposed method, the accuracy rate has increased further in the COVID class. In the COVID class, the number of TN is 255 and the number of FP is 58. For the COVID class, the accuracy rate is 81.5%, and the error rate is 18.5%. For the Non-COVID class, the FN number is 16, and the number of TP is 291. The class accuracy rate is 94.8%, the error rate is 5.2%.

4. CONCLUSION

Despite the COVID-19 outbreak, people continue their routine daily life. With the arrival of the winter months, the affected by this epidemic begin to rise significantly. Within the scope of this study, a COVID-19 diagnosis system was proposed to support clinical research. It is based on CNN architecture and utilizes transfer learning. The deep learning method has automatic feature decoding capability and provides higher performance than handmade feature extraction engines. In this way, COVID-19 cases can be detected with high performance by using CT images. The method used to achieve 88.06% ACC, 81.47% SEN, 94.79% SPE, 94.10% PRE, 87.33% F1-Score, 76.87% MCC and 76.16% Kappa classification performance. When the proposed method is evaluated clinically, it is predicted that it can support the decision-making process of experts. With this method, it has been proven that the error of misdiagnosis can be reduced, and the test times can be reduced from days.

REFERENCES

Afshar, P., Heidarian, S., Naderkhani, F., Oikonomou, A., Plataniotis, K. N., & Mohammadi, A. (2020). Covid-caps: A capsule network-based framework for identification of covid-19 cases from x-ray images. arXiv preprint arXiv:2004.02696.

Albahri O.S., Zaidan A.A., Albahri A.S.,. Zaidan B.B, Abdulkareem K. H., Al-qaysi Z.T., Alamoodi A.H., Aleesa A.M., Chyad M.A., Alesa R.M., Kem L.C., Lakulu M. M., Ibrahim A.B., Rashid N. A. (2020). Systematic review of artificial intelligence techniques in the detection and classification of COVID-19 medical images in terms of evaluation and benchmarking: Taxonomy analysis, challenges, future solutions and methodological aspects. Journal of Infection and Public Health, 13 (10), 1381-1396.

Barstugan, M., Ozkaya, U., & Ozturk, S. (2020). Coronavirus (covid-19) classification using ct images by machine learning methods. arXiv preprint arXiv:2003.09424.

Elaziz, M. A., Hosny, K. M., Salah, A., Darwish, M. M., Lu, S., & Sahlol, A. T. (2020). New machine learning method for image-based diagnosis of COVID-19. Plos one, 15(6), e0235187.

Fan, D. P., Zhou, T., Ji, G. P., Zhou, Y., Chen, G., Fu, H., ... & Shao, L. (2020). Inf-Net: Automatic COVID-19 Lung Infection Segmentation from CT Images. IEEE Transactions on Medical Imaging.

He, K., Zhang, X., Ren, S., & Sun, J. (2016). Deep residual learning for image recognition. In Proceedings of the IEEE conference on computer vision and pattern recognition (pp. 770-778).

Hemdan, E. E. D., Shouman, M. A., & Karar, M. E. (2020). Covidx-net: A framework of deep learning classifiers to diagnose covid-19 in x-ray images. arXiv preprint arXiv:2003.11055.

Jaiswal, A., Gianchandani, N., Singh, D., Kumar, V., & Kaur, M. (2020). Classification of the COVID-19 infected patients using DenseNet201 based deep transfer learning. Journal of Biomolecular Structure and Dynamics, 1-8.

Mirjalili, S., & Lewis, A. (2016). The whale optimization algorithm. Advances in engineering software, 95, 51-67.

Nour, M., Cömert, Z., & Polat, K. (2020). A novel medical diagnosis model for COVID-19 infection detection based on deep features and Bayesian optimization. Applied Soft Computing, 106580.

Pereira R. M., Bertolini D., Teixeira L. O., Silla C. N., Costa Y. M.G. (2020). COVID-19 identification in chest X-ray images on flat and hierarchical classification scenarios. Computer Methods and Programs in Biomedicine, 194.

Pham, T.D. (2020). A comprehensive study on classification of COVID-19 on computed tomography with pretrained convolutional neural networks. Nature, Sci Rep 10, 16942.

Randhawa, G. S., Soltysiak, M. P., El Roz, H., de Souza, C. P., Hill, K. A., & Kari, L. (2020). Machine learning using intrinsic genomic signatures for rapid classification of novel pathogens: COVID-19 case study. Plos one, 15(4), e0232391.

Sahlol, A. T., Yousri, D., Ewees, A. A., Al-Qaness, M. A., Damasevicius, R., & Abd Elaziz, M. (2020). COVID-19 image classification using deep features and fractional-order marine predators algorithm. Scientific Reports, 10(1), 1-15.

Shi, F., Xia, L., Shan, F., Wu, D., Wei, Y., Yuan, H., ... & Shen, D. (2020). Large-scale screening of covid-19 from community acquired pneumonia using infection size-aware classification. arXiv preprint arXiv:2003.09860.

Simonyan, K., & Zisserman, A. (2014). Very deep convolutional networks for large-scale image recognition. arXiv preprint arXiv:1409.1556.

Singh, D., Kumar, V., Yadav, V., & Kaur, M. (2020). Deep Neural Network-Based Screening Model for COVID-19-Infected Patients Using Chest X-Ray Images. International Journal of Pattern Recognition and Artificial Intelligence, 2151004.

Soares, E., Angelov, P., Biaso, S., Froes, M. H., & Abe, D. K. (2020). SARS-CoV-2 CT-scan dataset: A large dataset of real patients CT scans for SARS-CoV-2 identification. medRxiv.

Sun, L., Mo, Z., Yan, F., Xia, L., Shan, F., Ding, Z., ... & Yuan, H. (2020). Adaptive feature selection guided deep forest for covid-19 classification with chest ct. IEEE Journal of Biomedical and Health Informatics.

Ozturk, T., Talo, M., Yildirim, E. A., Baloglu, U. B., Yildirim, O., & Acharya, U. R. (2020). Automated detection of COVID-19 cases using deep neural networks with X-ray images. Computers in Biology and Medicine, 103792.

Öztürk, Ş., & Özkaya, U. (2020). Gastrointestinal tract classification using improved LSTM based CNN. Multimedia Tools and Applications, 1-16.

Öztürk, Ş., Özkaya, U., & Barstuğan, M. (2020). Classification of Coronavirus (COVID-19) from X-ray and CT images using shrunken features. International Journal of Imaging Systems and Technology.

Ucar, F., & Korkmaz, D. (2020). COVIDiagnosis-Net: Deep Bayes-SqueezeNet based Diagnostic of the Coronavirus Disease 2019 (COVID-19) from X-Ray Images. Medical Hypotheses, 109761.

Vaishya, R., Javaid, M., Khan, I. H., & Haleem, A. (2020). Artificial Intelligence (AI) applications for COVID-19 pandemic. Diabetes & Metabolic Syndrome: Clinical Research & Reviews.

Wang X., Deng X., Fu Q., Zhou Q., Feng J., Ma H., Liu W., and Zheng C. (2020). A Weakly-Supervised Framework for COVID-19 Classification and Lesion Localization From Chest CT. IEEE Transactions on Medical Imaging, 39(8) , 2615-2625.

Wu, Z., Ling, Q., Chen, T., & Giannakis, G. B. (2020). Federated variance-reduced stochastic gradient descent with robustness to byzantine attacks. IEEE Transactions on Signal Processing, 68, 4583-4596.

Zu, Z. Y., Jiang, M. D., Xu, P. P., Chen, W., Ni, Q. Q., Lu, G. M., & Zhang, L. J. (2020). Coronavirus disease 2019 (COVID-19): a perspective from China. Radiology, 200490.

GÖRÜNTÜ İŞLEMEDE NESNE KOORDİNAT ÖZELLİKLERİNİ KULLANARAK BAKLİYAT SAYMA İŞLEMİNE BİR YAKLAŞIM

¹Muhammet Üsame ÖZİÇ iD **, ²Nihat ÇANKAYA** iD **, ³Muciz ÖZCAN** iD **, ⁴Barış GÖKÇE** iD

¹Necmettin Erbakan Üniversitesi, Mühendislik ve Mimarlık Fakültesi, Biyomedikal Mühendisliği Bölümü, Konya, TÜRKİYE
²Necmettin Erbakan, Meram Meslek Yüksekokulu, Gıda İşleme Bölümü, Konya, TÜRKİYE
³Necmettin Erbakan Üniversitesi, Mühendislik ve Mimarlık Fakültesi, Elektrik-Elektronik Mühendisliği Bölümü, Konya, TÜRKİYE
⁴ Necmettin Erbakan Üniversitesi, Mühendislik ve Mimarlık Fakültesi, Mekatronik Mühendisliği Bölümü, Konya, TÜRKİYE

¹ muozic@erbakan.edu.tr, ² ncankaya@erbakan.edu.tr, ³ mozcan@erbakan.edu.tr, ⁴ bgokce@erbakan.edu.tr

ÖZ: Nesne sayma, gıda, medikal, endüstri ve günlük yaşamda farklı görevler için kullanılan bir süreçtir. Bu çalışmada, nesne sayma işleminin gerçekleştirilebilmesi için görüntü işleme tabanlı sistemler incelenmiş ve uygulamalar yapılmıştır. Uygulamalar için nesnelerin bir silo üzerinden akarak serici üzerinden eğimli bir şekilde ilerleyebileceği bir deney düzeneği tasarlanmıştır. Nesnelerin akışını gözlemleyebilecek endüstriyel bir kamera ve lens sistemi kullanılmıştır. Nesnelerin akışını izleyebilmek için sadece arka aydınlatma kullanılmıştır. Nesnelerin akış hızı ve nesnelerin serici çıkışı akabileceği eğim açısı değiştirilebilmektedir. Endüstriyel kamerada fps, piksel frekansı, pozlama süresi, görüntünün çözünürlüğü, ilgilenen alan seçimi, renkli ve renksiz görüntü alımı, görüntüdeki piksellerin kaç bit ile örnekleneceği kullanıcı tarafından seçilebilmektedir. Algoritma tasarımı için Python yazılımı ve OpenCV kütüphanesi kullanılmıştır. Nesne sayımı için 100 adet nohut tanesi belirlenmiş ve belirli bir süre kameradan video kaydı elde edilmiştir. Video üzerinde arka plan çıkarma işlemi uygulanarak sadece nesnelerin beyaz renk olarak görülebileceği ikinci bir video elde edilmiştir. Binary formata dönüştürülen videoda nesne çevresi sınırlayıcı en küçük dikdörtgen koordinat değerleri ve nesne ağırlık merkezi koordinat değerleri elde edilmiştir. Video görüntüsü üzerinde sabit tek ve çift sanal çizgiler çekilerek sayma işleminin gerçekleştirileceği metotlar geliştirilmiştir. Koordinat değerlerinin ve sanal çizgilerin sayma işlemi için kullanılmasında ortaya çıkan avantaj ve dezavantajlar bu çalışma sonucunda tartışılmıştır.

Anahtar Kelimeler: *Nesne Sayma, Görüntü İşleme, Kamera, Python, OpenCV*

An Approach to Counting Legumes Using Coordinate Features in Image Processing

ABSTRACT: Object counting is a process used for different tasks in food, medical, industry and daily life. In this study, image processing-based systems have been examined and applications have been made to perform the object counting process. For the applications, an experimental setup has been designed in which the objects can flow over a silo and proceed in an inclined manner over the spreader. An industrial camera and lens system that can observe the flow of objects were used. Only backlighting was used to monitor the flow of objects. The flow rate of objects and the angle of inclination through which objects can flow out of the spreader can be changed. In the industrial camera, fps, pixel frequency, exposure time, image resolution, area of interest selection, color and mono image acquisition, how many bits the pixels in the image will be sampled can be selected by the user. Python software and OpenCV library were used for

algorithm design. For the object counting, 100 chickpea seeds were determined and the video was recorded from the camera for a certain period of time. By applying a background subtraction process on the video, a second video was obtained in which only the objects can be seen as white. The smallest rectangular coordinate values bounding the object and the object centroid coordinate values were obtained in the video converted into binary format. Methods have been developed for counting by drawing single and double virtual lines in the video. The advantages and disadvantages of using coordinate values and virtual lines for counting have been discussed as a result of this study.

Key Words: *Object Counting, Image Processing, Camera, Python, OpenCV*

GİRİŞ (INTRODUCTION)

Görüntü sensörleri ile nesne sayma süreçleri, endüstri, gıda, medikal, güvenlik gibi geniş bir sektörde kullanımına ihtiyaç duyulan teknolojilerdir. Nesne sayısının küçük ve çok fazla olması, nesnelerin aynı anda hareketli olması manuel bir şekilde insan gücüne bağlı olan sayma işlemlerini oldukça zorlaştırmaktadır. İnsan gözünün bir video görüntüsünden çoklu nesne takibini kaçırabilmesi, bir bant üzerinden veya serbest düşme ile akan nesnelerin hızını yakalayamaması sayma işlemini zorlaştırmakta, süre problemini ortaya çıkarmakta ve hata yapmaya açık süreçlerin ortaya çıkmasına neden olmaktadır. Bundan dolayı görüntü sensörlerini kullanan endüstriyel kamera teknolojilerinin yapay görü, makine öğrenmesi, yapay zekâ, görüntü işleme ve gerçek zamanlı hızlı işlemler yapabilen donanımlar ile beraber entegre bir şekilde kullanılmasına dönük birleşik sistemler son zamanlarda endüstride talep gören teknolojilerdir. Görüntü sensörlerinin ucuzlaması ve görüntü işleme cihazlarının makul düzeylerde olması, ürün sayma çözümlerini kolay ulaşılabilir hale getirmiştir. Hazır olarak kullanılan var-yok sensörler yerine daha karmaşık nesnelerin veya ürünlerin sayılması için görüntü sensörleri tercih edilmektedir. Sayım ve ölçüm için uzman kontrolünün gerektiği durumlarda tamamen temassız çözümler geliştirilebilmektedir. Otomobil yedek parçaları, çuvallar, tohumlar, ilaçlar, bitkiler, meyveler, sebzeler, hırdavat parçaları, küçük boyutlu oyuncaklar gibi ticari değeri olan birçok endüstriyel ürün için özel çözümler gerçekleştirilebilmektedir. Sadece endüstriyel ürünler değil aynı zamanda özel kurum ve kuruluşların giriş çıkışlarının denetimi, kamu kurumlarının giriş çıkışlarının denetimi, mağazalar ve alışveriş merkezleri, güvenlik amaçlı sayma, trafik yoğunluğu, otopark doluluğu gibi sivil hayatta karşılık bulan kullanımları giderek artmaktadır (Barbedo, 2012; Raman ve Sukanya, 2012; Perera ve diğ., 2013; Thammasorn ve diğ., 2013; Pandit ve diğ., 2014; Baygin ve diğ., 2018). Alan taramalı kameralar ile yapılan sayma işlemlerinde, nesnenin kadraja girip çıktığı ana kadar kendine ait benzersiz bir kimliğe sahip olması gerekmektedir. Videoda nesne sürekli hareket halinde olduğu için hız, birbirine yapışık veya üst üste binmiş nesneler, kameranın çekim parametre ayarları, aydınlatma yöntemi gibi birçok faktör nesne sayma işlemini zorlaştırmaktadır. Bundan dolayı nesneye özel uygulama düzeneğinin geliştirilmesi görüntü işleme algoritma performansını etkileyecek en önemli etkendir. Nesne sayma metotları nesne algılama ve sayma, yörünge kümeleme ile sayma, global regresyon ile sayma ve nesne yoğunluk tahminine dayalı sayma olmak üzere genel olarak dört başlık atında toplanmaktadır. Nesne algılama ve temel eşik kuralına göre sayma en sık kullanılan yöntemlerden biridir. Bu yöntemin en önemli avantajı çok hızlı sayma gerçekleştirmesidir, dezavantajı ise birden fazla nesnenin birbirine yaklaşması durumunda sayım performansının düşmesidir (Lin ve diğ., 2010; Wang ve Wang, 2011; Arteta ve diğ., 2012). Yörünge kümeleme tekniği kullanılarak yapılan sayma işleminde ise kalabalık olan hareketli nesneler sayılır (Antonini ve diğ., 2006; Rabaud ve Belongie, 2006). Bu yöntem yalnızca istenilen yörüngeler doğrultusunda nesneleri izlemek için uygulanır. Bu yöntemin en önemli dezavantajlarından bir tanesi ise yüksek hesaplama maliyetine ihtiyaç duymasıdır. Bu sebeple bu yöntemin düşük maliyetli bir çözüm olarak sunulması mümkün değildir. Ayrıca global regresyon yöntemi ile yapılan sayma işleminde hızlı eğitim ve test prosedürleri kullanıldığından tahminlerde iyi bir sonuç vermektedir. Bununla birlikte tüm görüntü boyunca tahmin yapılacak nesne sayısı, yoğunluk haritasının integrali olarak hesaplanır. Bu yöntem diğer yöntemlerden farklı olarak görüntü boyunca nesne dağılımının analizi

için nesnenin yoğunluk haritasını verir (Chan ve diğ., 2008; Ryan ve diğ., 2009; Chan ve Vasconcelos, 2011; Chen ve diğ., 2013). Son dönemlerde popüler yöntemlerden biri olan derin öğrenme yöntemleri de sayma işlemleri için kullanılmaya başlanmıştır. Ancak derin öğrenme yöntemlerinin hesapsal maliyetleri oldukça fazladır (Zhang ve diğ., 2015; Onoro-Rubio ve López-Sastre, 2016; Zhang ve diğ., 2016). Görüntü işlemede nesne sayma için derin öğrenme yaklaşımı aslında tek yönlü bir regresyondur. Bu ağlar, olası çıktı birimlerinin sayısının eğitim verilerine dayalı olarak önceden tanımlanmış bir sınıflandırma mimarisini benimser (Öztürk ve Özkaya, 2020). Bunun yanında sayılacak nesnenin toplam sayısına mümkün olduğunca yakın gerçek bir değer üreten tek bir çıktı birimine sahiptir (Aich ve Stavness, 2017; Aich ve diğ., 2018). Her iki durum da yüksek boyutlu doğrusal olmayan regresyon modelleri kategorisi altında sınıflandırılabilir. Burada dikkat edilmesi gereken tahmin edicilerin sayısı giriş piksellerinin sayısı ile orantılıdır. Son dönemlerde derin öğrenme kütüphanelerinin versiyon güncellemeleri ile beraber Tensorflow ve YOLO kütüphanelerinin nesne sayma API'leri (Application Programming Interface) pratik kullanımlar sunmaktadır (Mazurek, 2020; Özlü, 2020). Bu çalışmada, tasarlanan bir deney düzeneği ile sabit bir bant üzerinde ilerleyen 100 adet nohut tanesinin videosu elde edilmiş ve nesnelerin sayma işlemi yapılmıştır. Uygun video çekimi için kamera parametreleri optimum şekilde ayarlamış ve nesne arkasından aydınlatma işlemi yapılmıştır. Video görüntülerinde arka plan çıkarma işlemi yapılarak nohut taneleri ön plana çıkarılmıştır. Binary formata dönüştürülen videoda nesnelerin çevresini sınırlayan en küçük dikdörtgenin koordinat değerleri ve nesnenin ağırlık merkezi koordinat değerleri elde edilmiştir. Video görüntüsü üzerinde çizilen tek ve iki sanal çizgi referansı ile nesne koordinat değerlerinin çizilen sanal çizgilerden geçip geçmediği tespit edilerek sayma işlemi gerçekleştirilmiştir. Kullanılan yöntemlerin sayma problemi için avantaj ve dezavantajları tartışılmıştır.

MATERYAL VE METOT (MATERIAL AND METHOD)

Deney Düzeneği (Experimental Setup)

Hareketli nesne görüntüsünün alınması için, nesnelerin silo içerisinden serici üzerine düştüğü ve sabit eğimli bir bant üzerinde ilerlediği bir düzenek tasarlanmıştır. Serici hızı ve bandın eğimi kullanıcı tarafından ayarlanabilmektedir. Deney düzeneğinde IDS marka (UI-3290SE-HQ) renkli bir endüstriyel kamera ve AZURE marka bir lens sistemi (35mm) kullanılmıştır. Aynı zamanda gelecek çalışmalar için küçük nesne ölçümlerinin yapılabileceği telesentrik bir lens temin edilmiştir. Bu kameranın çalışma için seçilme nedeni, üreticinin bu modeller için Python desteği sunması ve gelecek çalışmalarda GPU denemeleri için NVIDIA Jetson kartları desteklemesidir. IDS firması kamera kullanımı için bir arayüz (cockpit) sunmakta ve kameranın birçok parametresi buradan değiştirilebilmektedir. Çözünürlük, fps, piksel frekansı, pozlama süresi, kazanç, gama faktörü, gain faktörü, renk örnekleme bit seviyesi gibi video çekimini etkileyecek birçok parametre değiştirilebilmektedir. Bu parametreler üretici firmanın sunmuş olduğu Python kütüphanesi fonksiyonları ile gerçek zamanlı geliştirilebilecek yazılım içerisinden de kontrol edilebilmektedir. Nesnelerin sadece tane sayısı hesaplandığı, renk veya çürük gibi özellikler ile ilgilenilmediği için arka plan aydınlatma kullanılmıştır. Düzeneğin etrafı siyah bir naylon ile kaplanarak diğer ışık kaynaklarından etkilenmesi engellenmiştir. Şekil 1a'da deney düzeneği, Şekil 1b'de arka plan aydınlatma, Şekil 1c'de kamera ve lens çeşitleri verilmiştir.

Şekil 1. (a) Deney Düzeneği (b) Arka plan aydınlatma (c) Kamera ve lens çeşitleri
Figure 1. (a) Experimental Setup (b) Background illumination (c) Camera and lens types

Nesneler sericiden gelerek sabit eğimli bir bant üzerinden aktıkları için hızlı ilerlemektedir. Bundan dolayı pozlama süresi (exposure time) olabildiğince kısa tutulmuştur. Diğer parametreler kamera üretici firmanın sunmuş olduğu arayüz üzerinden manuel bir şekilde ayarlanmış ve yine arayüz üzerinden kullanıcıya sunulmuş olan video kayıt sistemi ile kayıt işlemi yapılmıştır. Çizelge 1'de çalışma için kullanılan kamera parametreleri verilmiştir.

Çizelge 1. Video kaydı için kamera parametreleri
Table 1. Camera parameters for video recording

Kamera Parametreleri	
FPS	46.14 kare/saniye
Pozlama süresi	1.410 ms
Piksel Frekansı (Pixel Clock)	395 MHz
Gain Faktörü	20
Gamma Faktörü	1.6
Renk Seviyesi	RGB32 (B8 G8 R8)
Toplam görüntü kare sayısı	2399
Görüntü boyutu	1144x774 (binning 2x)

GÖRÜNTÜ İŞLEME (IMAGE PROCESSING)

Segmentasyon (Segmentation)

Videoda ilerleyen hareketli nesnelerin koordinat özelliklerinin bulunabilmesi için nesnelerin arka plandan ayrılarak binary formata dönüştürülmesi gerekmektedir. Bu işlem için çalışmada basit bir eşik değeri, otsu eşikleme metodu, adaptif gaussian eşikleme (adaptive gaussian thresholding) ve adaptif ortalamalar eşikleme (adaptive means thresholding) algoritmaları denenmiş ancak yeterli performans alınamamıştır (OpenCV, 2020a). Özellikle basit ve otsu eşikleme yöntemlerinde deney düzeneğindeki arka plan aydınlatma platformunun ışık homojensizliğinden kaynaklı olarak yetersiz segmentasyon işlemi ortaya çıkmıştır. Adaptif gaussian eşikleme ve adaptif ortalamalar eşikleme algoritmaları ışık homojensizliğinden diğer eşikleme yöntemleri kadar etkilenmese de görüntüde çok fazla gürültü ortaya

çıkmaktadır. Bir diğer segmentasyon yöntemi ise OpenCV kütüphanesinin sunmuş olduğu video görüntülerinde hareketli nesne arka plan çıkarıcılardır (OpenCV, 2020b). Çalışmada gaussian karışım modelini kullanan MOG2 metodu arka plan çıkarma için kullanılmıştır. Bu yöntem kullanılarak sadece hareketli nesneler ortaya çıkarılmakta, böylece ışık homojensizliğinden kaynaklı problemlerden algoritma etkilenmemektedir. Hareketli nesne kenarlarının bazı bölgelerinde farklı gri tonlar ortaya çıktığı için basit bir eşikleme ile görüntü binary formata dönüştürülmüştür. Segmente edilmiş video görüntüsü üzerindeki ufak gürültü parçacıklarının bir nesne gibi işlem görmemesi için iki iterasyonluk erozyon işlemi uygulanmıştır. Şekil 2a'da video kaydından 1563. görüntü karesi, Şekil 2b'de MOG2 arka plan çıkarma işlemi, Şekil 2c'de adaptif ortalamalar eşikleme, Şekil 2d'de adaptif gaussian eşikleme Şekil 2e'de basit eşik değeri, Şekil 2f'de otsu eşikleme sonuçları 1563. görüntü karesi üzerinden verilmiştir.

(a)   (b)

(c)   (d)

(e)   (f)
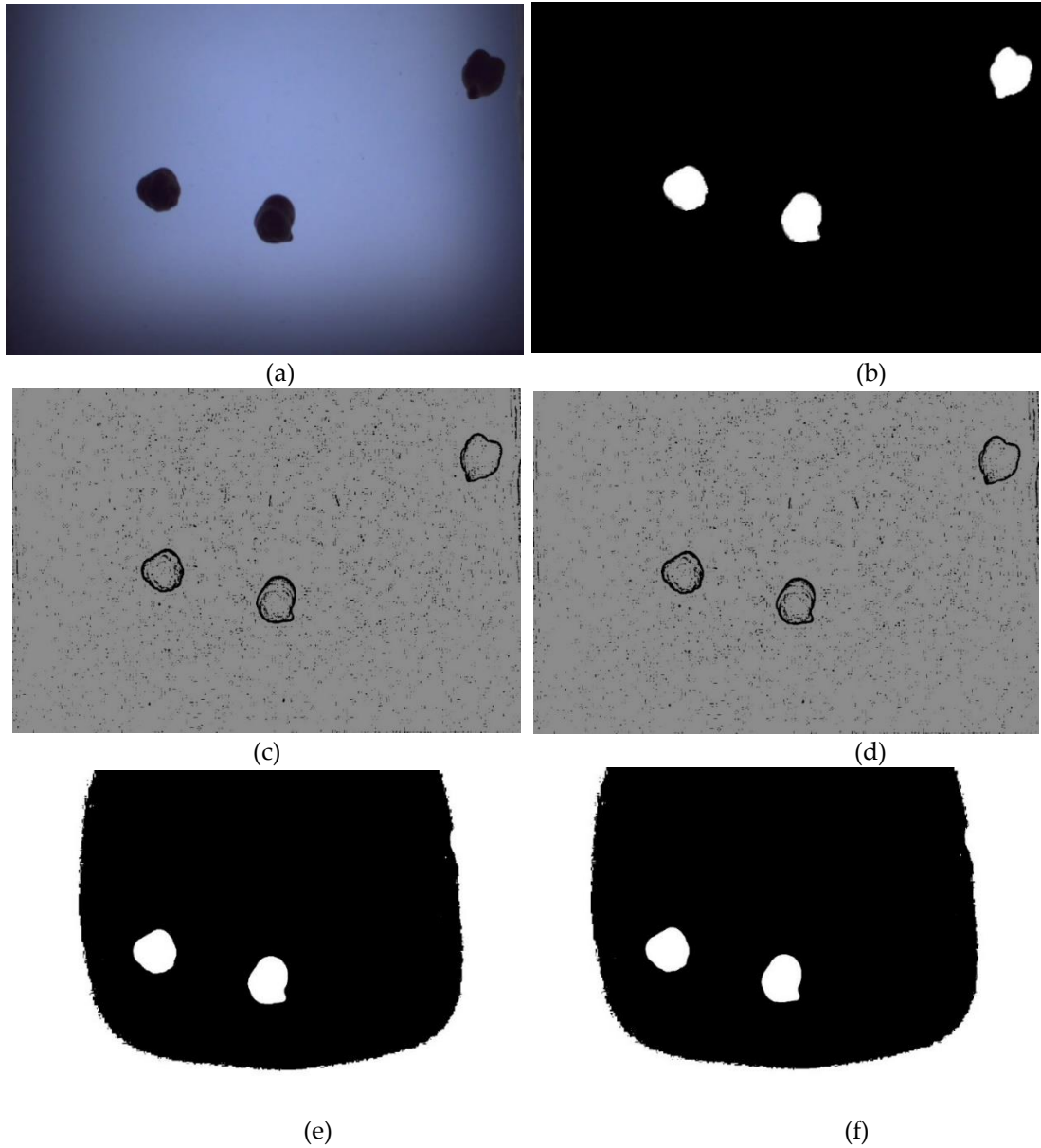
Şekil 2. (a) Video 1563. görüntü karesi (b) MOG2 arka plan çıkarıcı (c) Adaptif ortalamalar eşikleme (d) Adaptif gaussian eşikleme (e) Basit eşikleme (f) Otsu eşikleme
Figure 2. (a) Video 1563. frame (b) MOG2 background subtractor (c) Adaptive means thresholding (d) Adaptive gaussian thresholding (e) Simple thresholding (f) Otsu thresholding

Koordinat Noktaları (Coordinate Points)

Videodaki hareketli nesnelerin ağırlık merkezi koordinatları (centroid) ve en küçük dikdörtgen içine sığabilecek kutu koordinatları (bounding box) sayma işlemi için referans olarak kullanılacaktır. Binary formata dönüştürülen görüntülerde OpenCV'nin kontur (contours) metodu ile özellikler elde edilerek ilgili koordinat noktaları elde edilmiştir (OpenCV, 2020c). OpenCV'nin dikdörtgen sınırlayıcı metodu ile (BoundingRect) nesnelerin en küçük dikdörtgen kutuya sınırlayıcı koordinatları olan (x, y, w, h) noktaları her bir görüntü karesinde tek tek bulunmuştur (OpenCV, 2020d). (x,y) noktası nesneyi sınırlayan dikdörtgenin sol üst köşesini göstermektedir. Nesnelerin ağırlık merkezi koordinatları kontur özelliklerinin momentleri bulunarak hesaplanmaktadır. Momentlerden m10, m00, m01 çıktıları kullanılarak ağırlık merkezi (x1,y1) noktaları bulunmuştur (OpenCV, 2020d). Şekil 3a'da nesnelerin sınırlayıcı kutu içine alınması ve (x,y) sol üst köşe koordinat değerleri, Şekil 3b'de ağırlık merkezi ve (x1,y1) koordinat değerleri gösterilmektedir.

(a)   (b)
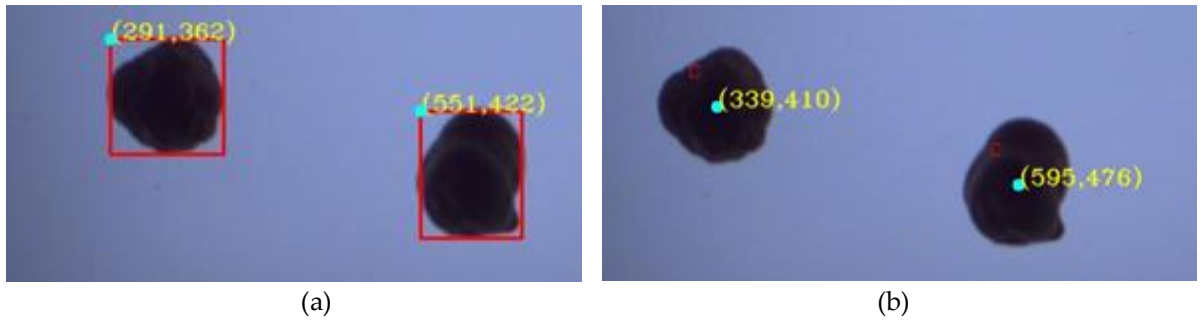
Şekil 3. (a) Nesnenin en küçük dikdörtgene sığdırılması ve (x,y) sol üst köşe koordinatları (b) Nesnelerin ağırlık merkezi (x1, y1) koordinat noktaları

Figure 3. (a) Fitting the object to the smallest rectangle and (x, y) upper left corner coordinates (b) The centroid of objects (x1, y1) coordinate points

Sayma İşlemi (Counting Process)

Çalışmada, video görüntüleri üzerine tek ve iki sanal çizgi çizilmiş, koordinat noktaları referans alınarak geliştirilen metotlar ile sayma performansları ölçülmüştür. İlk olarak video görüntülerinin y=300 ve y=410 noktalarından x ekseni boyunca sanal çizgiler çizilmiştir. Ağırlık merkezi ve sınırlayıcı dikdörtgen y koordinat değeri iki çizgi arasından geçince sayaç değeri bir arttırılmıştır. İki sanal çizgi arasından geçen nesneler ya fazla ya da az sayma işlemi yapmaktadır. Şekil 4a'da iki sanal çizgi arasından geçen sınırlayıcı dikdörtgen koordinat değerlerinin 1563. görüntü karesinden geçişi, Şekil 4b'de iki sanal çizgi arasından geçen ağırlık merkezi koordinat değerlerinin 1563. görüntü karesinden geçişi verilmektedir. İkinci yöntem olarak y=300 noktasından x ekseni boyunca tek bir sanal çizgi çekilmiştir. Tek sanal çizgi ile nesne saymada, nesnelerin çizgiye girmeden önce ve girdikten sonraki görüntü karesinden aynı nesne olup olmadığını kontrol eden bir metot uygulanmıştır. Bir görüntü karesinde bulunan nesnelerin x,y ve x1,y1 koordinat değerlerinin, bir sonraki görüntü karesindeki nesnelerin x,y koordinat değerlerine uzaklıkları x = x(t)-x(t-1), y=y(t)-y(t-1) eşitlikleri ile hesaplanarak eksenlerdeki tüm nesne yer değiştirmeleri belirlenmektedir. Nesnenin hareketinden kaynaklı yer değiştirme uzaklığı $x^2 + y^2$ eşitliği ile hesaplanmaktadır. Bu işlemden sonra yer değiştirme uzaklığı daha yakın olan nesne bir önceki ve bir sonraki görüntü karesindeki aynı nesne olarak işaretlenmektedir. Böylece nesne kadrajdan girip çıktığı ana kadar uzaklık ölçütüne göre takip edilebilmektedir. Bu hesaplamalar yapılırken nesne koordinatının y=300 sanal çizgisinden geçip geçmediği kontrol edilmekte, geçtiği anda sayaç bir defa arttırılmakta ve aynı nesne için tek bir sayım işlemi yapılmaktadır. Şekil 4c'de tek sanal çizgi arasından geçen sınırlayıcı dikdörtgen koordinat değerlerinin 1563. görüntü karesinden geçişi, Şekil 4d'de tek sanal çizgi arasından geçen ağırlık merkezi koordinat değerlerinin 1563. görüntü karesinden geçişi verilmektedir.
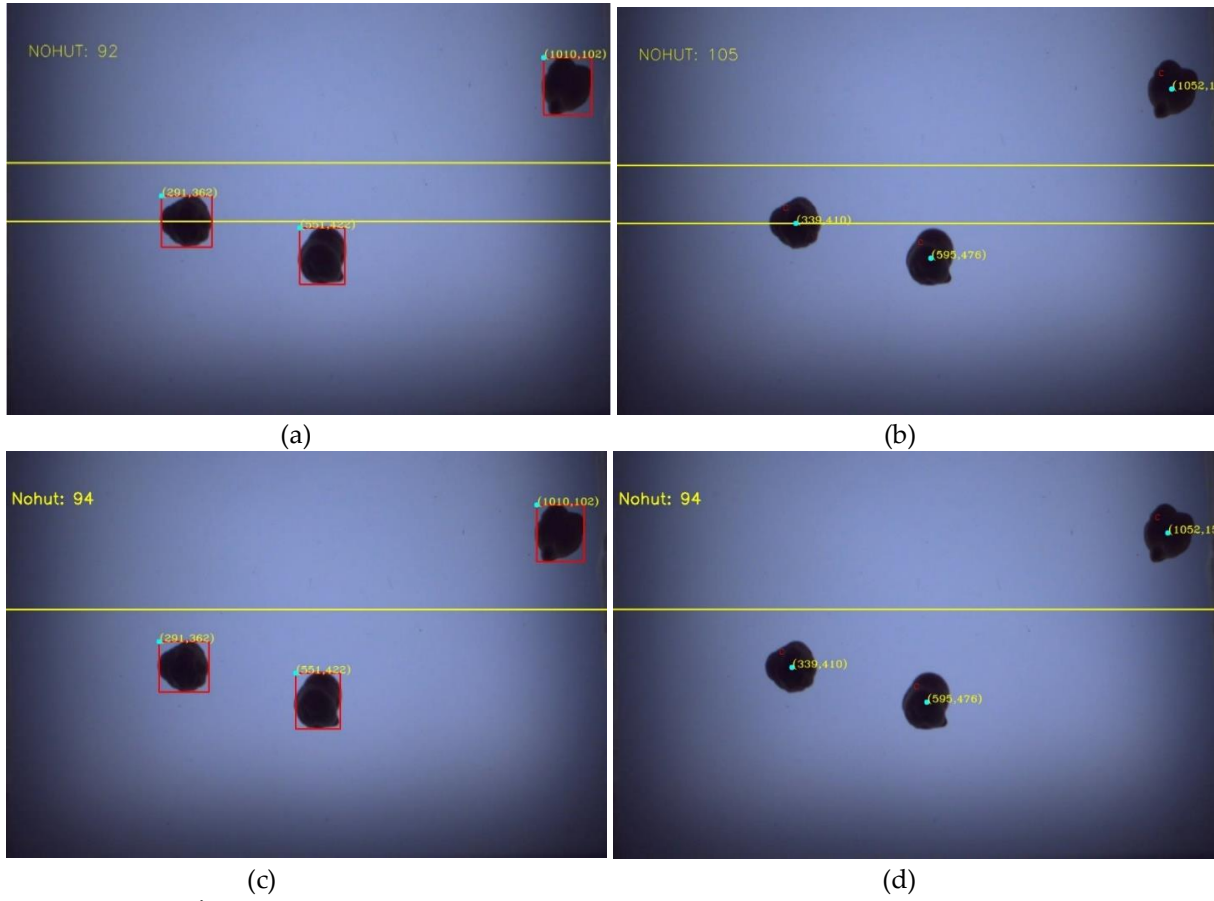
Şekil 4. (a) İki sanal çizgi arasından sınırlayıcı dikdörtgen koordinat değerlerinin geçmesi ve sayma işlemi (b) İki sanal çizgi arasından ağırlık merkez koordinatlarının geçmesi ve sayma işlemi (c) Tek sanal çizgi üzerinden sınırlayıcı dikdörtgen koordinat değerlerinin geçmesi ve sayma işlemi (d) Tek sanal çizgi üzerinden ağırlık merkez koordinatlarının geçmesi ve sayma işlemi

Figure 4. (a) Bounding rectangular coordinate values passing between two virtual lines and counting process (b) Centroid coordinates passing between two virtual lines and counting process (c) Bounding rectangular coordinate values passing over single virtual line and counting process (d) Centroid coordinates passing over single virtual line and counting process

SONUÇ ve TARTIŞMALAR (RESULTS and DISCUSSIONS)

Bu çalışmada, kamera sistemi ve bir deney düzeneği kullanılarak kaydedilen video görüntüsünden hareketli nohut tanelerinin saydırılması işlemi gerçekleştirilmiştir. Videoda segmentasyon işlemi ile nesneler ön plana getirilmiş ve arka plan videodan atılmıştır. Klasik segmentasyon algoritmaları ve eşikleme metotları ile başarılı sonuçlar elde edilememiştir. Bunun nedeni arka plan aydınlatmanın homojen olmamasından kaynaklı heterojen piksel intensite dağılımıdır. Videodan arka plan çıkarma işlemi OpenCV kütüphanesinin sunmuş olduğu MOG2 metodu ile gerçekleştirilmiştir. Daha sonra eşikleme işlemi yapılarak akan nesnelerin binary olarak elde edildiği görüntü kareleri elde edilmiştir. Yapılan karşılaştırmalar sonucunda OpenCV'nin sunmuş arka plan çıkarıcılar videoda arka planı atmak ve istenen nesneyi ön plana getirmek için klasik görüntü segmentasyon algoritmalarına göre kullanışlı sonuçlar verdiği belirlenmiştir. Arka plan çıkarıcılar görüntü üzerindeki piksel intensite dağılımı yerine sadece görüntü kareleri arasında değişen piksel değerlerine odaklandığı için daha yüksek doğrulukta sonuçlar vermektedir. Binary formata dönüştürülmüş video üzerindeki nesnelerin en küçük dikdörtgen içine sığdığı koordinatlar ve nesnenin ağırlık merkezi koordinatları OpenCV'nin moment ve kontur metodu ile elde edilmiştir. Bu koordinatlar nesne hareket ettiği sürece her bir görüntü karesinde tek tek hesaplanmaktadır. Burada temel problem nesne kadraja girdiği andan çıktığı ana kadar benzersiz bir kimliği olması gerekliliğidir. Aksi takdirde nesne her bir görüntü karesinde tekrar tekrar saydırılır. Bu

çalışmada elde edilen koordinat değerlerinin ilerleyişi iki farklı sanal çizgi yaklaşımı ile değerlendirilmiş ve sayma performansları ölçülmüştür. İki sanal çizgi arasından ilgili nesne koordinatları geçtiğinde tekrar sayma, fazla sayma ve az sayma gibi problemler ile karşılaşılmıştır. Bunun sebebi iki sanal çizgi arasında nesnenin görüntü karesindeki ilerleme hızına bağlı olarak tekrar görülmesi ya da çok hızlı geçmesidir. Bundan dolayı geliştirilen yazılım fazla veya eksik saymaktadır. İki sanal çizgi arasından nesnelerin sayılması işleminde nesne üzerinde hakimiyet kurulamamaktadır. Tek çizgi ile yapılan çalışmada nesnelerin bir önceki ve bir sonraki görüntü kareleri arasında koordinat değerlerine göre uzaklık değerlerinin bulunması, uzaklık değerine göre çizgiden geçip geçmediğinin kontrol edilmesi %100 sayma sonucu vermiştir. Şekil 5a'da iki sanal çizgi arasından geçen sınırlayıcı dikdörtgen koordinat değerlerine göre son nesne sayma işlemi, Şekil 5b'de iki sanal çizgi arasından geçen ağırlık merkezi koordinat değerlerine göre son nesne sayma işlemi, Şekil 5c'de tek sanal çizgi üzerinden geçen sınırlayıcı dikdörtgen koordinat değerlerine göre son nesne sayma işlemi, Şekil 5d'de tek sanal çizgi üzerinden geçen ağırlık merkezi koordinat değerlerine göre son nesne sayma işlemi verilmiştir.
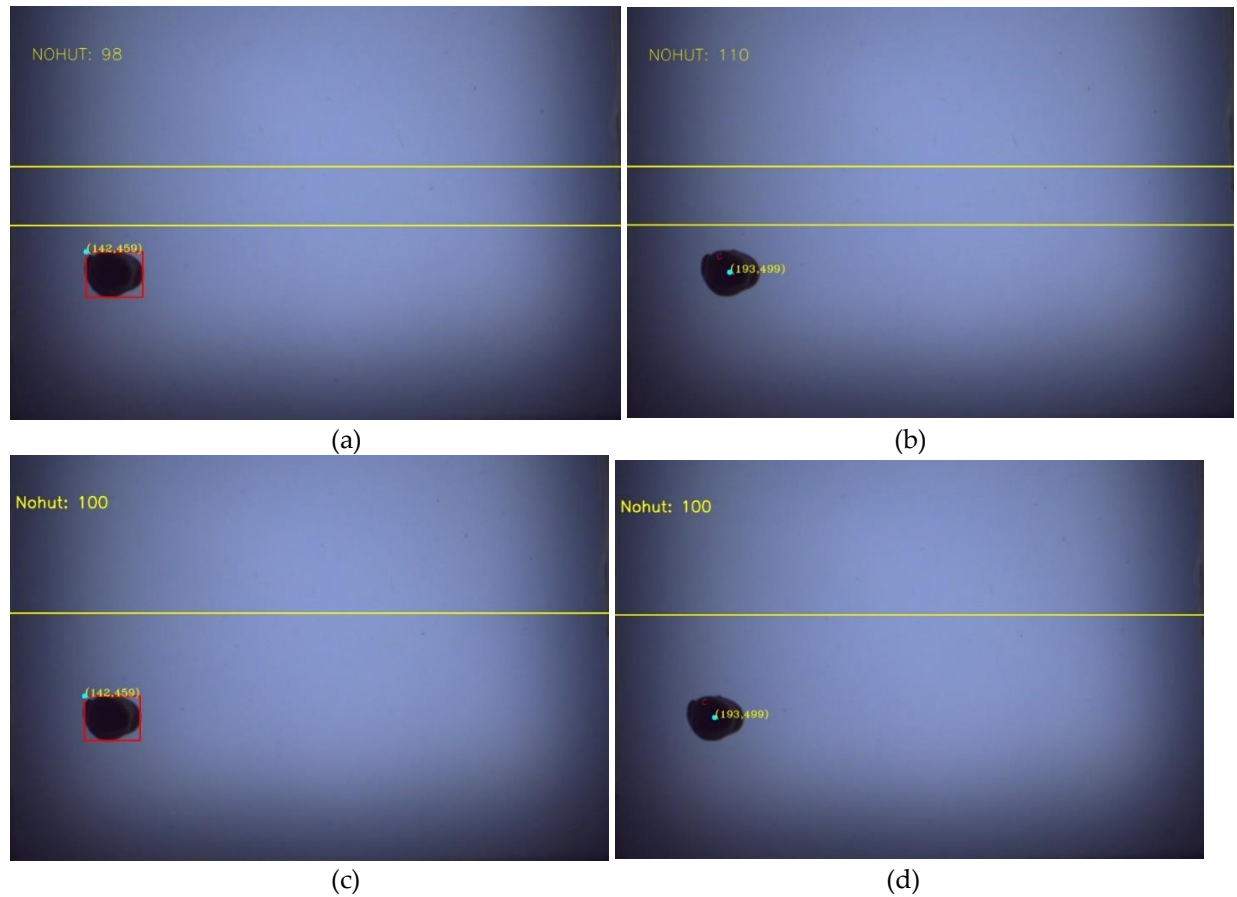

Şekil 5. (a) İki sanal çizgi arasından geçen sınırlayıcı dikdörtgen koordinat değerlerine göre son nesne sayma işlemi (b) İki sanal çizgi arasından geçen ağırlık merkezi koordinat değerlerine göre son nesne sayma işlemi (c) Tek sanal çizgi üzerinden geçen sınırlayıcı dikdörtgen koordinat değerlerine göre son nesne sayma işlemi (d) Tek sanal çizgi üzerinden geçen ağırlık merkezi koordinat değerlerine göre son nesne sayma işlemi

Figure 5. (a) The process of counting the last object with respect to the bounding rectangular coordinate values passing between the two virtual lines (b) The process of counting the last object with respect to the centroid coordinate values passing between the two virtual lines (c) The process of counting the last object with respect to the bounding rectangular coordinate values passing over the single virtual line (d) The process of counting the last object with respect to the centroid coordinate values passing over a single virtual line

Nesne sayma çözümleri hem zaman açısından hem de insan gücü bakımından maliyetleri azalttığı için tercih edilen endüstriyel uygulamalardır. Boyut olarak küçük, adet bakımından çok fazla olan ürünlerin sayılması ve paketlenmesi için kamera ve görüntü işleme tabanlı sistemler pratik kullanımlar sunmaktadır. Ancak ürün boyutunun çok küçük olması, malzemenin kamera önünden çok hızlı geçmesi, pozlama süresi, çözünürlük, fps oranı, malzemelerin ilerlerken üst üste binmesi veya yapışık ilerlemesi, nesne kadraja girip çıkıncaya kadar tek bir kimliğe sahip olması gerekliliği, segmentasyon, aydınlatma gibi birçok problemi beraberinde getirmektedir. Birçok farklı parametrenin görüntü işleme algoritma performansını doğrudan etkilediği bu durumlarda sadece ilgilenen nesneye özel bir uygulama tasarlanması veya nesneye göre adaptif bir sistem tasarlanması zorunluluğu ortaya çıkmaktadır. Bu çalışmada, hareketli nesnelerin video görüntüleri kaydedilerek sayma işlemi gerçekleştirilmiş, ileri uygulamalar için bir ön çalışma yapılmıştır. Önerilen iki farklı koordinat noktasına ve uzaklık ölçme kriterine göre tek bir sanal çizgi kullanılarak %100 sayma işlemi gerçekleştirilmiştir. Gelecek çalışmalarda serici hızı ve banttan ilerleyen nesne sayısı arttırılarak gerçek zamanlı çözümler gerçekleştirilecektir. Tensorflow ve YOLO gibi derin öğrenme kütüphanelerinde bulunan nesne sayma ve nesne tespiti API'leri kullanılarak uygulama geliştirilmesi ve bu uygulamaların hızlı sonuç vermesi için GPU teknolojisi kullanan NVIDIA Jetson kartlarında yazılımın koşturulması hedeflenmektedir.

KATKI BELİRTME (ACKOWLEDGEMENT)

KAYNAKLAR (REFERENCES)

Aich, S., Stavness, I., "Leaf counting with deep convolutional and deconvolutional networks", *Proceedings of the IEEE International Conference on Computer Vision Workshops*, Venice, Italy, 2080-2089, 22-29 Oct. 2017.

Aich, S., Josuttes, A., Ovsyannikov, I., Strueby, K., Ahmed, I., Duddu, H. S., Pozniak, C., Shirtliffe, S., Stavness, I., "Deepwheat: Estimating phenotypic traits from crop images with deep learning", *IEEE Winter Conference on Applications of Computer Vision (WACV)*, Lake Tahoe, NV, USA, 323-332, 12-15 March 2018.

Antonini, G., Thiran, J.-P. J. I. T. o. C., Technology, S. f. V., 2006, "Counting pedestrians in video sequences using trajectory clustering", *IEEE Transactions on Circuits and Systems for Video Technology*, Vol. 16, No. 8, pp. 1008-1020.

Arteta, C., Lempitsky, V., Noble, J. A., Zisserman, A., "Learning to detect cells using non-overlapping extremal regions", *International Conference on Medical Image Computing and Computer-Assisted Intervention*, Berlin, Heidelberg, 348-356, 2012.

Barbedo, J. G. A., "Counting clustered soybean seeds", *2012 12th International Conference on Computational Science and Its Applications*, Salvador, Brazil, 142-145, 2012.

Baygin, M., Karakose, M., Sarimaden, A., Akin, E. J. a. p. a., 2018, "An image processing based object counting approach for machine vision application", *arXiv preprint* arXiv:1802.05911.

Chan, A. B., Liang, Z.-S. J., Vasconcelos, N., "Privacy preserving crowd monitoring: Counting people without people models or tracking", *IEEE Conference on Computer Vision and Pattern Recognition*, Anchorage, AK, USA, 1-7, 2008.

Chan, A. B., Vasconcelos, N. J. I. T. o. I. P., 2011, "Counting people with low-level features and Bayesian regression", *IEEE Transactions on Image Processing* , Vol. 21, No. 4, pp. 2160-2177.

Chen, K., Gong, S., Xiang, T., Change Loy, C., "Cumulative attribute space for age and crowd density estimation", *Proceedings of the IEEE conference on computer vision and pattern recognition*, Portland, OR, USA, 2467-2474, 2013.

Lin, Z., Davis, L. S. J. I. T. o. P. A., Intelligence, M., 2010, "Shape-based human detection and segmentation via hierarchical part-template matching", *IEEE Transactions on Pattern Analysis and Machine Intelligence*, Vol. 32, No. 4, pp. 604-618.

Mazurek, P., YOLO-Object-Counting-API, https://github.com/tugot17/YOLO-Object-Counting-API, Ziyaret Tarihi: 28.09.2020

Onoro-Rubio, D., López-Sastre, R. J.,"Towards perspective-free object counting with deep learning", *European Conference on Computer Vision*, Amsterdam, Netherlands, 615-629, 11-14 October, 2016.

OpenCV, 2020a, Image Thresholding, https://docs.opencv.org/3.4/d7/d4d/tutorial_py_thresholding.html, Ziyaret Tarihi: 28.09.2020.

OpenCV, 2020b, Motion Analysis, https://docs.opencv.org/master/de/de1/group__video__motion.html, Ziyaret Tarihi: 28.09.2020.

OpenCV, 2020c, Contours : Getting Started, https://docs.opencv.org/master/d4/d73/tutorial_py_contours_begin.html, Ziyaret Tarihi: 28.09.2020.

OpenCV, 2020d, Structural Analysis and Shape Descriptors, https://docs.opencv.org/3.4/d3/dc0/group__imgproc__shape.html#ga103fcbda2f540f3ef1c042d6a9b35ac7, Ziyaret Tarihi: 28.09.2020.

Özlü, A., 2020, Tensorflow Object Counting API, https://github.com/ahmetozlu/tensorflow_object_counting_api, Ziyaret Tarihi: 28.09.2020.

Öztürk, Ş., Özkaya, U., 2020, "Skin Lesion Segmentation with Improved Convolutional Neural Network", *Journal of Digital Imaging*.

Pandit, A., Rangole, J., Shastri, R., Deosarkar, S., "Vision system for automatic counting of silkworm eggs", *International Conference on Information Communication and Embedded Systems (ICICES2014)*, 1-5, Chennai, India, 2014.

Perera, P., Fernando, W., Herath, H., Godaliyadda, G., Ekanayake, M., Wijayakulasooriya, J.,"A generic object counting algorithm under partial occlusion conditions", *IEEE 8th International Conference on Industrial and Information Systems*, Peradeniya, Sri Lanka, 554-559, 17-20 Dec. 2013.

Rabaud, V., Belongie, S., "Counting crowded moving objects", *IEEE Computer Society Conference on Computer Vision and Pattern Recognition (CVPR'06)*, New York, NY, USA , 705-711, 17-22 June 2006.

Raman, M. S., Sukanya, M., 2012, "A novel labelling algorithm for object counting", *2012 Third International Conference on Computing, Communication and Networking Technologies (ICCCNT'12)*, Coimbatore, India , 1-7, 26-28 July 2012.

Ryan, D., Denman, S., Fookes, C., Sridharan, S., "Crowd counting using multiple local features", *Digital Image Computing: Techniques and Applications*, Melbourne, VIC, Australia, 81-88, 1-3 Dec. 2009.

Thammasorn, P., Boonchu, S., Kawewong, A., "Real-time method for counting unseen stacked objects in mobile", *IEEE International Conference on Image Processing*, Melbourne, VIC, Australia, 4103-4107, 15-18 Sept. 2013.

Wang, M., Wang, X., "Automatic adaptation of a generic pedestrian detector to a specific traffic scene", *CVPR 2011*, Providence, RI, USA , 3401-3408, 20-25 June 2011.

Zhang, C., Li, H., Wang, X., Yang, X., "Cross-scene crowd counting via deep convolutional neural networks", *Proceedings of the IEEE conference on computer vision and pattern recognition*, Boston, MA, USA , 833-841, 7-12 June 2015.

Zhang, Y., Zhou, D., Chen, S., Gao, S., Ma, Y., "Single-image crowd counting via multi-column convolutional neural network", *Proceedings of the IEEE conference on computer vision and pattern recognition*, Las Vegas, NV, USA, 589-597, 27-30 June 2016.

AN OPERANT CONDITIONING APPROACH FOR LARGE SCALE SOCIAL OPTIMIZATION ALGORITHMS

[1]Seyit Alperen CELTEK iD **, [2]Akif DURDU** iD

[1]*Karamanoğlu Mehmetbey University, Engineering Faculty, Energy Systems Engineering, Karaman, TURKEY*
[2]*2Konya Technical University, Engineering Faculty, Electric and Electronic Engineering, Konya, TURKEY*
[1]salperenceltek@kmu.edu.tr, [2]adurdu@ktun.edu.tr

ABSTRACT: The changes that positive or negative results cause in an individual's behavior are called Operant Conditioning. This paper introduces an operant conditioning approach (OCA) for large scale swarm optimization models. The proposed approach has been applied to social learning particle swarm optimization (SL-PSO), a variant of the PSO algorithm. In SL-PSO, the swarm particles are sorted according to the objective function and all particles are updated with learning from the others. In this study, each particle's learning rate is determined by the mathematical functions that are inspired by the operant conditioning. The proposed approach adjusts the learning rate for each particle. By using the learning rate, a particle close to the optimum solution is aimed to learn less. Thanks to the learning rate, a particle is prevented from being affected by particles close to the optimum point and particles far from the optimum point at the same rate. The proposed OCA-SL-PSO is compared with SL- PSO and pure PSO on CEC 13 functions. Also, the proposed OCA-SL-PSO is tested for large-scale optimization (100-D, 500-D, and 1000-D) benchmark functions. This paper has a novel contribution which is the usage of OCA on Social Optimization Algorithms. The results clearly indicate that the OCA is increasing the results of large-scale SL-PSO.

Key Words: *Operant Conditioning, Large Scale Optimization, Operant Conditioning Approach, Swarm Optimization Algorithm.*

Büyük Ölçekli Sosyal Optimizasyon Algoritmaları İçin Edimsel Koşullandırma Yaklaşımı

ÖZ: Olumlu veya olumsuz sonuçların bir bireyin davranışında neden olduğu değişikliklere Edimsel Koşullandırma denir. Bu makale, büyük ölçekli sürü optimizasyon modelleri için bir edimsel koşullandırma yaklaşımı (OCA) sunar. Önerilen yaklaşım, PSO algoritmasının bir varyantı olan sosyal öğrenme parçacık sürüsü optimizasyonuna (SL-PSO) uygulanmıştır. SL-PSO'da sürü parçacıkları amaç işlevine göre sıralanır ve tüm parçacıklar diğerlerinden öğrenilerek güncellenir. Bu çalışmada, her parçacığın öğrenme hızı, edimsel koşullanmadan esinlenen matematiksel fonksiyonlar tarafından belirlenir. Önerilen yaklaşım, her parçacık için öğrenme oranını ayarlar. Öğrenme oranını kullanarak, optimum çözüme yakın bir parçacığın daha az öğrenmesi amaçlanmaktadır. Öğrenme oranı sayesinde bir parçacığın çözüme yakın partikül ile çözüme uzak partiküllerden aynı oranda etkilenmesinin önüne geçilmektedir. Önerilen OCA-SL-PSO, CEC 13 işlevlerinde SL-PSO ve saf PSO ile karşılaştırılır. Ayrıca, önerilen OCA-SL-PSO, büyük ölçekli optimizasyon (100-D, 500-D ve 1000-D) karşılaştırma işlevleri için test edilmiştir. Bu yazının, Sosyal Optimizasyon Algoritmalarında OCA'nın kullanımı olan yeni bir katkısı vardır. Sonuçlar açıkça OCA'nın büyük ölçekli SL-PSO sonuçlarını artırdığını göstermektedir.

Anahtar Kelimeler: *Edimsel koşullanma, Büyük Ölçekli Optimizasyon, Edimsel Koşullandırma Yaklaşımı, Sürü Optimizasyon Algoritması.*

1. INTRODUCTION

Optimization can be called the process of finding the best solution to a problem or system (Celtek *et al.*, 2020) (Pham and Karaboga, 2012). The optimization's main purpose is to find the parameters that achieve the minimum cost and the shortest time(Karaboğa, 2014). The particle swarm optimization (PSO), which is based on a simple mechanism that mimics societal animals' swarming behaviors, is one of the most used to optimize engineering problems. PSO has given successful results in many engineering problems (Cui and Lee, 2013; Yalcin *et al.*, 2015; ASLAN *et al.*, 2018; Eldem and Ülker, 2020; Song *et al.*, 2020). The PSO consists of particles with a position and velocity and represents a candidate solution for the optimization problem(Eberhart and Kennedy, 1995).

While classical PSO can perform well in low dimensional optimization problems, it is weak in large-scale optimization problems and cannot get expected results (Wang *et al.*, 2013). For this reason, many PSO variations have been proposed to improve the PSO's search performance (Clerc and Kennedy, 2002; Premalatha and Natarajan, 2009; Wang *et al.*, 2020).

The social learning particle swarm optimization (SL-PSO) is one variant of the PSO algorithm (Cheng and Jin, 2015). Social learning plays an important role in behavior learning in the swarm. It provides particles to learn behaviors from other's experiences without incurring the costs of particle trials-and-errors. Unlike the studies in the literature recommended improving the PSO's search performance, no global and local best values are kept in SL-PSO. Instead, the swarm particles are sorted according to the objective function, and all particles except the best are updated with learning from other better particle. Unlike the classic PSO, the update process in SL-PSO is achieved by learning all the particles from the others.

In this study, each particle's learning rate is determined by the mathematical functions that are inspired by the operant conditioning. The changes that pleasant and unpleasant consequences cause in individuals' behavior are called Operant Conditioning (Holland and Skinner, 1961). If an individual's behavior results in something pleasant, the individual tends to do it repeatedly.

It is suggested an operant conditioning approach (OCA) to SL-PSO. The main goal of the proposed method is to arrange the learning rate. This method provides the necessary learning for every particle. For instance, one of the particles with good results is intended to learn less and not be affected by the worst particles. If not, in the bad particle case, the learning rate will be high and the particle will be trained more.

This study consists of four sections. In Section 2, the mathematical background of particle update in PSO and SL-PSO methods is given. Then, Section 3 gives information about operant conditioning -the inspiration source for this work- and explains operant conditioning's mathematical modeling. Section 4 gives results in different dimensions of CEC 13 functions. Of proposed approach. In Section 5, the study is terminated by comparing the proposed approach with pure PSO and SL-PSO.

2. PSO and SL-PSO

The PSO, developed by Eberhart and Kennedy in 1995, is a population-based metaheuristic optimization technique (Eberhart and Kennedy, 1995). PSO, which is inspired by birds, is assumed that each particle can update its position and velocity by using global and local best values. Detailed coverage of PSO can be found in (Eberhart *et al.*, 2001).

The position and velocity equations (1-2) for a conventional PSO are as follows;

$$V_i(t+1) = \omega V_i(t) + c_1 R_1(t)\big(pbest_i(t) - X_i(t)\big) + c_2 R_2(t)\big(gbest(t) - X_i(t)\big) \tag{1}$$
$$X_{i,j}(t+1) = X_{i,j}(t) + V_i(t+1) \tag{2}$$

In these equations, t, $V_i(t)$ and $X_i(t)$ indicate respectively the number of iterations, the speed of the i_{th} particle and the position of the i_{th} particle. Also, ω is the inertia weight, c_1 and c_2 are acceleration vectors, and R_1 and R_2 are random vectors generated at 0-1 interval.

As mentioned above, classical PSO can perform well in low dimensional optimization problems. Unfortunately, as the dimension of the problem increases, the PSO success rate falls. The social learning particle swarm optimization (SL-PSO), which is one variant of the PSO algorithm, has proposed improving the search performance (Cheng and Jin, 2015).

Like the classical PSO, in the SL-PSO approach, a randomly initialized initial vector (Xij) is created, which first constitutes a candidate solution. Then, the swarm particles are sorted according to the ascending order of the fitness function results. As a result, every particle learns from other particles (as it is in the same social learning mechanism) and corrects its behavior. The social learning between the particles takes place as follows;

$$X_{i,j}(t+1) = \begin{cases} X_{i,j}(t) + \Delta X_{i,j}(t+1), & if\ p_i(t) \le P_i^L \\ X_{i,j}(t), & otherwise \end{cases} \tag{3}$$

where $X_{(i,j)}(t)$ is the particle that learns, X_{ij} is the particle that teaches, P_i is the probability of learning. In detail, $\Delta X_{i,j}(t+1)$ is constructed as follows;

$$\Delta X_{i,j}(t+1) = r_1(t)\Delta X_{i,j}(t) + r_2(t)I_{i,j}(t) + r_3(t)\epsilon C_{i,j}(t) \tag{4}$$
$$I_{i,j}(t) = X_{k,j}(t) - X_{i,j}(t) \tag{5}$$
$$C_{i,j}(t) = \overline{X}_j(t) - X_{i,j}(t) \tag{6}$$

As can be seen in Equation 4, there are three components for updating to position in SL-PSO. First one is is $X_{i,j}(t)$ the same as the inertia component in the canonical PSO. Second component is the called as demonstrators $I_{i,j}(t)$ (Equation 5). As mentioned above, SL-PSO uses demonstrators for position correction (Equation 6) instead of gbest or pbest in PSO. The third one is called social influence factor. There are three random coefficients r1, r2 and r3, which will be randomly generated within [0; 1].

Specifically, the j-element in the behavior vector of the particle i; $X_{ij}(t)$ simulates $X_{kj}(t)$, the j-th element in the behavior vector of the particle k_i. In SL-PSO, the particle learns from different indicators in the current swarm, and this behavior is controlled randomly.

As the higher the search size, the harder it is to solve the problem, and the lower the likelihood of a particle being willing to learn from others. In SL-PSO, the relationship between learning possibility and problem dimensionality is inversely related to the following relation;

$$P_i^L = \left(1 - \frac{i-1}{m}\right)^{\alpha \log\left(\left\lceil \frac{n}{M} \right\rceil\right)} \tag{7}$$

Where P_i^L the is the learning probability for each particle I, M is the dimension of problem, m is the swarm size, n is the number of the dimensionality and α is the smooth coefficient (α =0.5).

3. OPERANT CONDITIONING and OCA-SL-PSO

The main challenge of social swarm methods is learning from just better particles can cause the results to stick to the local optimum points. This study aims at a social learning network that a particle learns from other particles with the learning rate. Thus, the learning rate controls each particle's learning from the other particles.

It is inspired by the actual condition used in social life for the determination of learning rates. In operant conditioning, for every situation that an individual has experienced before, positive or negative consequences arise. These positive or negative consequences arise from past experiences and are largely influential in their future behavior. The changes that positive or negative consequences lead to an individual's behavior are called "Operant Conditioning." If the individual has already had an attitude and has a positive outcome due to this behavior, he or she is directed to the same behavior again. Similarly, if

the individual has had a previous behavior and has received a negative reaction due to this behavior, he/she is striving for similar behavior.

In this study, the operant conditioning is applied to the swarm, not to the individual. In this way, it is possible to benefit from the experiences of all the individuals. The pseudo code of the OCA-SL-PSO is given in Algorithm 1.

Algorithm 1. The pseudo code of the OCA-SL-PSO
1   Initialization
2   t = 0 (generation index), n = dimension.
3   M = 100 (swarm size).
4   Divide into groups like in SL-PSO [11]
5   Set the social impact factor like in SL-PSO [11]
6   Create a solution vector for each group.
7   Sort solutions from large to small.
8   Set the best solutions as a pointer.
9   Find the best, worst and average value of each particle.
10 Calculate the learning rate of each particle.
11 Train the particles.
• Calculate P_{best}.
• Calculate the random coefficients.
• Train the particles with new components.
12 Run the objective function for the solution and create the solution vector.
13 If the FEs number is not completed, go back to Step 7.
14 End.

The learning rates in this study are determined by a function that depends on the best distance and the particle's worst distance. If the particle yields a good result, there are two situations; in the first case, the particle should achieve better by imitating the better particles. Another case, the result of the particle is that it is local rather than global, which is overcome by imitating worst particles. The learning rate are defined as P_{best};

$$Pbest = \frac{|Xi - Xbest|}{|Xbest - Xworst|} \tag{8}$$

$$X_{i,j}(t+1) = \begin{cases} X_{i,j}(t) + \Delta X_{i,j}(t+1), & if \ p_i(t) \leq Pbest \\ X_{i,j}(t), & otherwise \end{cases} \tag{9}$$

As mentioned above, Equation 9 is used for finding $\Delta X_{i,j}(t+1)$. In our scenario, the coefficients will be randomly generated within [0,1] under one condition. The condition is;

$$r_2(t) > r_3(t) > r_1(t) \tag{10}$$

4. RESULTS

The proposed approach in this study was tested with CEC 13 functions. The CEC 13 benchmark functions consist of 28 benchmark functions. 13 of 28 benchmark functions are using in this paper. The used functions are given in Table 1. The proposed approach first tries with n = 100 dimensions and FEs = 3E6 and the results are given in Table 2. The number of fitness evaluations (FEs) is the number of times you evaluate a solution in the meta-heuristic algorithm. The proposed approach has tried with n = 500 dimensions and FEs = 3E6 and the results are given in Table 3. The program has been run 10 times in order to get all results on the tables.

Table 1. CEC 13 Test Functions

Number	Function Name
f1	Sphere Function
f2	Rotated High Conditioned Elliptic Function
f3	Rotated Bent Cigar Function
f4	Rotated Discus Function
f5	Different Powers Function
f6	Rotated Rosenbrock's Function
f7	Rotated Schaffers F7 Function
f8	Rotated Ackley's Function
f9	Rotated Weierstrass Function
f10	Rotated Griewank's Function
f11	Rastrign's Functions
f12	Rotated Rastrign's Function
f13	Non-Contious Rotated Rastrign Function

Table 2. OCA-SL-PSO 100 D Results, FEs=6E5

	Best	Worst	Mean	STD
f1	0,00E+00	0,00E+00	0,00E+00	0,00E+00
f2	6,27E-229	4,07E-221	4,07E-222	0,00E+00
f3	9,18E+00	2,53E+04	1,36E+04	9,26E+03
f4	3,21E-36	9,47E-34	1,68E-34	2,96E-34
f5	9,57E+01	3,06E+02	1,38E+02	6,44E+01
f6	0,00E+00	2,00E+00	7,00E-01	8,23E-01
f7	5,72E-02	8,28E-02	6,97E-02	8,30E-03
f8	5,30E+03	8,58E+03	6,80E+03	1,01E+03
f9	7,96E+01	2,02E+02	1,12E+02	3,59E+01
f10	1,33E-14	2,04E-14	1,62E-14	2,80E-15
f11	0,00E+00	1,48E-02	2,22E-03	4,99E-03
f12	4,71E-33	4,71E-33	4,71E-33	0,00E+00
f13	1,35E-32	1,47E-32	1,39E-32	5,95E-34

Table 3. OCA-SL-PSO 500 D Results, FEs=6E5

	Best	Worst	Mean	STD
f1	5,88E-27	7,32E-11	7,32E-12	2,31E-11
f2	9,59E-01	3,39E+01	2,64E+01	1,26E+01
f3	4,46E+05	9,57E+05	6,58E+05	1,78E+05
f4	5,96E+01	7,82E+01	7,00E+01	5,18E+00
f5	1,07E+03	1,77E+03	1,36E+03	2,38E+02
f6	1,00E+01	7,50E+02	2,66E+02	2,87E+02
f7	8,06E-01	9,67E-01	8,80E-01	5,57E-02
f8	3,84E+04	4,41E+04	4,07E+04	2,11E+03
f9	1,46E+03	2,22E+03	1,94E+03	2,46E+02
f10	9,83E-01	2,30E+00	1,67E+00	4,56E-01
f11	6,66E-16	1,01E-02	2,56E-03	4,17E-03
f12	2,89E+00	6,29E+00	4,58E+00	1,08E+00
f13	7,79E-23	6,78E-02	9,07E-03	2,12E-02

The proposed approach model is tested for n = 1000 dimensions and FEs=1,2E5, FEs=6E5, FEs=3E6 and the results are given in Table 4, Table 5 and Table 6, respectively.

Table 4. OCA-SL-PSO 1000 D Results, FEs=1,2E5

	Best	**Worst**	**Mean**	**STD**
f1	2,09E+05	3,16E+05	2,81E+05	4,27E+04
f2	1,00E+20	1,00E+20	1,00E+20	
f3	9,48E+06	1,28E+07	1,09E+07	1,61E+06
f4	8,26E+01	8,71E+01	8,53E+01	1,77E+00
f5	1,39E+07	3,61E+07	1,94E+07	9,35E+06
f6	2,03E+05	2,85E+05	2,43E+05	3,81E+04
f7	1,80E+02	6,64E+02	4,61E+02	2,31E+02
f8	3,93E+05	4,02E+05	3,99E+05	3,48E+03
f9	1,21E+04	1,24E+04	1,23E+04	1,36E+02
f10	1,91E+01	1,92E+01	1,92E+01	6,51E-02
f11	2,20E+03	3,41E+03	2,63E+03	4,73E+02
f12	6,90E+06	1,72E+07	1,12E+07	4,07E+06
f13	2,35E+07	5,77E+07	3,99E+07	1,49E+07

Table 5. OCA-SL-PSO 1000 D Results, FEs=6E5

	Best	**Worst**	**Mean**	**STD**
f1	1,15E+04	2,43E+04	1,84E+04	4,65E+03
f2	1,00E+20	1,00E+20	1,00E+20	
f3	4,85E+06	9,65E+06	6,97E+06	2,20E+06
f4	8,05E+01	8,54E+01	8,28E+01	1,87E+00
f5	1,30E+04	4,37E+05	9,95E+04	1,89E+05
f6	8,60E+03	2,95E+04	1,67E+04	8,69E+03
f7	1,68E+00	1,85E+00	1,78E+00	6,68E-02
f8	2,69E+05	2,94E+05	2,80E+05	1,08E+04
f9	8,28E+03	1,20E+04	1,05E+04	1,90E+03
f10	1,56E+01	1,72E+01	1,64E+01	7,30E-01
f11	1,11E+02	1,95E+02	1,53E+02	3,27E+01
f12	1,19E+02	1,29E+04	3,24E+03	5,42E+03
f13	1,42E+03	2,53E+03	1,80E+03	4,28E+02

Table 6. OCA-SL-PSO 1000 D Results, FEs=3E6

	Best	**Worst**	**Mean**	**STD**
f1	4,33E+00	5,17E+02	1,80E+02	1,84E+02
f2	1,00E+20	1,00E+20	1,00E+20	
f3	2,12E+06	3,80E+06	2,68E+06	5,99E+05
f4	7,69E+01	8,21E+01	8,01E+01	1,59E+00
f5	4,35E+03	6,41E+03	5,00E+03	5,65E+02
f6	7,91E+02	6,77E+03	2,80E+03	1,93E+03
f7	1,29E+00	1,52E+00	1,42E+00	9,11E-02
f8	1,08E+05	1,21E+05	1,13E+05	4,71E+03
f9	3,25E+03	6,38E+03	4,78E+03	1,12E+03
f10	5,19E+00	6,37E+00	5,66E+00	4,47E-01
f11	1,33E+00	1,53E+01	4,71E+00	5,98E+00
f12	5,90E+00	7,48E+00	6,73E+00	6,25E-01
f13	2,26E+00	4,42E+00	3,63E+00	1,19E+00

The comparison between the proposed approach in Table 7 and SL-PSO (Cheng and Jin, 2015) and classical PSO (Zambrano-Bigiarini *et al.*, 2013) is given. It is clear from Table 7 that the proposed approach

achieves a more efficient result than the standard PSO or SL-PSO. Moreover, the SL-PSO and PSO data in the table are the results of 50-dimensional studies. The success of the proposed method comes to the forefront if SL-PSO and pure PSO are driven from the idea that the results will get worse when operated in more sizes. From the 13 test functions, OCA-SL-PSO produces the most successful result in 9 functions. The proposed 500-dimensional approach works better than SL-PSO and PSO at 8 out of 13 test functions. The proposed 1000-dimensional approach is more successful than SL-PSO and PSO in five of the 13 test functions.

Table 7. The Comparison Results

	Proposed (n=50)	Proposed (n=100)	Proposed (n=500)	SL-PSO (n=50)	PSO (n=50)
f1	0,00E+00	**0,00E+00**	**5,88E-27**	7,19E-13	-1,400E+3
f2	0,00E+00	**6,27E-229**	9,59E-01	5,90E+5	3,776E+05
f3	4,12E+00	**9,18E+00**	4,46E+05	2,13E+07	1,99E+07
f4	**2,11E-117**	**3,21E-36**	5,96E+01	3,11E+6	3,113E+04
f5	8,61E+00	9,57E+01	1,07E+03	**6,23E-11**	-1,000E+03
f6	0,00E+00	**0,00E+00**	1,00E+01	2,33E0	-8,816E+02
f7	0,00E+00	**5,72E-02**	8,06E-01	1,51E0	-7,439E+02
f8	1,65E+04	5,30E+03	3,84E+04	**3,44E-02**	-6,790E+02
f9	3,54E+00	7,96E+01	1,46E+03	**1,75E0**	-5,548E+02
f10	0,00E+00	**1,33E-14**	9,83E-01	1,06E-1	-4,999E+02
f11	0,00E+00	0,00E+00	**6,66E-16**	5,87E0	-2,498E+02
f12	0,00E+00	**4,71E-33**	2,89E+00	2,11E+1	-1,378E+02
f13	**1,25E-227**	**1,35E-32**	7,79E-23	2,45E+1	1,196E+02

5. CONCLUSION AND FUTURE WORKS

This study proposes a new approach to swarm-based optimization methods inspired by operant conditioning. The focus point is creating better learning for each particle. Thus, the proposed approach adjusts the learning rate for each particle. The learning rate encourages a particle close to the optimum solution to learn from better particles and learn less from the worse particle. Thanks to the learning rate, a particle is prevented from being affected by particles close to the optimum point and particles far from the optimum point at the same rate. The experiment results on CEC 13 functions clearly prove that our strategy is successful for large scale problem.

Furthermore, we are now investigating our approach on different swarm-based methods like as applied to SL-PSO. We will also apply the proposed method to real engineering problems. In our future work, we will consider other colony-based optimization techniques

6. ACKNOWLEDGEMENT

REFERENCES

Aslan, S., Aksoy, A. and Gunay, M., 2018, Performance of parallel artificial bee colony algorithm on solving probabilistic sensor deployment problem, *2018 International Conference on Artificial Intelligence and Data Processing (IDAP)*, 1-5.

Celtek, S. A., Durdu, A. and Alı, M. E. M., 2020, Real-time Traffic Signal Control with Swarm Optimization Methods, *Measurement*.

Cheng, R. and Jin, Y. J. I. S., 2015, A social learning particle swarm optimization algorithm for scalable optimization, 291, 43-60.

Clerc, M. and Kennedy, J., 2002, The particle swarm-explosion, stability, and convergence in a multidimensional complex space, *IEEE Transactions on Evolutionary Computation*, 6 (1), 58-73.

Cui, C.-Y. and Lee, H.-H., 2013, Distributed traffic signal control using PSO based on probability model for traffic jam, In: Intelligent Autonomous Systems 12, Eds: Springer, p. 629-639.

Eberhart, R. and Kennedy, J., 1995, A new optimizer using particle swarm theory, *MHS'95. Proceedings of the Sixth International Symposium on Micro Machine and Human Science*, 39-43.

Eberhart, R. C., Shi, Y. and Kennedy, J., 2001, Swarm intelligence, Elsevier, p.

Eldem, H. and Ülker, E., 2020, A Hierarchical Approach Based on ACO and PSO by Neighborhood Operators for TSPs Solution, *International Journal of Pattern Recognition and Artificial Intelligence*, 2059039.

Holland, J. G. and Skinner, B. F., 1961, The analysis of behavior: A program for self-instruction.

Karaboğa, D., 2014, Yapay Zeka Optimizasyon Algoritmalari, Nobel Akademik Yayıncılık, p.

Pham, D. and Karaboga, D., 2012, Intelligent optimisation techniques: genetic algorithms, tabu search, simulated annealing and neural networks, Springer Science & Business Media, p.

Premalatha, K. and Natarajan, A., 2009, Hybrid PSO and GA for global maximization, *Int. J. Open Problems Compt. Math*, 2 (4), 597-608.

Song, B., Wang, Z. and Zou, L., 2020, An improved PSO algorithm for smooth path planning of mobile robots using continuous high-degree Bezier curve, *Applied Soft Computing*, 106960.

Wang, H., Sun, H., Li, C., Rahnamayan, S. and Pan, J.-S., 2013, Diversity enhanced particle swarm optimization with neighborhood search, *Information Sciences*, 223, 119-135.

Wang, Z.-J., Zhan, Z.-H., Kwong, S., Jin, H. and Zhang, J., 2020, Adaptive Granularity Learning Distributed Particle Swarm Optimization for Large-Scale Optimization, *IEEE transactions on cybernetics*.

Yalcin, N., Tezel, G. and Karakuzu, C., 2015, Epilepsy diagnosis using artificial neural network learned by PSO, *Turkish Journal of Electrical Engineering & Computer Sciences*, 23 (2), 421-432.

Zambrano-Bigiarini, M., Clerc, M. and Rojas, R., 2013, Standard particle swarm optimisation 2011 at cec-2013: A baseline for future pso improvements, *2013 IEEE Congress on Evolutionary Computation*, 2337-2344.

X-BAND EPR STUDIES OF GAMMA IRRADIATED A NEW ISOQUINOLINE SULFONAMIDE: $C_{17}H_{20}BrNO_3S$

[1]Özgül KARATAŞ ID **, [2]Yusuf CEYLAN** ID

[1]*Konya Technical University, Vocational School of Technical Sciences, Department of Electric and Energy, Konya, TURKEY*
[2]*Selçuk University, Faculty of Science, Department of Physics, Konya, TURKEY*
[1] okaratas@ktun.edu.tr, [2] yceylan@selcuk.edu.tr

ABSTRACT: A new epoxyisoquinoline sulfonamide as a fused heterocycle compound (**I**), (4aS,7S,8aR)-8a-bromo-7-methyl-2-tosyl-2,3,4,7,8,8a-hexahydro-1H-4a,7-epoxyisoquinoline was synthesized using green and cascade progress which was then irradiated by ^{60}Co-gamma (γ) ray source with a dose speed of 0.981 kGy/h at the room temperature for 72h. EPR spectra of **I** compound were measured at different orientations in magnetic field with X-band EPR spectrometer along the temperatures between 150-340 K. Isotropic spectrum was obtained without depending on temperature and radical structure, CH_3H was observed. Radical was simulated using the Bruker software WinEPR-Simfonia and the experimental isotropic g-value with hyperfine coupling constant of radical was calculated.

Key Words: EPR, Irradiation effects, Radical, Synthesis, Sulfonamide.

Gama Işınları ile Işınlanmış Yeni Bir Isoquinoline Sulfonamide ($C_{17}H_{20}BrNO_3S$) Maddesinin X-Bant EPR Çalışması

ÖZ: Kaynaşık bir heteroksil bileşiği olan yeni epoxyisoquinoline sulfonamide maddesi (**I**), (4aS,7S,8aR)-8a-bromo-7-methyl-2-tosyl-2,3,4,7,8,8a-hexahydro-1H-4a,7-epoxyisoquinoline, yeşil ve kademeli bir süreç ile sentezlendi. Daha sonra doz hızı of 0.981 kGy/h olan ^{60}Co-gama (γ) kaynağı ile oda sıcaklığında 72 saat ışınlandı. **I** bileşiğinin EPR spektrumları, 150-340 K sıcaklık aralığında X-bant EPR spektrometresi kullanılarak manyetik alanda üç farklı yönelimde kaydedildi. Elde edilen sonuçlara göre, örneğe ait izotropik spektrumların olduğu görüldü ve CH_3H radikalinin varlığı gözlemlendi. Sonuçlar, Bruker WinEPR-Simfonia programı kullanılarak fit edildi. Radikalin aşırı ince yapı sabiti (A) ile deneysel izotropik spektroskopik değeri (g) hesaplandı.

Anahtar Kelimeler: EPR, Işınlama Etkileri, Radikal, Sentez, Sulfonamide.

1. INTRODUCTION

The Intra Molecular Diels–Alder cycloaddition of Furan, called IMDAF is one of the most widely used synthetic tool for the construction of heterocyclic ring systems since furan's diene character (Padwa and Flick (2013), Schindler and Carreira (2009), Takao *et al.* (2005), Brieger and Bennett (1980)). IMDAF process does allow obtaining usually fused heterocycles like isoquinoline which are extremely important in pharmaceutical field (Alonso and Garcia (2013)). Isoquinolines particularly are important heterocyclic

motifs; its derivatives also have been identified as ligands for a variety of receptors and as agents for the treatment of a number of pathologies (Glushkov and Shklyaev (2001), Dieudonne *et al.* (2012), Pettit *et al.* (2003)). On the other hand, sulfonamides are also widely used class of compounds as anti-inflammatory and antiviral agents, therefore general and efficient synthesis of sulfonamides under mild conditions is of continuing interest among pharmacists (Jafarppour *et al.* (2011), Supuran *et al.*(2003), Scozzafava *et al.* (2003), Greenfield and Grosanu (2008)).

Irradiation (gamma, UV, x-ray) has a significant role and widely used in organic and inorganic chemistry (Chatterjee and Mahata (2004), Yarbası *et al.* (2011), Yordanov and Aleksieva (2019)) such as sterilization of drugs, killing the pathogens in contaminated foods, producing free radicals or modification of physical properties etc. (Sayin *et al.* (2012), Asik *et al.* (2004)). The EPR spectroscopy is one of the most powerful methods for identifying irradiation damage centers over molecules containing unpaired electrons (Dereli *et al.* (2011), Usta *et al.* (2011), Karatas and Aras (2012), Eaton and Eaton (2008), Gordy (1980), Pshezhetskii and Kotov (1973), Atherton (1973)). Furthermore, this method has been in preference for a long time to produce paramagnetic centers for Electron Paramagnetic Resonance (EPR) technique in order to identification of paramagnetic defect centers and also provides a detailed description for structures mentioned above (Karatas *et al.* (2016), Yarbası *et al.* (2011), Yordanov and Aleksieva (2019), Sayin *et al.* (2012)). There are known two EPR parameters (g-value and hyperfine constant (A)) giving the most complete and valuable information about the geometry and electronic structure of radical species and centers (Dereli *et al.* (2011), Gordy (1980), Aras *et al.* (2014)).

In this study, we wish to report synthesis of new isoquinoline sulfonamide, N-(2-bromoallyl)-4-methyl-N-(2-(5-methylfuran-2-yl) ethyl) benzenesulfonamide, **I** using environmentally benign and one pot cascade sequence. The free radical was generated on the structure I by EPR using ^{60}Co-gamma (γ) ray source with a dose speed of 0.981 kGy/h for 72 hours at ambient temperature. Simulated EPR parameters were also calculated, compared with experimental result.

2. MATERIAL AND METHOD

2.1. Synthesis of (4aS,7S,8aR)-8a-bromo-7-methyl-2-tosyl-2,3,4,7,8,8a-hexahydro-1H-4a,7-epoxyisoquinoline (I) C17H20BrNO3S

One-pot protocol for the construction of complex heterocycle through furan tethered terminal bromoalkenes was afforded under catalyst free condition during the synthesis of isoquinoline sulfonamide (**I**). Compound **I** was obtained from overall four step reactions; in the first step, Henry reaction was carried out between **II** and nitromethane in the presence of base to give **III** in quantitative yield (Luzzio (2001)). Reduction of the nitrovinyl group from **III** with lithiumaluminum hydride under refluxing in tetrahydrofuran (THF) is the second step and produced **IV** in good yield. Resulting amine **IV** was then treated with 2,3-dibromopropene and potassium carbonate in THFn gave **V** in third step. In the last step, secondary amine, **V**, tosyl chloride and potassium carbonate were stirred in aqueous media and heated at 368 K for four days to afford **I** in 62% yields. This last step is a one pot cascade sequence in which sulfonyl part of the tosyl group attaches to nitrogen **VI** and followed by intramolecular Diels-Alder cycloaddition progress (Scheme 1).
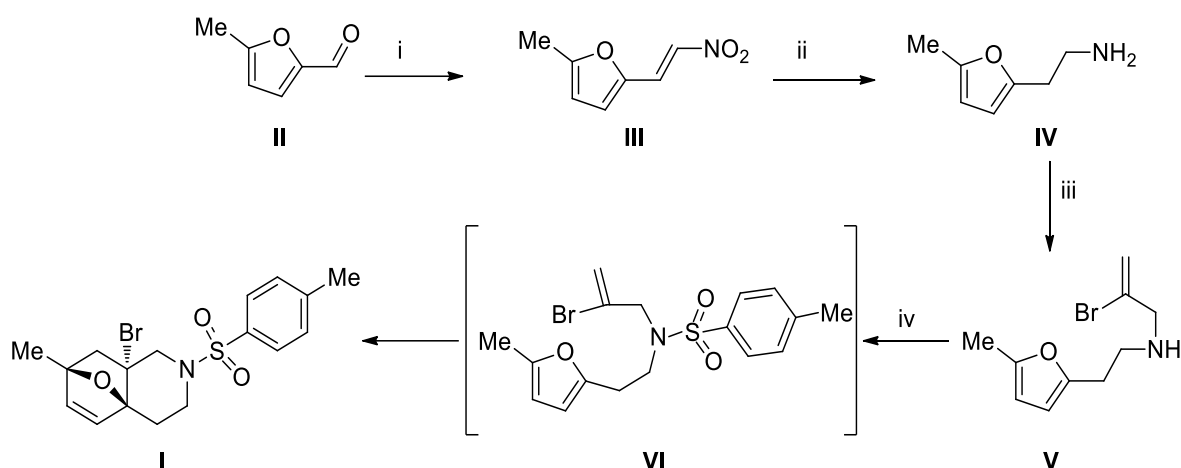
Scheme 1. Synthesis of $C_{17}H_{20}BrNO_3S$: (i. CH_3NO_2, NaOH, Acetone, 273 K, 95%; ii. $LiAlH_4$, THF, reflux, 4h, 72%; iii. 2,3-dibromopropene, K_2CO_3, 4 days, 85%; iv. Tos-Cl, H_2O, K_2CO_3, 4 days, 368 K, 62%).

2.2. Procedure for (4aS,7S,8aR)-8a-bromo-7-methyl-2-tosyl-2,3,4,7,8,8a-hexahydro-1H-4a,7-epoxyisoquinoline ($C_{17}H_{20}BrNO_3S$) I:

Reactions requiring anhydrous conditions were conducted in flame dried or oven dried apparatus under atmosphere of a dry nitrogen except last step. All solvents and reagents were obtained from commercial sources and used without further purification unless otherwise stated. Tetrahydrofuran (THF) was dried by distillation from sodium / benzophenone under an atmosphere of nitrogen and stored over activated 4Å molecular sieves. ChemBioDraw Ultra V12 programme was used for nomenclature of molecules according to IUPAC rules.

IR Spectrum was taken in Niğde Ömer Halisdemir University Research Laboratory on Perkin Elmer BXII, ^1H Nuclear magnetic resonance (NMR) spectra were recorded at 300 MHz on a Bruker DPX 400 instrument in Selçuk University. Chemical shifts are reported in parts per million (ppm) relative to residual $CHCl_3$ (δ 7.27ppm) or tetramethylsilane as the internal reference (δ 0.00 ppm). The following abbreviations are used to describe the multiplicity of a given signal: s = singlet, d = doublet, t = triplet, q = quartet, p = pentet, sex = sextet, m = multiplet, br = broad. Coupling constants, J, are given in Hertz. ^{13}C Nuclear magnetic resonance spectra were recorded either at 100.78 MHz on a Jeol Ex400 FTNMR instrument or at 75.43 MHz, on a Bruker DPX 400 instrument. Chemical shifts are reported in parts per million (ppm) relative to CDCl3 (central line of triplet δ 77.0 ppm).

2-Bromo-N-(2-(5-methylfuran-2-yl) ethyl) prop-2-en-1-amine **V** (0.65g, 2.66mmol, 1equivalent) and Tosyl chloride (0.6g, 3.20 mmol, 1.2 equivalent) were dissolved in 50 mL distilled water. Potassium carbonate (0.46g, 3.2mmol, 1.2 equivalent) were added and the reaction mixture was stirred at 368 K for four days. The reaction mixture was cooled to room temperature then ethyl acetate (100 mL) was added, followed by extraction of aqueous phases using 2x50 mL ethyl acetate. Combined organic phases was evaporated, resulting residue was turned to brown solid phase, which was recrystallized employing dichloromethane, hexane mixture. The titled compound was collected as pale-yellow crystals 0.66g, 62% yield.

IR: υ_{max} (thin film)/cm^{-1} :3014(w,C-H) , 2948(s,C-H), 1585 (w, C=C) ,1479(m,C-N), 708(C-Br), ^1H NMR (400 MHz, CDCl3, δ ppm): 7.60(d, J 8Hz, 2H), 7.26 (d, J 8Hz, 2H), 6.23(d, J 5.6 Hz, 1H), 6.07(d, J 5.6 Hz, 1H), 4.07(d, J 2Hz, 1H), 3.85(d, J 2Hz, 1H), 2.64(m, 2H), 2.52(m, 2H), 2.36(s, 3H), 1.95(d, J 12.8Hz, 1H), 1.71(d, J 12.8Hz, 1H), 1.44(s, 3H). ^{13}C NMR (100 MHz, CDCl3, δ ppm): 143.9, 140.1, 138.1, 134.2, 129.9(2xC), 127.8(2xC), 87.4, 87.2, 60.3, 58.8, 48.7, 42.7, 25.4, 21.8, 19.1.

2.3. EPR Measurements

In this study, its polycrystal form was produced, after synthesis of isoquinolin sulfonamide **I**. This polycrystal sample was irradiated at room temperature for 72h using ^{60}Co gamma (γ)-ray source with dose speed of 0,981 kGy/h at Saraykoy Establishment of Turkish Atomic Energy Agency (TAEK) in Ankara. Afterwards, the EPR spectra of isoquinolin sulfonamide **I** were recorded between 150K and 340K in the magnetic fields using Bruker EMX 081 (Germany) X-Band EPR spectrometer. EPR measurements were performed at 150 K in steps of 10º intervals along each of three perpendicular planes (x, y, z) during the experiment using temperature control unit of EPR spectrometer. The spectrometer was set as follows: the microwave power was 4mW, the modulation frequency was 100kHz, and modulation amplitude was 4G. Low and high temperature measurements were performed using variable temperature-control unit of EPR spectrometer. Radical was simulated by using the Bruker software WinEPR-Simfonia and the g value of radical was found by comparison with a DPPH sample (g= 2.0036) (Weil and Wertz (1994), Ceylan *et al.* (2013), Ceylan *et al.* (2015),).

3. RESULTS AND DISCUSSION

EPR signals were not detected on non-irradiated isoquinolin sulfonamide **I** compound, so the sample irradiated for 72h by using ^{60}Co gamma (γ)-ray source and about 71kGy dose have been used for investigating of free radical in isoquinolin sulfonamide **I**. After irradiation, recorded EPR signals showed that free radical was produced over the sample by gamma irradiation. EPR signals of free radical produced by γ-irradiation in **I** compound were able to observe between 150K- 340K temperatures (Figure 2.). The best spectra of isoquinolin sulfonamide **I** was observed at 150K, so we recorded detailed EPR spectra for three mutually perpendicular axes by rotating the crystals around the x, y and z crystallographic axes in steps of 10º at 150K during the experiment using temperature control unit of EPR spectrometer (Figure 1.).
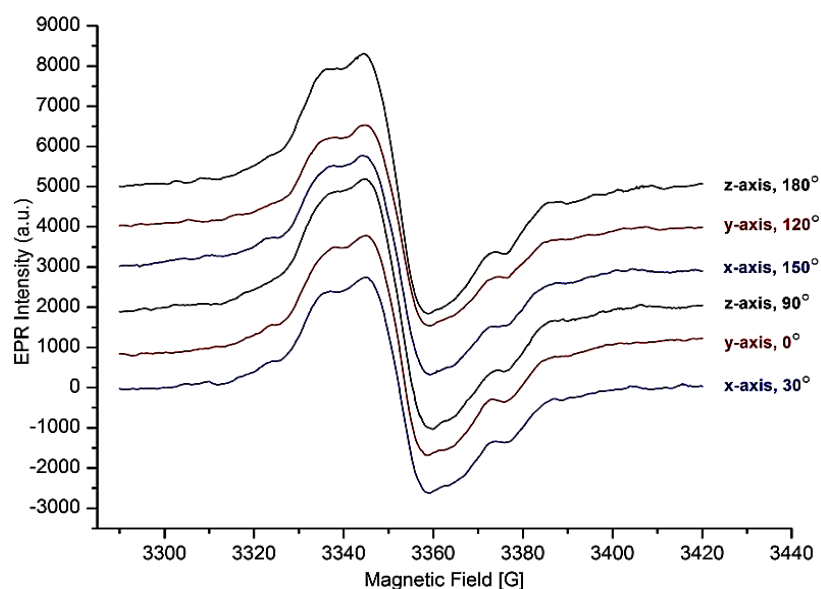

Figure 1. The EPR spectra of gamma (γ)-irradiated isoquinolin sulfonamide **I** at different angles towards the x, y, z axes in magnetic field at 150K.

These measurements showed that only a single peak was observed in these ranges. And also, the distances between the lines were similar and isotropic behaviors were shown in the spectra. It was understood that isotropic properties were observed due to spectra were independent on the magnetic field in the planes which are perpendicular to each other (Figure 1.). In addition to the shapes and intensities

of the lines in the spectra were not changed along with temperature (Figure 1.), so it was deduced that isotropic spectrum was obtained without depending on temperature and radical structure, too.
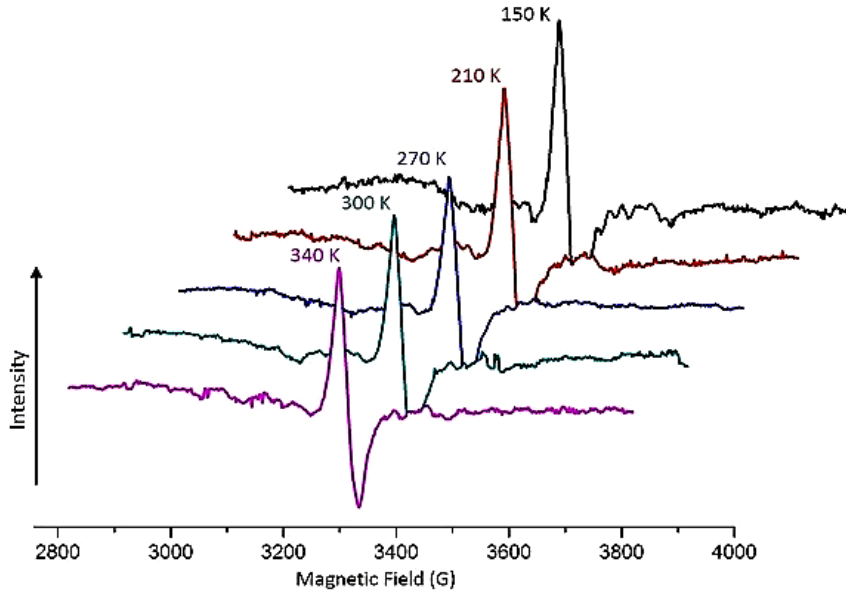

Figure 2. The temperature dependency of EPR spectrum of gamma (γ)-irradiated isoquinolin sulfonamide **I**.

Taking account to recorded EPR spectra and molecular structure, it was deduced that one radical structure was formed under the gamma-rays. The free radical in **I** compound was identified as $\dot{C}H_3H$. After the conduct of an in-depth analysis, it was determined that the spectrum was splitted into 1:3:3:1 intensity ratio from hydrogen atoms in CH_3 ($I_H = 1/2$) according to $2nI+1$ formula firstly, because H protons directly attached to the carbon (C). Then each of these lines was splitted into 1:1 intensity ratio due to the other hydrogen atom which is magnetically nonequivalent in CH_3. Therefore spectrum slightly changed due to the overlap and also all splitting were observed 1:4:6:4:1 intensity ratios. As a result, we obtained the computer simulation of spectra (Figure 3.) which gives the best agreement with our experimental values and we attributed these spectra to $\dot{C}H_3H$ radical.
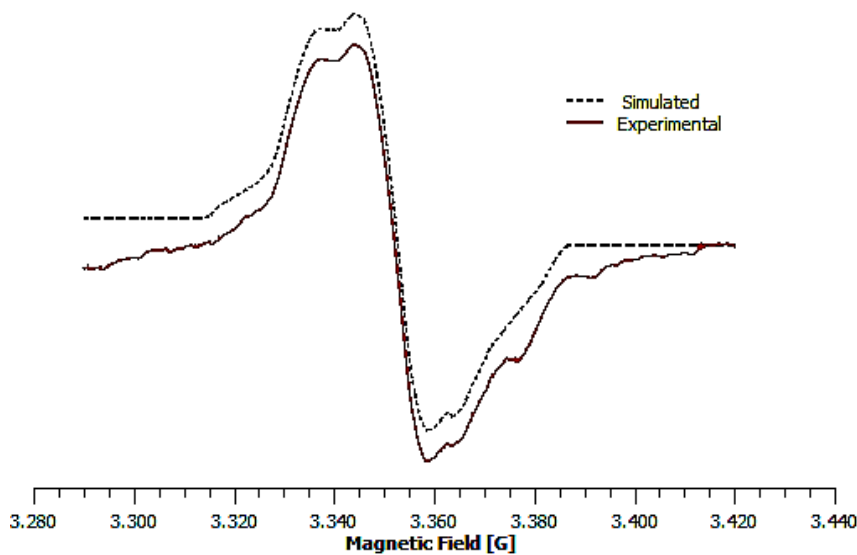

Figure 3. The EPR spectrum of gamma (γ)-irradiated $C_{17}H_{20}BrNO_3S$ polycrystal when the magnetic field oriented to yz plane at angle of 0º and its simulation.

The compound **I** was characterized spectroscopically, well defined and peaks in excellent agreement with the structure which was then taken into EPR analyze. In the most cases the EPR spectra of radical from isoquinolin sulfonamide **I** were poorly resolved, and the hyperfine coupling constants were deduced from the overall width and intensities distributions then verified by computer simulation. Isotropic g-factor was calculated as 2,005841 by resonance equation (hv=gβH) and isotropic hyperfine coupling constants were determined A_{CH3}= 27,12 G, A_H= 15,93 G from the experimental spectra of radical. These parameters were then slightly modified until a reasonable agreement between simulated and experimental spectra was reached (Figure 3.).

4. CONCLUSIONS

A new isoquinoline sulfonamide **I** was efficiently synthesized using an environmentally benign cascade methodology and its radicalic behavior was investigated by EPR. Non-irradiated isoquinoline sulfonamide **I** polycrystal did not give any EPR signal and have stability. The radical generated on isoquinoline sulfonamide **I** and measurement at 150-340 K by gamma irradiation at EPR shows isotropic hyperfine coupling constants and g-factors were determined in this investigation. We observed that the simulation and experimental result are in good harmony. The simulation we used here, promises to be employed more efficiently on different substances as well.

5. ACKNOWLEDGE

REFERENCES

Alonso, R., and N-Garcia, O, 2013, *J. Org. Chem.,* Vol. 78, pp. 2564-2570.

Aras, E., Karatas, O., Meric, Y., Abbass, H.K., Birey, M., and Kılıç, A., 2014, *Radiat. Effects&Defects in Solids,* Vol. 169(9), pp. 754-758.

Asik, B., Aras, E., Caliskan, B., Eken, M., and Birey, M., 2004, *Radiat. Eff. Def. Solids,* Vol. 159, pp. 55-60.

Atherton, N.M., 1973, "Electron Spin Resonance", *John Wiley&Sons,* New York.

Brieger, G., and Bennett, J.N., 1980, *Chem. Rev.,* Vol. 80, pp. 63-97.

Ceylan, Usta, A., Usta, K., Durmaz, F., and Coskun, A.,2013, *J. Mol. Struct.,* Vol. 1050, pp. 69-72.

Ceylan, Y., Usta, K., Usta, A., Aydogmus, H.Y., and Guner, A., 2015, *J. Mol. Struct.,* Vol. 1100, pp. 180-183.

Chatterjee, D., and Mahata, A., 2004, *J. Photochem. Photobiol. A.,* Vol. 165, pp. 19-23.

Dereli, O., Türkkan, e., Özmen, A., and Yüksel, H., 2011, *Radiat. Phys. And Chems.,* Vol. 80, pp. 742-749.

Dieudonne-Vatran, A., Azoulay, M., and Florent, J.-C, 2012, *Org. Biomol. Chem.,* Vol.10, pp. 2683-2691.

Eaton, S.S., and Eaton, G.R, 2008, *R. Soc. Chem.,* Vol. 21, pp. 59-75.

Glushkov, V.A., and Shklyaev, Y.V., 2001, *Chem. Heterocycl. Compd.,* Vol. 37, pp. 663-687.

Gordy, W., 1980, "Theory and Applications of Electron Spin Resonance", *John Wiley&Sons,* New York, Toronto.

Greenfield, A., and Grosanu, C., 2008, *Tetrahedron Lett.,* Vol. 49, pp. 6300-6303.

Jafarppour, M., Rezaeifard, A., and Golshani, T., 2011, *Phosphorus, Sulfur Silicon Relat. Elem.,* Vol. 186, pp. 140-148.

Karatas, O. and Aras, E., 2012, *J. Mol. Struct.,* Vol. 1027, pp. 49-52.

Karatas, O, Aras, E., Karadag, A.H., and Islek, Y., 2016, *Radiat. Effects&Defects in Solids,* Vol. 171(7-8), pp. 651-657.

Luzzio, F.A., 2001, *Tetrahedron,* Vol. 57, pp. 915-945.

Padwa, A. And Flick, A.C., 2013, *Adv. Hererocycl. Chem,* Vol. 110, pp. 1-41.

Pettit, G.R., Meng, Y., Herald, D.L., Graham, K.A.N., Pettit, R.K., and Doubek, D.L., 2003, *J. Nat. Prod.,* Vol. 66, pp. 1065-1069.

Pshezhetskii, S. Ya., and Kotov, A.G., 1973, "EPR of Free Radicals in Radiation Chemistry", *John Wiley&Sons,* New York.

Sayin, U., Dereli, O., and Türkkan, E., 2012, *J. Mol. Struct.,* Vol. 1007, pp. 179-184.

Schindler, C.S. and Carreira, E.M., 2009, *Chem. Soc. Rev.,* Vol. 38, pp. 3222-3241.

Scozzafava, A., Owa, T., Mastrolorenzo, A., and Supuran, C.T., 2003, *Curr. Med. Chem.,* Vol. 10, pp. 925-953.

Supuran, C.T., Casini, A., and Scozzafava, A., 2003, *Med. Res. Rev.,* Vol. 5, pp. 535-558.

Takao, K.-i., Munakata, R. And Tadano, K.-i., 2005, *Chem. Rev.,* Vol. 105, pp. 4779-4807.

Usta, A., Filiz, A., Birey, M., and Ozmen, A., 2011, *Concepts Magn. Reason. Part A,* Vol. 38(3), pp. 102-106.

Weil, J.A., and Wertz, J.R., 1994, Electron Paramagnetic Resonance Elemantary Theory and Practical Applications, *John Wiley&Sons Inc.,* New York.

Yarbası, Z., Karabulut, B., and Karabulut, A., 2011, *Spectrochimica Acta Part A,* Vol. 83, pp. 337-339.

Yordanov, N.D. and Aleksieva, K., 2019, *Radiation. Phys. Chem.,* Vol. 78, pp. 213-216.

PANDEMİ SÜRECİNDE ONLİNE ANKET UYGULAMASI

¹Yalçın EZGİNCİ ᴵᴰ

¹Konya Teknik Üniversitesi, Mühendislik ve Doğa Bilimleri Fakültesi, Elektrik Elektronik Mühendisliği Bölümü, Konya, TÜRKİYE
¹ yezginci@ktun.edu.tr

ÖZ: Covid-19 pandemisi nedeniyle Üniversitemizde alt yapı imkânları nispetinde ve paydaşların etkin katılımı ile 23 Mart 2020 tarihinde uzaktan eğitime geçilmiştir. Elektrik ve Elektronik Mühendisliği Bölümünde Devre Analizi Laboratuvar dersi, dönem başından pandemi kısıtlamalarının başladığı tarihe kadar (ilk 5 hafta) normal yüz yüze laboratuvar uygulamaları olarak gerçekleştirildi. Pandemi kısıtlarından itibaren uzaktan eğitim, Öğretim Yönetim Sistemleri (ÖYS) üzerinden asenkron videolar, ders notları ve canlı ders uygulamaları ile yapılmıştır. Eğitimin değerlendirilmesinde, ara sınav ve final sınavları yerine, her bir öğrenciye farklı bir çalışma içeren ödev uygulaması tercih edilmiştir. Kamuoyunda uzaktan eğitim ve sınavları hakkında yapılan tartışmaların öğrencilerde bir karşılığının olup olmadığını araştırmak üzere 28 soru içeren bir anket hazırlanmıştır. Ankette öğrencilerin uzaktan eğitime katılım, eğitimin değerlendirilmesi ve derslerdeki uygulamaları içeren sorular yer aldı. Anket, ara sınavdan hemen sonra dersin ÖYS sayfalarında ilan edildi. Dersi alan öğrencilerin sayısı 115 ve ankete katılan öğrenci sayısı 42 olup ankete katılım oranı %36,5 olarak gerçekleşmiştir. Anket sorularına ait temel istatistikler ve bazı yorumlar çalışmanın sonuna eklenmiştir.

Anahtar Kelimeler: Anket, Koronavirüs (Covid-19), uzaktan eğitim, Laboratuvar Eğitimi, Moodle ÖYS, ödev.

Application of Online Survey during Pandemic

ABSTRACT: Due to the Covid-19 pandemic, distance education was started on March 23, 2020 with the active participation of stakeholders and in line with the infrastructure possibilities at our university. The Circuit Analysis Laboratory course in the Department of Electrical and Electronics Engineering was carried out as regular face-to-face laboratory practices from the beginning of the semester until the beginning of the pandemic restrictions (the first 5 weeks). Since the pandemic restrictions, distance education has been carried out over Learning Management Systems (LMS) with asynchronous videos, lecture notes and live course applications. In the evaluation of learning, each student was given a homework application containing a different study, instead of midterm and final exams. A questionnaire containing 28 questions was prepared to investigate whether the students also participated in the discussions about distance education and exams in the public. The questionnaire included questions about students' participation in distance education, evaluation of education, and practices in lessons. The questionnaire was announced on the LMS pages of the course right after the midterm exam. The number of students taking the course was 115, but the number of students participating in the survey was 42, and the rate of participation in the survey was 36.5%. Basic statistics and some comments regarding the survey questions have been added at the end of the study.

Key Words: Survey, Coronavirus (Covid-19), Distance Education, Laboratory Training, Moodle LMS, Assignments

GİRİŞ (INTRODUCTION)

Pandemide Uzaktan Eğitime Geçiş Süreci (Transition to Distance Education in Pandemic)

Yeni tip koronavirüs pandemisi, üniversitelerdeki eğitimi kesintiye uğrattı ve değişime zorladı (Tarhan, 2020). Bulaşma riski nedeniyle ve Sağlık Bilim Kurulunun önerisiyle önce 16 Mart'ta okullar bir haftalığına kapatıldı. Sonra yükseköğrenimde Uzaktan Öğretim Yol Haritası çizilerek (YÖK, 2020) beş alanda (Mevzuat, altyapı, insan kaynakları, içerik ve uygulama) gerekli düzenlemeler ve alınan kararlar çerçevesinde tüm öğretim kademelerinde 23 Marttan itibaren tamamen uzaktan eğitime geçildi. Eğitim faaliyetlerini, koronavirüs tehlikesine karşı, can güvenliğini riske atmadan bilgi ve iletişim teknolojilerine dayalı olarak sürdürme imkânının olması bu kararda etkili oldu (Emin, 2020). Okulların kapanmasının ani etkilerini hafifletmek ve eğitimin devamlılığını sağlamak üzere, uzaktan eğitim seçeneği kurumlar, yöneticiler ve uzmanlar tarafından da teşvik edildi (Unesco, 2020). Böylece Uzaktan Eğitimin, kriz süreçlerinde eğitimi destekleme, geliştirme ve etkinleştirme potansiyeline sahip olması vb. nedenler, uzaktan öğretim yaklaşımının kolay ve uygulanabilir çözüm olarak devreye girmesini sağlamıştır (Yamamoto, 2020).

Türkiye'de Uzaktan Eğitim (Distance Education in Turkey)

Yükseköğrenimde zaten var olan açık, uzaktan ve harmanlanmış eğitim sistemlerini yürüten Üniversiteler açısından, tamamen uzaktan eğitime geçiş kolay olmuştur. Kurumların hazır bulunuşluklarıyla orantılı olarak, özellikle üniversiteler hızlı bir şekilde uzaktan eğitime geçiş yapabildiler (Tarhan, 2020). Acil planlamalar ve mevcut yetenekler ortaya konarak kısa sürede gerekli tedbirler alındı ve uzaktan eğitim aktif hale getirdi (Dikmen ve Bahçeci, 2020). Bu sayede, belirli bir aşamaya gelmiş olan uzaktan eğitimde, koronavirüs baskısı ile dijital dönüşüm hızlanmıştır.

Türkiye'deki üniversitelerin çoğunluğu gerekli teknolojik alt yapıya sahip olması ve açık veya harmanlanmış eğitim uygulamalarını zaten yapıyor olmaları, uzaktan eğitime geçişi kolaylaştırdı. Ayrıca Yüksek Öğretim Kurulu (YÖK) 'nun iki yıl öncesinde uygulamaya koyduğu "Dijital Dönüşüm Projesi" ile yeni üniversitelerde bu açığı kapatma yolunda önemli adımlar atmıştı. Pandemide YÖK, eğitim ve öğretime muhtemel etkileri üzerine belli senaryolar üzerinde çalışma başlatmış ve üniversitelerdeki UZEM'ler (Uzaktan Öğretim Uygulama ve Araştırma Merkezinin) etkin hale getirilmiştir (YÖK, 2020). Bu süreçte yapılan araştırmalar, uzaktan eğitim merkezlerinin ders içerikleri, senkron eğitim ve altyapı başta olmak üzere, yoğun bir çalışma gerçekleştirdikleri, belli aşamaları kaydettikleri görülmekle birlikte, yeteri kadar uzman eleman, ders materyali ve sunum teknolojisi bakımından eksiklikleri olduğunu göstermiştir. Örnek olarak Articulate, Captivate, iSpring gibi zengin çoklu ortam araçları kullanılarak eğitim içerikleri hazırlanmalı ve bu sunumları yapacak öğreticilerin desteklenmesi gerekli görülmektedir (Yamamoto, 2020).

Uzaktan Eğitimin Yeterliliği (Competence of Distance Education)

Uzaktan eğitimde senkron dersler, eğitici ile öğrencilerin internet üzerinden canlı olarak karşı karşıya olduğu sınıf uygulamasıdır. Senkron ders için her iki tarafın hazır oluşlukları yanında teknolojik alt yapılarının uygunluğu da gerekir. Eğitici, normal ders anlatımının dışında, bir DJ gibi ders araçlarını kullanabilme ve online ortamda sınıfı yönetme becerilerini kazanmış olması gerekir. Online dersin, eğitici ile karşılıklı soru-cevap dışında yüz yüze derste yapılamayan anket, kısa sınav uygulamalarını gerçekleştirebilme avantajları vardır. Uzaktan eğitim sürecini başında kısa bir hazırlıktan sonra dersler çoğunlukla asenkron olarak ve ÖYS'nin tüm yetenekleri kullanılmadan yapıldı. Bunun yanında eğitimin ölçüm ve değerlendirmesi aşamasında bir miktar belirsizlik altında sınavlar etkin şekilde yapılamadı.

Toplum olarak, bu dönemde üniversitelerin ve özellikle Milli Eğitimin gerçekleştirdiği uzaktan eğitim uygulamaları tanınmış, uzaktan eğitim hizmetlerinin önemi anlaşılmış ve yapılabilirliği kabul edilmiştir. Bununla birlikte uzaktan eğitimde niceliğin yanında aynı zamanda niteliğin de önemi görülmüş ve

sorgulanmaya başlamıştır. Pandemi sürecinin uzaktan eğitim veren akademisyenler ve eğitim alan öğrenciler üzerindeki etkileri ve değişkenlerin aracılık rolünün araştırılması gerekli görülmüştür (Dikmen ve Bahçeci, 2020).

Pandemiden önce sınavlar örgün sisteme göre hazırlanmakta ve sınıflarda kontrollu ve şeffaf bir şekilde yapılmaktaydı. Bununla yanında harmanlanmış derslerde internet üzerinden dönem içi ödev ve kısa sınav gibi uygulamalar yine sınıfta ve belli kontroller dâhilinde idi. Pandemiye gelindiğinde dersler belli oranda gerçekleştirilebildi, ancak genel olarak sınavlarda yeterli denetim yapılamadı. Uzaktan eğitim için etkili bir şekilde ölçme ve değerlendirme kurgulanamadı. Çünkü kısa vadede geçici bir çözüm olarak bakıldı. Ancak pandeminin devamında, bu şekildeki uzaktan eğitimin sürdürülmesi mümkün değildir. Bu geçiş döneminin ardından süreklilik kazanacak olan ve yeni normal olarak adlandırılan devre için gerçekçi çözümler üretilmelidir. Her şeye rağmen salgın nedeniyle yaşadığımız bu zorunlu süreç bize, temel ve orta düzey eğitimin en azından bir bölümünün uzaktan eğitimle yapılabileceğini gösterdi. Yeni normal devrede yüz yüze eğitim daha az ama daha değerli hale geleceğini görebilmekteyiz. Nitekim bütün dünyada yüz yüze eğitimle uzaktan eğitimin iç içe olduğu karma bir modele doğru gidilmektedir. Covid19 salgının sağladığı adaptasyonla dijital öğrenme deneyimleri geliştirilecek ve dijital öğrenme, yenilenen teknoloji ve sistemlerin de katkısıyla işlevselliği artarak ana öğrenme yapısı haline gelecektir (Yamamoto, 2020). Bu sayede öğrencilere, sosyal ve duygusal öğrenme deneyimleri ile tasarım ve beceri aktiviteleri için zaman ve imkan kazandırma şansımız olacaktır.

Sınavlar, Öğrenciler, Beklentiler ve Anket (Exams, Students, Expectations and Survey)

Eğitimde ölçme ve değerlendirme, öğrenme sürecini, gelişimini ve ne ölçüde gerçekleştiğini bulmak, neyi ne kadar öğrendiğini belirlemek, eğitimin verimliliğini tespit etmek ve eğitim sürecindeki hataları ortaya çıkarmak için yapılmaktadır. Uzaktan eğitimde öğrencilerin öğrenme ihtiyaçlarını nasıl ve ne ölçüde karşılayabildiği, ne ölçüde geri besleme alınabildiği, ders başarılarını ölçme ve değerlendirme işlemlerinin nasıl gerçekleştirildiği hakkında ciddi belirsizlikler vardır ve bunlar hakkında kapsamlı araştırmalara ihtiyaç bulunmaktadır. Dijital dönüşümde etkili öğrenmenin nasıl olacağı, öğrenmenin gerçekleştiğinin nasıl ölçüleceği, sınav ve değerlendirmelerin nasıl yapılacağı sorularına en doğru cevaplar bulunmalıdır.

Kim ve diğ. (2008), öğrenci başarısının değerlendirilmesinin öğretimin ayrılmaz bir parçası olduğuna işaret ederek değerlendirmenin rolü ve çevrimiçi öğrenme ortamı içinde test, ödev, elektronik portföy, çevrimiçi tartışma, öz değerlendirme, takım ve akran değerlendirmesi yöntemlerinin kullanılılarak nasıl yapılması gerektiğini ayrıntılı bir şekilde ortaya koymuşlardır.

Karşılaştığımız kısıt ve problemleriyle yaşadığımız bu pandemi dönemi, eğitim örgütlerini öğretim yöntem ve tekniklerini değiştirmeye, programlarını gözden geçirmeye zorluyor. Bu yeni dönemde, kendi kimliğimizi koruyarak etkin bir biçimde yerimizi almalıyız. Öğrencilerimizi bir yandan çağın gereği dijital dünyaya hazırlarken, diğer yandan öz değerlerine sahip çıkan ve bu değerleri özümseyen, insanlığın ortak değeri olması gereken erdemlere sahip olarak yetiştirmeye çalışmalıyız (Dönmez, 2020).

Yükseköğretim Kurulu Başkanlığı, önlisans ve lisans programları için çevrim içi sınav ve ödev uygulamaları için tavsiye ve yönergeler yayınlamıştır. Buna rağmen, ülkemiz kamuoyunda pandemi döneminde yapılan internet tabanlı sınav uygulamalarına ilişkin sınavların güvenliği hakkında endişeler ve tartışmalar yer almıştır. Bu tartışmalarda, sınav sorularının sosyal medya gruplarında ve kapalı gruplarda paylaşıldığı, geçmiş yıllarda sorulmuş aynı soruların tekrar sorulduğu, ücret karşılığında başkasının yerine sınava girme olaylarının olduğu, yaygın bir şekilde kopya çekildiği, öğrenci başarısının objektif olarak belirlenemediği, soruların çözümlerine internet üzerinden kolaylıkla erişilebildiği iddia edilmektedir. Bu tür online ve denetimsiz sınavlarda, sınavın güvenliği ile güvenirliğinin sağlanması ve objektif bir uygulama olması bakımından gerekli koşulların sağlanması büyük önem taşımaktadır (Can, 2020).

Bu pandemide sürecinde sınavlar geleneksel alışkanlıklar etkisinde hazırlandı ve genelde denetimsiz bir şekilde gerçekleştirildi. Bu durumda öğrenmenin ne ölçüde sağlandığı doğal olarak bir sorgulama konusu haline geldi. Yapılan değerlendirme ile verilen notların adaletli olmadığı endişesini doğurdu.

Çünkü sınav yerine yapılan ödev veya online sınav uygulamaları bir şekilde etkisiz hale geldi, hatta bir formaliteye dönüştü. Bu ara dönemde bazı sınıflarda öğrencilerin, tüm derslerden AA başarı notu aldığı gözlemlendi. Bu durum yapılan eğitimin ve sınavların, güvenilirliğini ve geçerliliğini ciddi şekilde tehlikeye atmıştır.

Bu çalışmada zorunlu olarak aniden yapmak durumunda kaldığımız uzaktan eğitimin hakkında önemli bir paydaşı ve araştırılacak verilerin kaynağı durumunda olan öğrencilerle bir anket yaparak, onların görüşlerini almak ve sorunlar hakkında düşüncelerini ortaya çıkarmak amaçlandı. Malum olduğu üzere anket, doğrudan birincil kaynaktan düzenli ve sistematik bir veri toplama yöntemidir. Eğitim süreçlerini değerlendirmenin yollarından birisidir, ancak anketin iyi hazırlanması ve güvenilir olması gerekir. İnternet üzerinden yapılan anketler hızlı, etkin ve düzenli kayıtları nedeniyle önem kazanmaktadır (Ezginci, 2013).

Öğrenciler mail, sms, whatsApp ve cep telefonu üzerinden eğiticileri ile iletişim kurabilmektedirler. Anketin farkı ise dolaylı olarak ve kümülatif sonuçlara göre eğiticiye mesaj verebilme özelliğine sahip olmasıdır. Eğitici ile öğrenciler arasında daha objektif bir değerlendirme ve bir diyalog yolu olabilir. Anketlerin doğru bir şekilde düzenlenmesi ve değerlendirilmesi ile ihtiyaç duyulan çıkarımlar elde edilebilir. Böylece anket etkileşimini takiben sonuçların uygulamaya geçirilmesi, eğitimin sağlıklı yürümesine katkı sağlayacaktır.

MATERYAL VE METOD (MATERIAL AND METHOD)

Elk.-Elt. Mühendisliği bölümünde Devre Analizi Lab. Dersi, dönem başında ilk 5 hafta normal, yüz yüze laboratuvar uygulamaları olarak gerçekleştirilmiştir. Uzaktan eğitim başladıktan sonra dersler, Öğrenim Yönetim Sistemleri (ÖYS) üzerinden yürütüldü. Deney çalışmaları için videolar çekildi, ÖYS'ye aktarıldı ve asenkron olarak sistemde öğrencilere sunuldu. İlave olarak, canlı derslerde deney ile ilgili örnek soru çözümleri yapıldı, diğer yardımcı materyaller dosya olarak eklendi. Dönem başında yüz yüze eğitim sürecinde laboratuvar, deney öncesi, deney sırası ve deney sonrası çalışmaların değerlendirilmesi ile öğrencilerin performans notu belirlenmişti. Vize ve final sınavları, ödev uygulaması yöntemiyle yapıldı. Ara sınav notu, pandemiden önce aldığı performans notu %40 ve pandemide aldığı ödev notu %60 oranında etki etmesiyle elde edilmiştir. Pandemi sırasındaki ara sınav ödevinde, her öğrenci farklı olmak üzere bir konu derleme çalışması ile her öğrenci farklı konfigürasyonda bir DC devresine ait problemin analiz edilerek çözümü istenmiştir (Şekil 1). Derleme özeti, sınırlı bir konuda tanım, ilgili konuyu formül ve grafikle açıklama ve örnek bir problem çözümü içermekteydi.

OGRENCINO	Ödev konusu
111202009	DC da seri RC devresi, R üzerinde oluşan akım, gerilim
121202102	DC da seri RC devresi, C üzerinde oluşan akım, gerilim
121202103	DC da seri RC devresi, zaman sabiti, RC gerilim
131202110	DC da seri RL devresi, R üzerinde oluşan akım, gerilim
141202081	DC da seri RL devresi, L üzerinde oluşan akım, gerilim
151202035	DC da seri RL devresi, zaman sabiti, RL gerilim
151202052	AC seri RC faz ve fazör işlemleri
151202111	AC seri RL faz ve fazör işlemleri
151202113	AC seri RLC faz ve fazör işlemleri (VC > VL)

Şekil 1. Ara Sınav için Öğrenciler Verilen Derleme ödevi konu listesi
Figure 1. Compilation Homework Subject List Given to Students for Midterm Exam

Toplam katılımın 115 öğrenci olduğu ara sınavlarında, sınıfın yüz yüze laboratuvar performans not ortalaması, 29,9/40 (%75) ve bu notlara ait standart sapma 9,07 olarak bulunmuştur. Pandemi döneminde ara sınavda verilen ödev uygulamasına ait sınıf ortalaması ise, 44.2/60 (%74) ve bu dağılımın standart sapması 12,44 olarak gerçekleşmiştir. Buradan pandemi öncesi ve pandemi sonrası etkinliklerde elde edilen not başarı oranı yaklaşık aynı olmuştur. Bu sonuç her iki ödevin düzeyleri aynı olduğunun bir

göstergesi kabul edilebilir. Her iki grubun notları arasındaki ilişkiye (korelasyona) bakıldığında ise r=0,20 değeri elde edilmiştir. Bu sonuç iki değerlendirme yöntemi arasında anlamlı bir ilişki olmadığını söyler. Yani bu sonuca göre ilk uygulamada alınan notlar ile ikinci uygulamada alınan notların paralel olmadığını göstermektedir. Bir başka ifade her iki çalışmada öğrencilerin aynı oranda başarı göstermediklerini ifade etmektedir. Bazı öğrencilerin notu yükseldi, bazılarınki düştü, bazılarınki de aynı seviyede kaldı demektir. Bir başka yönden baktığımızda yüz yüzede yapılan uygulama ile ödev ile yapılan uygulamaya öğrencilerin reaksiyonu bir birinden farklı gerçekleşmiştir.

Anket soruları genel olarak öğrencilerin uzaktan eğitime katılımlarını, uzaktan eğitim programını değerlendirmelerini ve uzaktan eğitim uygulamasından memnuniyetlerini, yaşadıkları sorunlarını ve onların bakışı ile gördükleri eksikliklerini ortaya çıkarmayı amaçlamaktadır. Ayrıca pandeminin bu ilk döneminde tartışmalara konu olan sınav uygulamaları ve bu sınavların değerlendirilmesi, öğrenciler arasında nasıl bir yansıma oluşturduğu ortaya çıkarılmak istenmiştir.

Öğrencilerin bu süreçte yapılan uzaktan eğitim uygulamaları, ders ve sınavlar hakkındaki görüşlerini almak üzere Çizelge 1'de listesi verilen anket soruları hazırlanmıştır. Anket soruları genel etik konular, dersler ve sınavlar hakkında bazı öğrenci tutumlarını sorgulayan soruları içermektedir. Bu anket soruları üniversitenin ÖYS üzerine yüklenmiş ve Şekil 2'de gösterildiği gibi, online olarak öğrencilerin gönüllü kullanımına açılmıştır.

Şekil 2. Online Anket sayfasından bir kesit
Figure 2. A snippet of the Online Survey page

Çizelge 1'de verilen 28 adet anket sorusu ÖYS'de tek bir sayfa olarak öğrencilere sunulmuştur. Ankete katılan öğrenciler eksiksiz olarak tüm soruları işaretlemiştir. Sorular için 1 den 5'e -en olumsuzdan en olumluya- artan sırada seçenekler sunulmuştur. Dersi alan öğrencilerin sayısı, 115 ve ankete katılan öğrenci sayısı, 42 ve katılım oranı [42/(115) =%36,5] olarak gerçekleşmiştir. Anket çalışması, uzaktan eğitim sırasında ve vize sınavları yapıldıktan sonra başladı, final sınavlarına kadar devam etmiştir.

Çizelge 1'de anket sorularının yanı sıra, ankette elde edilen veriler kullanılarak, her bir ankete ait ortalama ve standart sapma değerlerine de yer verilmiştir. Bunlara ilaveten en yüksek ve en düşük değerli ortalama ve standart sapma değeri gösteren anketlerin grafik dağılımları da bulgular bölümünde gösterilmiştir.

Çizelge 1. Anket Soruları, Ortalama ve Standart Sapma Değerleri
Table 1. Survey Questions, Mean and Standard Deviation Values

| Sıra No	Anket Soruları (PD: Pandemi Dönemi)	Ortalama	Standart Sapma
1	PD'nde dersleri düzenli ve yoğun şekilde takip edebildinizmi?	3,14	1,18
2	Uzaktan eğitimde canlı dersler yeterli işlenebildimi?	3,4	1,15
3	Genelde Uzaktan eğitimde canlı derslere bağlanmakta sorun yaşadınız mı?	2	1,25
4	Ödev ve sınavların değerlendirmesinde objektif ölçüler bulunmalı ve adil olmalıdır.	4,29	0,94
5	Bazıları maharet sanıyor ama Kopya çekmek övünülecek bir şey değildir.	4,57	0,91
6	Kopya çekme ve paylaşımlar bir çeşit sahteciliktir ve haksızlığa sebeb olmaktadır.	4,52	1,06
7	Kopya çekenler az çalışan, notları düşük ve kendine güveni olmayanlardır	4,36	1,21
8	Bu yeni şartlar ve eğitim sistemi kopya çekmeye zorluyor	2,19	1,31
9	Sınav ve ödevlerden emeğimin karşılığını alamıyorum	2,33	1,36
10	Normal zamanda Öğrenciler zayıf almamak için kopya çekiyor	3,02	1,35
11	Sınav ve ödevlerde küçük hatalardan çok not kırılması bizi endişendiriyor	3,98	1,2
12	Bu dönem notlarım yükseldi	3,62	0,88
13	PD'nde genelde herkes kopya çekiyor ve paylaşıyor	2,02	1,22
14	Ödev ve sınavlar anlaşılır, yapılabilir ve bilgi-beceri seviyelerini ortaya çıkarabilir olmalıdır.	4,36	1,1
15	Kopya ve paylaşımlarda arkadaşların teşvik ve zorlaması oluyor	1,88	1,19
16	Sınav ve ödevler öğrenciyi ölçmekten ziyade, zor ve kopyacılığı teşvik edecek şekilde hazırlanmaktadır	2,43	1,29
17	Devre Analizi Lab dersinde öğretim elemanlarının performansını başarılı buluyormusunuz	3,67	1,16
18	Sizce Devre Analizi Lab dersinde vize notları çalışmayanla çalışanı ayrıştırdımı?	3,62	1,4
19	Genel olarak (pandemi haricinde) sınavlar ve değerlendirmeleri ezberciliği teşvik etmektedir	3,86	1,2
20	PD'nde yapılan ödev ve sınav uygulamaları araştırma yönümü artırmaya neden oldu	4,26	1,08
21	PD'nde yapılan ödev ve sınav uygulamalarında, normal duruma göre daha çok çalışma fırsatım oldu	3,88	1,31
22	PD'nde yapılan ödev ve sınav uygulamalarında verilen süreler tam olarak yeterli geldi	3,36	1,38
23	PD'nde yapılan ödev ve sınav uygulamaları (şu ana kadar yapılanlar) çok emek istiyordu, zorlandım	3,4	1,04
24	PD'nde yapılan ödev ve sınav uygulamaları kendimi gerçekleştirmeme ve geliştirmeme yardımcı oldu	3,79	1,09
25	PD'nde herbir ödev ve sınav için en fazla bir gün harcadım	2,31	1,35
26	PD'nde Ödev ve sınavları çoğunlukla ders notları ve internetten araştırarak yaptım	4,14	0,95
27	PD'nde Ödev ve sınavları çoğunlukla arkadaşlarıma danışarak yaptım	2,14	1,05
28	Sizce PD'nde Ödev ve sınavlar para karşılığı mı yapılmaktadır	1,55	1,02

BULGULAR (RESULTS)

Bu anket çalışması, dönem arasında aniden uzaktan eğitime geçiş yapıldığından, önceden hazırlığı ve tasarımı yapılamamıştır. Bu nedenle istatistiksel değerlendirmenin en temel iki parametresi olan ortalama ve standart sapma değerleri üzerinden, yüzeysel olarak, mümkün olabilen çıkarımlar ve yorumlar yapılmıştır. Çizelge 1 incelendiğinde, öğrencilerin anketlerdeki ilk üç soruya verdikleri cevaplardan, pandemi döneminde uzaktan yapılan eğitimde derse katılımın ve sağlanan eğitim uygulamaların yeterli görüldüğü anlaşılmaktadır. Anketteki 12. Soru olan "Bu dönem notlarım yükseldi" ifadesine verdikleri değerlendirme 3,62 ve buna ait standart sapma 0,88 olmuştur. Bu 12. soruya verilen notların dağılımı Şekil 3'de gösterilmiştir. Bu öğrencilerin en yüksek uzlaşı sağladığı sorudur. Değerlendirmelerde en çok standart sapmaya sahip olan, "Sizce Devre Analizi Lab. dersinde vize notları çalışmayanla çalışanı ayrıştırdı mı?" sorusudur, buna ait standart sapma 1,4 olarak gerçekleşmiştir.

Öğrenci görüşlerinin en çok sapma gösterdiği bu soruya verilen ortalama değerlendirme notu, ilginç bir şekilde i önceki soruda olduğu gibi 3,62 olmuştur (Şekil 4).

S.Sapma : 0.88 (En küçük)
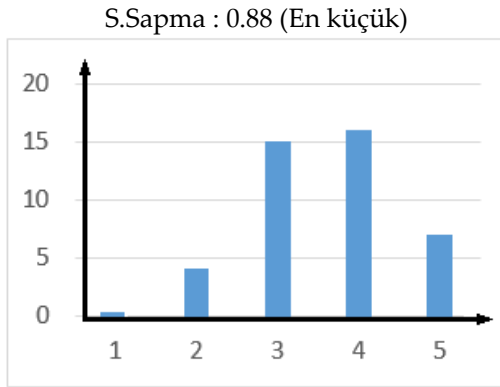
Şekil 3. 12 nolu anket dağılımı
Figure 3. 12. survey distribution

S.Sapma : 1.4 (En büyük)
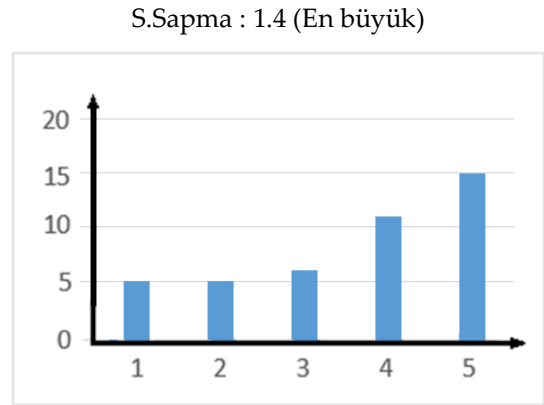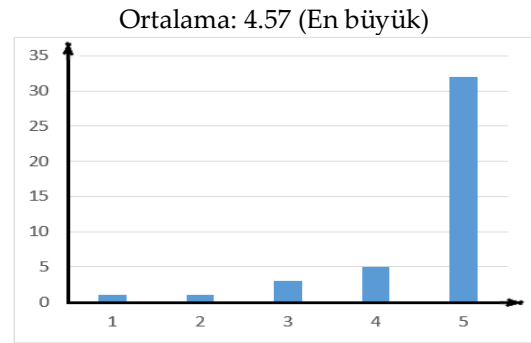

Şekil 4. 18 nolu anket dağılımı
Figure 4. 18. survey distribution

Anket soruları içinde en düşük ve en yüksek ortalama değerler, en dikkat çekici sorular olmak durumundadır. Şekil 5'de "Sizce PD'nde ödev ve sınavlar para karşılığı mı yapılmaktadır" sorusunun en düşük ortalama verilerek cevaplanmıştır. Şekil 6 ise ankette en çok geçen kopya ve internetten soru-cevap paylaşımı hakkında fikir verebilecek olan "Bazıları maharet sanıyor ama Kopya çekmek övünülecek bir şey değildir" sorusuna öğrenciler en yüksek değerlendirme ile hayır cevabı vermiş olmaktadırlar.

Ortalama: 1.55 (En küçük)
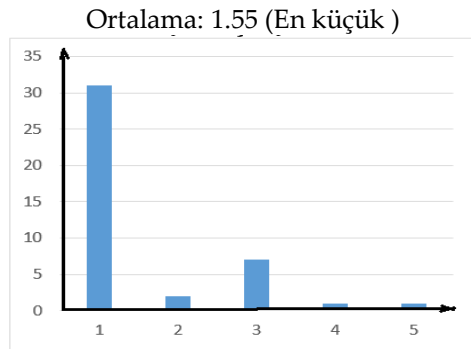


Şekil 5. 28 nolu anket dağılımı
*Figure 5. 28. survey distribution*

Ortalama: 4.57 (En büyük)

Şekil 6. 5 nolu anket dağılımı
Figure 6. 5. survey distribution

Ankette öğrencilerin uzaktan eğitim, etik değerler, okul ve dersler hakkındaki olumlu yön ile, buna karşın olumsuz durumları ifade eden sorular gruplandırılmış ve sonuçları Şekil 7'de gösterilmiştir. Olumlu yönde 5, olumsuz yönde 1, en iyi anlamındadır. İstatistikte her ikisi içinde standart sapma aynı çıkmıştır. Şekil 8'de farklı iki yönelimli anket sorusunun dağılımları karşılaştırılmak için aynı grafiğe yerleştirilmiştir. Olumlu yöndeki soru, "Uzaktan eğitimde canlı dersler yeterli işlenebildi mi?", olumsuz yönde beklenilenin sorusu "Genelde Uzaktan eğitimde canlı derslere bağlanmakta sorun yaşadınız mı?" şeklinde idi. Olumlu cevabın 5'e yaklaşması ile olumsuz cevabın 1'e yaklaşması aslında aynı cevap demektir ki bu anketi öğrencilerin dikkate alarak işaretleme yaptıklarının bir göstergesidir.
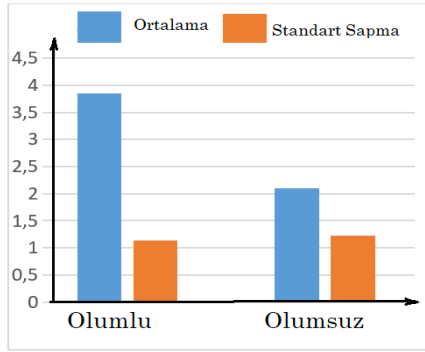
Şekil 7. Müsbet-Menfi kanaatler
Figure 7. Positive-Negative opinions
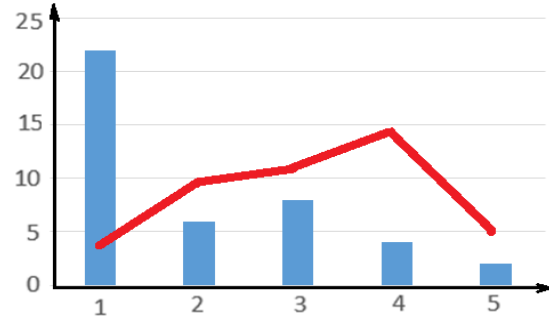
Şekil 8. Ters yönde benzer iki soruda dağılım
Figure 8. Distribution in two opposite similar questions

Anket sorularını kabul görmüş etik değerler, olaylara etki eden faktörler ve bunların sonuçları başlıkları atında gruplandırdığımızda Çizelge 2'yi elde ediyoruz. Çizelge 2'den idealler, etkenler ve neticeleri olarak veya yapılması gerekenler, etkenler altında bir miktar olumsuz etkilenerek sonuçlanıyor anlamı çıkarılabilir.

Çizelge 2. Etik değerler, etkenler ve neticeleri
Table 2. Ethical values, factors and consequences

Konu	Anket Soruları	Ortalama	Standart sapma
Kabul edilmiş ve etik değerler	4,5,6,7	4,435	1,03
Etkenler, faktörler	8,9,10,11,15,19	2,877	1,27
Sonuçlar, görüşler	12,20,21,24	3,887	1,09

Anket sorularından genel durum ve öğrenci görüşlerini almak olmasının yanı sıra, pandemide yapılan sınav ve ödevlerde öğrencilerin çözümleri paylaşmaları, bunların devamında normal bir not dağılımının oluşmaması nedeniyle eğitimi sorgulama amaçlı olarak hazırlanmıştır. Alınan cevaplara bakıldığında kopyacılığın etik olmadığı öğrenciler tarafından kabul edilmekte, ancak sınavlarda zorlandığı, zayıf alma endişesi, bazı arkadaşlarının yapması veya teşvik etmesi gibi etkenler nedeniyle kısmen kopya çekme ve soru-çözüm paylaşımı olduğu anlaşılabilmektedir. Ancak bu anket çalışmasına göre bu öğrenciler arasında sosyal medyada yer aldığı gibi para ile ödev veya soru yaptırılmadığı anlaşılıyor. Buradan bu yanlış tercihe gerek olmayacak şekilde, yani çok zor olmayan ve yapılabilir düzeylerde soru-ödev verildiği sonucu da çıkarılabilir.

Anketlerdeki bir başka dikkat çekici olumlu gözlemler ise, [20,21,22,23,24,26.] sorulara bakıldığında, PD'nde yapılan ödev ve sınav uygulamaları ile öğrencilerin, eğitimcileri memnun edecek davranışlar kazandığı söylenebilir. Bu davranışlar arasında araştırmaya daha fazla vakit ayırmaları, bazı derslere daha fazla çalıştığı, sınavlar için daha çok emek harcadığı ve emeklerinin karşılığını aldıklarına inandıkları gibi pozitif yorumlar elde edilmiştir.

SONUÇ ve TARTIŞMALAR (RESULTS and DISCUSSIONS)

Yapılan anket çalışmasında en yüksek, en düşük ortalama ve standart sapma gösteren sorular dikkat çekmektedir. En yüksek ortalama, kopyanın yanlış olduğunu (4,57) ifade eden 5. anket sorusudur. En düşük ortalama ise ödevlerin para karşılığı yapıldığı, 1,55 değerlendirmesi ile aslında ters yönde hayır cevabının verildiği sorudur. En yüksek uzlaşı ise notların yükseldiğini ifade eden 12 nolu soruda gerçekleşmiştir. En az uzlaşı ise sınavların çok çalışanla, az çalışanı ayırt etmesi ile ilgili olan 18. anket sorusudur. Öğrencilerin etik değerleri ifade eden anketlerde 4,44 değerlendirme ile uzlaşı içinde olmalarına rağmen başarıya etki eden faktörler bağlamındaki sorularda 2,8 değerlendirme ve 1,27'lik sapma ile görüş ayrılıkları olduğu görülmüştür. Bunlara ilaveten, anket sonuçlarından öğrencilerin uzaktan eğitime bağlanmakta ve uyum sağlamakta zorlanmadıkları, ödev ve sınav uygulamalarından

genel olarak memnun oldukları, normal döneme göre araştırma yapma imkanlarının ve isteklerinin arttığı şeklindeki olumlu çıkarımlar elde edilmiştir.

Koronavirüs salgını, ülkemizdeki eğitim kapasitesini ve üretebileceği tepkiyi ortaya koymuş, uzaktan eğitimdeki eksiklikleri ve geliştirilmesi gereken yönlerini göstermiştir. Yeni normale doğru giderken, her bir öğrenci için internet ve alt yapı erişim ve imkânının sağlanması, öğrenci merkezli eğitim, uzaktan eğitime uygun içerik ve materyallerin üretilmesi, ölçme - değerlendirme araç ve yöntemlerinin geliştirilmesi gerekmektedir.

KAYNAKLAR (REFERENCES)

Can E. (2020) Coronavirüs (Covid-19) pandemisi ve pedagojik yansımaları: Türkiye'de açık ve uzaktan eğitim uygulamaları, Açıköğretim Uygulamaları ve Araştırmaları Dergisi, AUAd 2020, Cilt 6, Sayı 2, 11-53

Dikmen S., Bahçeci F., Covid-19 Pandemisi Sürecinde Yükseköğretim Kurumlarının Uzaktan Eğitime Yönelik Stratejileri: Fırat Üniversitesi Örneği, Turkish Journal of Educational Studies, 7 (2) Mayıs 2020.

Dönmez B., "Pandemi döneminde uzaktan eğitim ve Türkiye'de eğitimin geleceği", https://www.hurriyet.com.tr/egitim/pandemi-doneminde-uzaktan-egitim-ve-turkiyede-egitimin-gelecegi-41529246 (Son Erişim tarihi: 6 Haziran 2020).

Emin M.N., Koronavirüs Salgını ve Acil Durumda Eğitim, SETA Perspektif, Nisan 2020, Sayı 268.

Ezginci Y., İnternet Destekli Temel Bilgisayar Bilimleri Dersinde Anket Uygulaması, Akademik Bilişim 2013 – XV. Akademik Bilişim Konferansı Bildirileri, sayfa 487-490, 23-25 Ocak 2013 – Akdeniz Üniversitesi, Antalya.

Kim N., Smith M.J., K. Maeng (2008) Assessment in Online Distance Education: A Comparison of Three Online Programs at a University, Online Journal of Distance Learning Administration, Volume X1, Number I, Spring 2008

Tarhan N., "Pandemi Döneminde Uzaktan Eğitimde Model Oluşturduk", https://uskudar.edu.tr/tr/icerik/5313/pandemi-doneminde-uzaktan-egitimde-model-olusturduk, (Son Erişim tarihi: 6 Haziran 2020).

UNESCO. (2020), "Education: From disruption to recovery", https://en.unesco.org/covid19/educationresponse (Son Erişim tarihi: 6 Haziran 2020).

Yamamoto G.T., Altun D., Coronavirüs ve Çevrimiçi (Online) Eğitimin Önlenemeyen Yükselişi, Üniversite Araştırmaları Dergisi, Nisan 2020, Cilt 3, Sayı 1, Sayfa: 25-34.

YÖK, 2020, Pandemi Günlerinde Türk Yükseköğretimi, https://covid19.yok.gov.tr/Sayfalar/HaberDuyuru/pandemi-gunlerinde-turk-yuksekogretimi.aspx, (Son Erişim tarihi: 15 Eylül 2020).

COMPARATIVE FAULT LOCATION ESTIMATION BY USING IMAGE PROCESSING IN MIXED TRANSMISSION LINES

[1]Serkan BUDAK [ID] , **[2]Bahadır AKBAL** [ID]

[1,2] *Konya Technical University, Engineering and Natural Sciences Faculty, Electrical and Electronics Engineering Department, Konya, TURKEY*
[1] sbudak@ktun.edu.tr, [2] bakbal@ktun.edu.tr

ABSTRACT: Overhead lines are generally used for electrical energy transmission. Also, XLPE underground cable lines are generally used in the city center and the crowded areas to provide electrical safety, so high voltage underground cable lines are used together with overhead line in the transmission lines, and these lines are called as the mixed lines. The distance protection relays are used to determine the impedance based fault location according to the current and voltage magnitudes in the transmission lines. However, the fault location cannot be correctly detected in mixed transmission lines due to different characteristic impedance per unit length because the characteristic impedance of high voltage cable line is significantly different from overhead line. Thus, determinations of the fault section and location with the distance protection relays are difficult in the mixed transmission lines. In this study, 154 kV overhead transmission line and underground cable line are examined as the mixed transmission line for the distance protection relays. Phase to ground faults are created in the mixed transmission line. overhead line section and underground cable section are simulated by using PSCAD/ EMTDC ™. The short circuit fault images are generated in the distance protection relay for the overhead transmission line and underground cable transmission line faults. The images include the R-X impedance diagram of the fault, and the R-X impedance diagram have been detected by applying image processing steps. Artificial neural network (ANN) and the regression methods are used for prediction of the fault location, and the results of image processing are used as the input parameters for the training process of ANN and the regression methods. The results of ANN and regression methods are compared to select the most suitable method at the end of this study for forecasting of the fault location in transmission lines.

Key Words: *Distance protection relay, Mixed transmission lines, Short circuit faults, Matlab regression learner, Fault location estimation, Artificial neural network*

Karma İletim Hatlarında Görüntü İşleme Kullanılarak Karşılaştırmalı Hata Konumu Tahmini

ÖZ: Havai hatlar genellikle elektrik enerjisi iletimi için kullanılır. Ayrıca XLPE yeraltı kablo hatları genellikle şehir merkezinde ve kalabalık alanlarda elektrik güvenliğini sağlamak için kullanılır, bu nedenle iletim hatlarında havai hat ile birlikte yüksek gerilim yeraltı kablo hatları kullanılır ve bu hatlar karma hatları olarak adlandırılır. Mesafe koruma röleleri, iletim hatlarındaki akım ve gerilim büyüklüklerine göre empedans tabanlı ölçüm sonucu arıza yerini belirler. Ancak yüksek gerilim kablo hattının karakteristik empedansı havai hattan önemli ölçüde farklı olduğundan, birim uzunluk başına farklı karakteristik empedans nedeniyle karma iletim hatlarında arıza konumu doğru bir şekilde tespit edilemez. Bu nedenle karma iletim hatlarında mesafe koruma röleleri ile arıza bölümünün ve yerinin tespiti zordur. Bu çalışmada, 154 kV havai iletim hattı ve yer altı kablo hattı, mesafe koruma röleleri için karma iletim hattı olarak incelenmiştir. Karma iletim hattında faz-toprak arızaları oluşturulur ve havai hat bölümü ve yeraltı kablo bölümü PSCAD / EMTDC ™ kullanılarak benzetimi yapılmıştır. Kısa devre

arıza görüntüleri, havai iletim hattı ve yer altı kablo iletim hattı arızaları için mesafe koruma rölesinde oluşturulur. Görüntüler, arızanın R-X empedans diyagramını içerir ve R-X empedans diyagramından elde edilen görüntüler görüntü işleme adımları uygulanmıştır. Arıza yeri tahmini için görüntü işleme sonuçlarından çıkarılan özellikler giriş parametresi olarak belirlenmiştir. Yapay sinir ağları (YSA) ve regresyon yöntemleri kullanılarak arıza yeri tahmini yapılmıştır. YSA sonuçları ve regresyon yöntemleri bu çalışmanın sonunda iletim hatlarında arıza yerinin tahmin edilmesi için en uygun yöntemin seçilmesi için karşılaştırılmıştır.

Anahtar Kelimeler: Mesafe koruma rölesi, Karma iletim hatları, Kısa devre arızaları, Regresyon metotları, Arıza yeri tahmini, Yapay sinir ağları

1. INTRODUCTION

Protection systems are one of the most important parts of power systems. Inside the protection and control systems used in the transmission of electrical energy, the most important task falls on protection relays.

Various places and various short circuit faults can occur in electrical power systems. When the causes of short circuit faults are examined, lightning strikes, high-speed winds, ice weight, earthquakes, fires, explosions, falling trees, flying objects, animals, people and other natural cases, as well as hardware failure, hardware aging, wrong hardware, wrong operation, wrong switching such as can cause. Protective relays are installed at different points and parts of the power system to make fast and selective protection.

Distance protection relays are one of the most preferred relays to protect transmission lines (Glover *et al.*, 2012). While distance protection relays are applied as main protection in transmission and distribution lines, they are widely used as backup protection for transformer, busbars and distant lines. Distance protection relays are adjusted to operate according to the impedance of the line by comparing the voltage and current values of the transmission line (Glover *et al.*, 2012). The distance of the point where the relay is connected to the fault is determined by measuring the impedance value. Short circuit impedance decreases at a certain rate as it approaches the feeding point of the line and thus the fault location is determined. Determining the fault location in transmission lines is an important feature used in protection systems. The increasing complexity of power transmission systems has greatly increased the importance of fault location investigation studies in recent years. If the location of a fault is known or can be estimate with high accuracy, the fault can be repair quickly. Quick troubleshooting is of great importance as it reduces customer complaints, downtime, operating cost, loss of revenue, and maintains the stability of the system.

Overhead line systems are dominant in the transmission of electrical energy. Overhead line systems are transmission lines that have proven their operational reliability and functional use. In addition, the installation costs of overhead lines are low and their useful life is high (Han and Crossley, 2013).

Nowadays, underground cables are used in distribution lines, especially in places where there is a high density of people, in order to ensure operational safety, human-environmental health and the economy of the enterprise. With new technological developments in insulation systems in high voltage XLPE underground cables, cables have been used in transmission lines. Underground power cable installations have started to replace some of the overhead transmission lines due to environmental factors in areas where the overhead line cannot pass and in densely populated areas (Han and Crossley, 2013).

When the operations of the distance protection relay in mixed transmission lines (lines consisting of overhead and underground cable sections) were examined, it was seen that it could not detect the correct fault location. Pinpointing the location of fault on transmission lines can significantly save labor force and speed up the repair process. For this reason, efforts are being made to use mixed transmission lines with high efficiency (Han and Crossley, 2013).

The main problem in transmission lines consisting of overhead lines with underground cables is that the positive and zero sequence impedance of underground cables and overhead lines are different. For

this reason, distance protection relays cannot accurately detect fault locations in mixed transmission lines. In mixed transmission lines, it is of major importance that the fault is in the overhead or underground cable line. Short circuit fault and failure to locate the fault cause many problems. Short circuit fault can occur in different ways in electrical installations. The sudden occurrence of short circuit in the form of impact causes the large short circuit currents passing through the circuit to be mechanically forced on the plant elements. Continuous short circuit currents passing through the circuit for a long time cause the plant elements to heat up and the material to be thermally forced. For this reason, both the facility and operating personnel may be harmed by this. As a result of the failures caused by the short circuit, the operation is partially or completely stopped and gradually the energy generation, transmission, distribution and consumption cannot continue normally.

In addition, the damage caused by the malfunction causes great repair costs. For this reason, fault and fault location that causes short circuit is of great importance. Artificial intelligence techniques have been used and recommended to quickly and accurately detect fault locations of faults in mixed transmission lines. Thanks to the artificial intelligence technique, the images obtained from the distance protection relay were processed and more accurate fault and fault location detection was made compared to conventional methods.

When the studies in the literature are examined, machine learning-based approaches (Ekici, 2012), (Livani and Evrenosoglu, 2013), (Thukaram *et al.*, 2005), (Khorashadi-Zadeh, 2004) and (Fan *et al.*, 2019) are also suggested to find transmission line failures. In Ekici (2012), proposes a support vector machine (SVM) to predict the transmission line fault location. It used a wavelet transform to process single-ended fault transient data and then used it as an input data set to the SVM network. In Livani and Evrenosoglu (2013), used the SVM network to predict fault locations with a separate wavelet transform to extract features from waves moving on arrival. In Thukaram *et al.* (2005), an ANN and SVM approach is presented to find errors in radial distribution systems. Unlike traditional fault section estimation methods, the proposed approach uses the measurements available at the substation, circuit breaker and relay situations. In Khorashadi (2004), A new scheme has been proposed for fast and reliable fault classification for a double-circuit transmission line. It has been shown that the algorithm can work quickly and accurately in different fault conditions such as fault type, fault resistance, fault initiation angle, fault location, pre-fault power flow direction and system short circuit level. In Fan *et al.* (2019), they offer a new single-ended fault location approach for transmission lines using modern deep learning techniques. They estimate the given error distance using single-ended voltage and current measurements.

Different techniques have been proposed in (Aziz *et al.*, 2006), (Niazy and Sadeh, 2013) and (Han and Crossley, 2013) when determining the fault location in mixed transmission lines. In Aziz *et al.* (2006), for transmission systems consisting of an overhead line coupled with an underground cable, a fault location diagram is proposed. Requires phasor synchronous measurements from both ends of the transmission line. In Niazy and Sadeh (2013), A new single-ended fault detection method has been proposed for underground cable coupled with overhead lines. In the proposed method, samples are taken from the transient voltages generated by the fault clearing action of the circuit breaker from the sending end of the cable line. When the wavelet transform is applied, the waves going to the fault detector are detected. The fault section, the overhead line section or the underground cable section is identified, and then the wave velocity is calculated and the fault location is accurately determined. In Han et al, proposed a new hybrid fault location scheme for fault section detection in a mixed transmission line (MTL) consisting of an overhead line (OHL) and an underground cable (UGC).

In this study, unlike the studies performed on mixed transmission lines, the fault location was estimated by using the R-X impedance diagram images of the distance protection relay at the time of short circuit by using ANN and Regression methods. ANN and Regression methods were compared with each other and the best method was determined. The use of image processing techniques and their comparison with different methods differs from other studies.

2. MATERIALS AND METHOD

Distance protection relays are used to protect transmission lines against short circuit faults and to determine the location of the fault. Since distance protection relays make impedance-based fault and fault location detection according to current and voltage magnitudes, it detects fault location in mixed transmission lines due to different impedance per unit length (Han and Crossley, 2013, 2015). In this study, images taken from the R-X impedance diagram were applied to image processing steps for short circuit faults occurring in the overhead transmission line and underground cable transmission line. Data sets were created to be used in ANN and Matlab Regression Learner applications. By comparing the performance results of ANN and Regression methods, fault location estimates are given in the results section of the study.

2.1. Mixed Transmission Lines

The underground cable line can replace a part of the existing overhead line in high voltage transmission lines, but the characteristic impedance of the cables differs according to the overhead line. The inductance of underground cable conductors is 30-50% less than an overhead line and its capacity is 30-40 times greater than an overhead line (Tziouvaras, 2006). Using the underground cable line and the overhead line together makes it difficult to determine the fault section and location in the transmission line (Tziouvaras, 2006).

Identifying the fault location accurately and quickly will reduce the costs of locating the fault. It will speed up the operations that need to be done quickly, such as repairing the fault and re-commissioning the transmission line, and reduce production, usage and income losses due to interruptions. For this reason, accurate and fast estimation and determination of the malfunction is very important in terms of operating continuity of the system, operating cost and operational safety.

2.2. Image Processing Method

Image processing is a method applied to obtain different information using different techniques over digitally transferred images. Image is used mathematically in the design and analysis of image processing systems. In the image processing method, many different information can be obtained that we cannot see with the eye.

When images are digitized using image processing method, a large size matrix is obtained. Using the large size matrix has a high error rate and long processing time during the training stage. For this reason, by applying various statistical methods, the matrix size is reduced and the processing time and error rate are reduced. This process is done by extracting the features of the images before proceeding to the training phase.

In this study, some statistical approaches used in feature extraction are used. With the Gray Level Co-occurrence Matrices (GLCM) function, we can obtain different statistical properties for each image. These are mean, entropy, variance, difference, contrast, inverse difference moment, energy, correlation, cluster shade, cluster prominence, sum entropy, sum mean, difference entropy, sum variance values. The training phase was started by extracting the statistical properties of 1x20 size images for each image (Budak and Akbal).

The training data set was created by using images image processing methods. The applied image processing steps are shown in Figure 1 (Budak and Akbal).
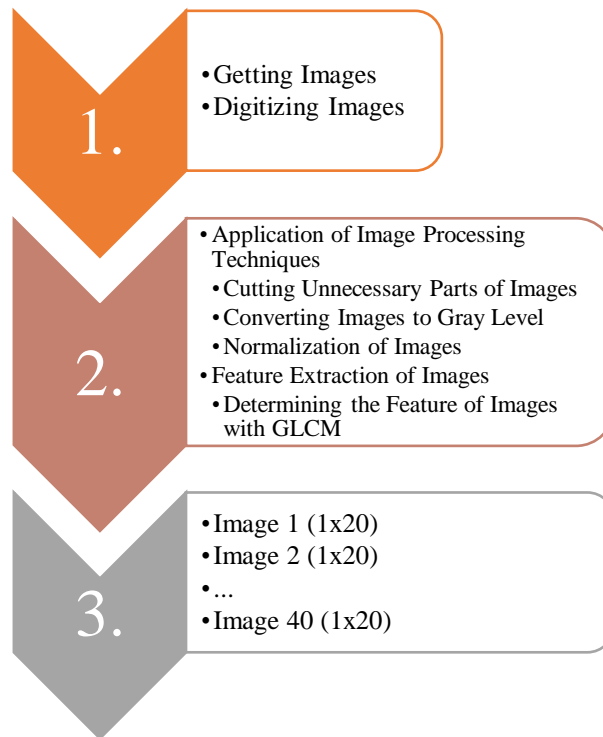
1.
- Getting Images
- Digitizing Images

2.
- Application of Image Processing Techniques
  - Cutting Unnecessary Parts of Images
  - Converting Images to Gray Level
  - Normalization of Images
- Feature Extraction of Images
  - Determining the Feature of Images with GLCM

3.
- Image 1 (1x20)
- Image 2 (1x20)
- ...
- Image 40 (1x20)

Figure 1. Applied image processing steps

2.3. Artificial Neural Networks

ANN emerged as a result of similarity with the working system of the human brain. It is an algorithm that resembles the working system of the human brain, which has abilities such as learning, associating, decision making, inference, recall, generalization, classification, new information generation, feature determination, optimization in computer environment.

In Figure 2, the general structure of ANN consists of three layers. These are the input layer, hidden layer, and output layer. The input layer has neurons that receive input from outside. Neurons in this layer transmit the input values to the hidden layer. A neuron in the hidden layer receives signals from all the neurons of the previous layer. After processing these neurons, it sends its output to all the neurons of the next layer. Output layer is a layer that contains neurons that transmit the outputs out. Neurons in the output layer process information from the hidden layer and output (Yegnanarayana, 2009).
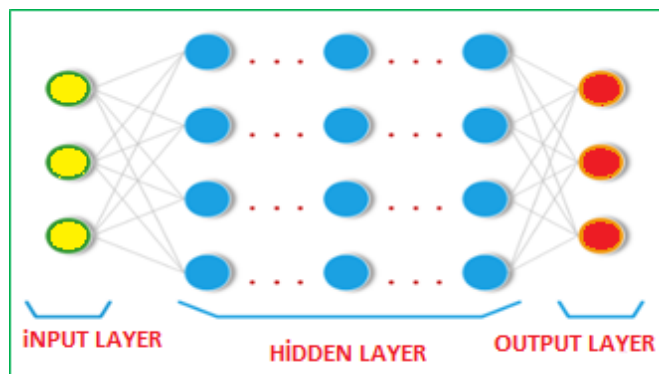

Figure 2. General structure of ANN

In ANN, the way the problem is given to the network, the structure of the network, the algorithm used, the learning strategy used by the network, the transfer function and learning rules affect the

performance of the network (Öztemel, 2012). In this study, various network types, learning functions, training functions and performance functions in ANN were tried to determine the most suitable network structure for the problem.

2.4. Matlab Regression Learner App

Regression Learner is an application that provides training, comparison and determination of the most appropriate method using machine learning methods widely used in the literature (MathWorks). Input and output data sets are given to the application, data is checked, features are selected, verification schemes are determined and performance results are obtained by training with different models. The results for each training model can be visualized as a Response Plot, Predicted vs. Actual Plot and Residual Plot. Performance criterion looked at to examine and evaluate the predictive accuracy of training models. Performance criterion determined the performance of the model and allow us to choose the best suitable model. The application also provides information on estimated training time and speed.

The training models used in Matlab Regression Learner application are Linear Regression, Tree, Ensemble Trees, Support Vector Machines (SVM), Gaussian Process Regression and their sub-methods (MathWorks). The best training model can be found automatically. In this way, there is no obligation to write separate and different code. It has the ability to automatically train and test multiple models at the same time (Özleyen, 2019).

2.5. Simulation Study

In the PSCAD ™ / EMTDC ™ simulation program, a mixed transmission line was formed by modelling 154 kV, 50 Hz, 200 km and 50 km two overhead transmission lines and 10 km of underground cable lines between the overhead lines. The transmission line is fed from two generator generation sources connected to two three-phase power transformers. For the overhead transmission line, 154 kV single circuit power transmission line, 1272 MCM conductor cross sections and 'PB' pole type are designed. 89/154 kV, 2XS(FL)2Y cable type is designed for underground cable transmission line. The low voltage side of the transformer has been selected as 11 kV delta, and the high voltage side as 154 kV star. A fixed load of 20 MW was used in the system (Budak, 2020).

In the study, the images of short circuit faults occurring both in the overhead transmission line and in the underground cable transmission line were observed in the R-X impedance diagram. Short circuit fault impedance is determined as constant $Zf=1\Omega$. Short circuit fault persists for 0.05 seconds and 0.3 seconds after the system operates for fixed periods. Studies have been carried out by creating a phase a-ground short circuit, which is the most common single-phase ground fault. Figure 3 shows the mixed transmission line model.
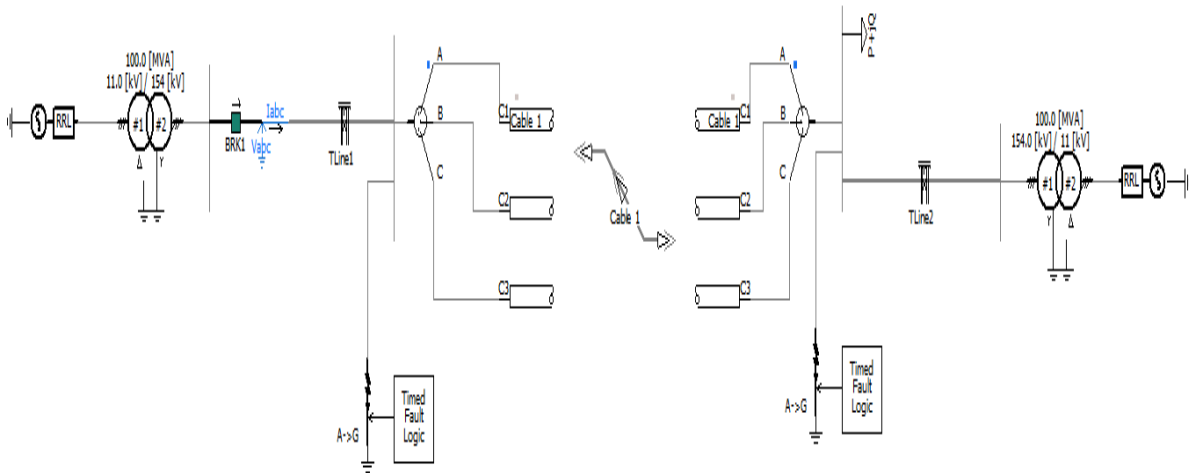
Figure 3. Mixed transmission line model

Figure 4 component computes the line-to-ground impedance as seen by a ground impedance relay.
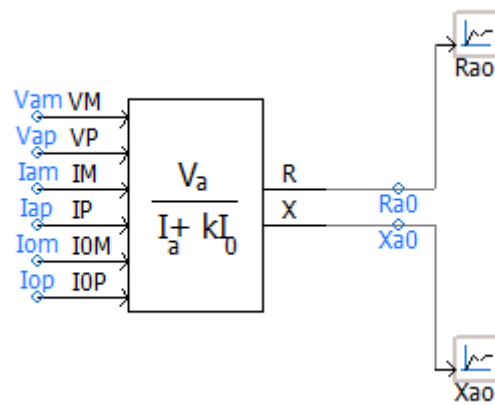

Figure 4. Line to ground impedance

The on-line ground impedance is calculated as follows Equation 1 :

$$Z_L = \frac{V_{phase}}{I_{phase} + k.I_o} \qquad (1)$$

Where,
$V_{phase} = Phase\ Voltage$
$I_{phase} = Phase\ Current$

$$I_o = \frac{1}{3}(I_A + I_B + I_C) \qquad (2)$$

$$k = \frac{Z_0 - Z_1}{Z_1} \qquad (3)$$

Z_o= Zero-sequence impedance as seen from the location of the relay to the end of the protected zone

Z_1= Positive-sequence impedance as seen from the location of the relay to the end of the protected zone

The Mho Circle component is classified as an 'Impedance Zone Element', which checks whether or not a point described by inputs R and X, lies inside a specified region on the impedance plane. R and X represent the resistive and reactive parts of the monitored impedance, and may be input in per-unit or ohms. Please note however, that the units of the component input parameters should match that of the R and X inputs. The component produces an output '1' if the point defined by R and X is inside the specified region, otherwise the output will be '0' (Yatendra *et al.*, 2019).
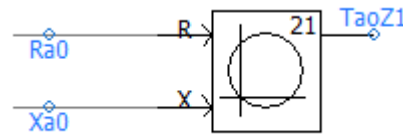
Figure 5. Mho circle

Figure 6 shows sample images occurring in phase a-ground short circuit faults formed at the 60th km of the overhead line section of the mixed transmission line and at the 5th km of the underground cable line section. Distance protection SIMENS SIPROTEC 7SA82 Sampling frequencies parameterizable from 1 kHz to 16 kHz high sampling frequency. The sampling frequency was chosen as 1 kHz in the study. Sampling Frequency is the number of data samples obtained per second.
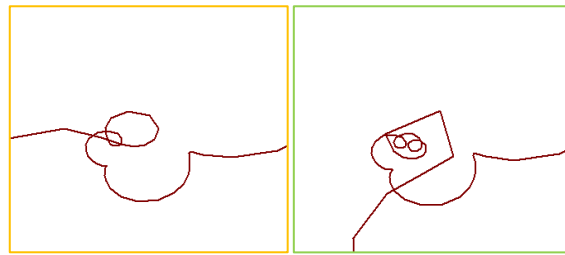

Figure 6. Sample images obtained from the R-X impedance diagram in mixed transmission lines

Root Mean Square Error (RMSE) and percentage error value were used to evaluate the results obtained in fault location estimation studies. The RMSE and error value are always positive, and close to zero indicates the best value. Equation 4 and Equation 5 contain percent error and RMSE equations, respectively (Karasu *et al.*, 2018).

$$\%Error\ Value = |\ \frac{Actual\ fault\ location - Calculated\ fault\ location}{Total\ length\ of\ the\ line} * |100 \qquad (4)$$

$$RMSE = \sqrt{\frac{\sum_{i=1}^{n}(xi - yi)^2}{n}} \qquad (5)$$

3. RESULTS

40 number phase a-ground faults were created at 5,10,15,… 200 km of the overhead transmission line simulated using PSCAD ™ / EMTDC ™ and 50 number phase a-ground faults were created at 0.2, 0.4,… 10 km of the underground cable transmission line.

In order to determine the fault location, three different network types, namely Feed Forward Backpropagation, Cascade Feed Forward Backpropagation and Elman Feedback Network, and five different training functions LM, CGB, OSS, GDX and SCG were used in the ANN. In the ANN model, the number of hidden layers, the number of neurons in hidden layers and which activation function will be used in hidden layers were determined by trial and error method. The tangent sigmoid activation function is used in the input and hidden layers of the specified network, and a linear activation function in the output layer. The number of neurons in the layers was determined as 1, 10 and 1, respectively. The iteration number was chosen as 1000. Of the 40 faults in the overhead transmission line data set, 32 were

used in the training set, 8 in the test set and of the 50 faults in the underground cable transmission line 40 were used in the training set and 10 were used in the test set.

In Table 1, the short circuit faults occurring in the overhead line and underground cable line are simulated and the methods and training errors used in the ANN are given (Budak, 2020).

Table 1. Methods and training errors used in ANN application

Method		RMSE OHL	RMSE UGC
Feed Forward Backpropagation	LM	**0.0048**	0.0082
	CGB	0.0106	0.0123
	OSS	0.0269	0.0176
	GDX	0.0124	0.0113
	SCG	0.0153	0.0098
Cascade Feed Forward Backpropagation	LM	0.0096	0.0139
	CGB	0.0106	0.0162
	OSS	0.0411	0.0159
	GDX	0.0400	0.0144
	SCG	0.0163	0.0151
Elman Feedback	LM	0.0062	0.0129
	CGB	0.0121	0.0135
	OSS	0.0146	0.0126
	GDX	0.0157	0.0110
	SCG	0.0143	0.0120

In Table 2, Fault location prediction training errors in overhead and underground cable transmission lines are given by using regression methods.

Table 2. Regression methods used and training errors

Method		RMSE OHL	RMSE UGC
Linear Regression	Linear	0.017721	0.010085
	Interactions Linear	0.025492	0.0064932
	Robust Linear	0.036589	0.010119
	Stepwise Linear	0.026962	**0.0060709**
Tree	Fine Tree	0.098382	0.061107
	Medium Tree	0.15016	0.12531
	Coarse Tree	0.23998	0.24734
SVM	Linear SVM	0.02837	0.016424
	Quadratic SVM	0.056601	0.020054
	Cubic SVM	0.21514	0.03174
	Fine Gaussian SVM	0.12044	0.071415
	Medium Gaussian SVM	0.065541	0.022517
	Coarse Gaussian SVM	0.06412	0.034763
Ensemble Trees	Boosted Trees	0.051223	0.046086
	Bagged Trees	0.075814	0.058129
Gaussian Process Regression	Spuared Exponential GPR	0.0078464	0.0092204
	Matern 5/2 GPR	0.010683	0.0087294
	Exponential GPR	0.023817	0.0093471
	Rational Quadratic GPR	0.0079423	0.0094911

Looking at the training errors obtained from ANN and Regression methods, the methods that give the best results were chosen. In Table 3 and Table 4, The estimation of fault locations are given as a result of short circuit fault occurring at the determined kilometres of the mixed transmission line and the percentage error values of these estimates.

Table 3. Estimated (km) fault locations and percentage error value as a result of short circuit occurring in overhead transmission line

Method	Fault Location (km)	Estimated Fault Location (km)	Error Value (%)
Feed Forward Backpropagation	20	19.1112	0.444
	45	42.4392	1.280
	70	70.3472	0.1736
	95	94.8647	0.0676
	120	119.8546	0.0727
	145	143.1658	0.9171
	170	169.8743	0.0628
	195	195.0882	0.0441

Table 4. Estimated (km) fault locations and percentage error value as a result of short circuit occurring in underground cable transmission line

Method used	Fault Location (km)	Estimated Fault Location (km)	Error Value (%)
Linear Regression Stepwise Linear	0.8	0.835775	0.357
	1.8	1.707975	0.921
	2.8	2.687975	1.121
	3.8	3.7623	0.377
	4.8	4.817025	0.17
	5.8	5.7321	0.679
	6.8	6.720675	0.794
	7.8	7.757025	0.43
	8.8	8.66965	1.304
	9.8	9.755	0.45

Figure 7 and Figure 8 show the graphics of the actual and estimate fault locations of the overhead and underground cable lines, respectively.
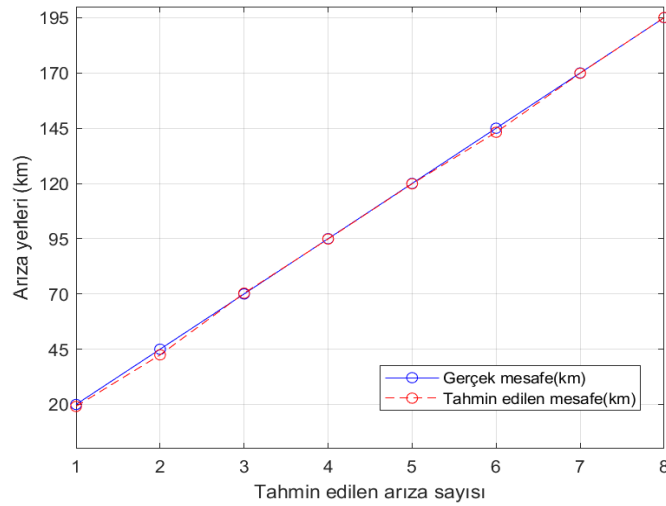
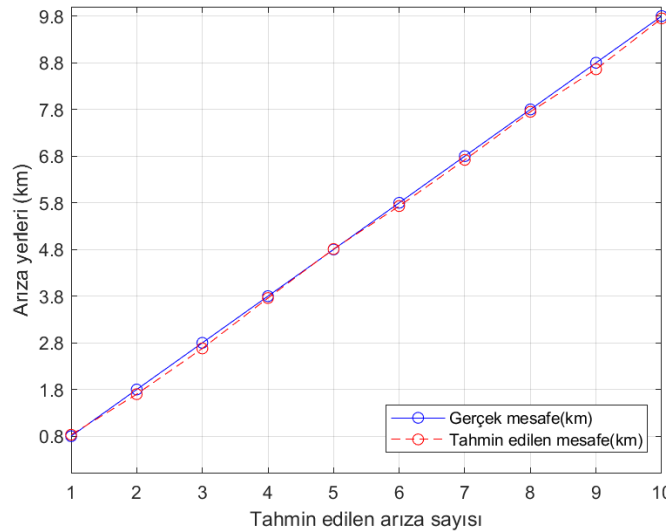**Figure 7.** Comparison graph of actual and estimated distances in overhead transmission lines

Figure 8. Comparison graph of actual and estimated distances in underground cable transmission lines

4. CONCLUSION

In this study, image processing is used for short circuit faults occurring in mixed transmission lines. The fault location was estimated using ANN and Regression methods. Considering the methods and training errors used as a result of the studies carried out on the mixed transmission line, it has been determined that the best training model is the Feed Forward Back Propagation LM network type in the overhead transmission line section. When we look at the underground cable line section, it was determined that the best training model was Linear Regression (Stepwise Linear). According to these results, it has been seen that better results can be obtained by using different methods.

According to the test results, the highest fault location estimation is 1.28% in the estimated distances in the overhead line section and 1.304% in the underground cable line part. In the study, fault location predictions can determine whether the fault is in the overhead line or underground cable line part in the case of short circuit failures occurring in the mixed transmission line and close to the actual fault location. Unlike other studies, high predictive values were obtained in different methods using image processing. The use of image processing in protection systems shows that it can be improved and used in different ways.

As a result, in long mixed transmission lines, in case of short circuit failure, the mixed transmission line does not affect fault location estimation studies and high predictive values are shown in the tables.

High estimation values, fast and accurate detection of the fault with artificial intelligence methods recommended in electricity transmission areas, rapid arrival of fault teams to the fault point, informing the fault in the overhead or underground cable line are of great importance. In addition, if the fault point is in the underground cable line, excavation works will take a short time. As a result, it can significantly save labor, speed up the repair process, and avoid large repair costs.

REFERENCES

Aziz, M. M. A., khalil Ibrahim, D., & Gilany, M. (2006). Fault location scheme for combined overhead line with underground power cable. *Electric Power Systems Research, 76*(11), 928-935.

Budak, S. (2020). *Karma iletim hatlarında mesafe koruma rölesi çalışmasının incelenmesi ve çalışma başarımlarının yükseltilmesi.* (Yüksek Lisans). Konya Teknik Üniversitesi Lisansüstü Eğitim Enstitüsü, Konya.

Budak, S., & Akbal, B. Fault Location Estimation by Using Machine Learning Methods in Mixed Transmission Lines. *Avrupa Bilim ve Teknoloji Dergisi*, 245-250.

Ekici, S. (2012). Support Vector Machines for classification and locating faults on transmission lines. *Applied soft computing, 12*(6), 1650-1658.

Fan, R., Yin, T., Huang, R., Lian, J., & Wang, S. (2019). *Transmission Line Fault Location Using Deep Learning Techniques.* Paper presented at the 2019 North American Power Symposium (NAPS).

Glover, J. D., Sarma, M. S., & Overbye, T. J. (2012). Power System. *Analysis and Design, Stamford: Cengage Learning*.

Han, J., & Crossley, P. A. (2013). *Fault location on mixed overhead line and cable transmission networks.* Paper presented at the 2013 IEEE Grenoble Conference.

Han, J., & Crossley, P. A. (2015). Traveling wave fault locator for mixed, overhead, and underground teed transmission feeders. *IEEJ Transactions on Electrical and Electronic Engineering, 10*(4), 383-389.

Karasu, S., Altan, A., Saraç, Z., & Hacioğlu, R. (2018). *Prediction of Bitcoin prices with machine learning methods using time series data.* Paper presented at the 2018 26th Signal Processing and Communications Applications Conference (SIU).

Khorashadi-Zadeh, H. (2004). *Artificial neural network approach to fault classification for double circuit transmission lines.* Paper presented at the 2004 IEEE/PES Transmision and Distribution Conference and Exposition: Latin America (IEEE Cat. No. 04EX956).

Livani, H., & Evrenosoglu, C. Y. (2013). A machine learning and wavelet-based fault location method for hybrid transmission lines. *IEEE Transactions on Smart Grid, 5*(1), 51-59.

MathWorks. Choose Regression Model Options. Retrieved from https://www.mathworks.com/help/stats/choose-regression-model-options.html

MathWorks. Train Regression Models in Regression Learner App. Retrieved from https://www.mathworks.com/help/stats/regression-learner-app.html#:~:text=Choose%20among%20various%20algorithms%20to,Models%20in%20Regression%20Learner%20App.

Niazy, I., & Sadeh, J. (2013). A new single ended fault location algorithm for combined transmission line considering fault clearing transients without using line parameters. *International Journal of Electrical Power & Energy Systems, 44*(1), 816-823.

Özleyen, Ü. (2019). *Hibrit güç sistemlerinde arıza tespiti.* (Yüksek Lisans). Fırat Üniversitesi Fen Bilimleri Enstitüsü, Elezığ.

Öztemel, E. (2012). Yapay Sinir Ağları, Papatya Yayıncılık Eğitim, 3. *Basım, İstanbul*.

Thukaram, D., Khincha, H., & Vijaynarasimha, H. (2005). Artificial neural network and support vector machine approach for locating faults in radial distribution systems. *IEEE Transactions on Power Delivery, 20*(2), 710-721.

Tziouvaras, D. (2006). *Protection of high-voltage AC cables.* Paper presented at the 59th Annual Conference for Protective Relay Engineers, 2006.

Yatendra, K., Tripathi, P., & Singh, R. (2019). *Impact of FACTS Device on Zonal Protection Scheme in Modified Dorsey-Chicago Transmission System.* Paper presented at the 2019 3rd International Conference on Recent Developments in Control, Automation & Power Engineering (RDCAPE).

Yegnanarayana, B. (2009). *Artificial neural networks*: PHI Learning Pvt. Ltd.

ANALYSIS OF ELECTRICAL ENERGY IN THERMOELECTRIC GENERATOR IN SANDWICH DESIGN

[1]Hakan TERZİOĞLU iD **, [2]Abdullah Cem AĞAÇAYAK** iD

[1]Konya Technical University, Faculty of Engineering and Natural Sciences, Department of Electrical-Electronics Engineering, Konya, TURKEY
[2] Konya Technical University, Vocational School of Technical Science, Department of Electrical, Konya, TURKEY
[1]hterzioglu@ktun.edu.tr, [2]acagacayak@ktun.edu.tr

ABSTRACT: Researchers and industry are seeking to manage energy better by increasing the efficiency of the energy system because of the increasing importance of energy in recent years. For this reason, a shift towards alternative energy sources to provide electricity has begun. As for alternative energy sources, interest in renewable energy sources is increasing day by day. Solar, wind and thermal sources are the most prominent renewable energy sources. Today we use of thermal sources in greenhouse, fish breeding, thermal facilities, city heating and electricity production. Nowadays, it is known that when we move thermal water from the source to the place to be used, it can be converted into electrical energy by utilizing the heat it emits around it. In this study, the effects of the type of the material and the placement of the thermoelectric generator (TEG) on the efficiency of two Thermoelectric Modules (TEM) were investigated by using thermal sources from renewable energy sources. Hot and cold water was passed through the sandwich blocks which were made from Copper, Aluminum and Brass materials, and the power produced in TEG was analyzed. As TEG, TEC1-12706 and TEC1-12710 materials were used. As a result of experimental studies, it is observed that the type of the material that conveys thermal water and the order of transmission of hot/cold water through sandwich blocks have an effect on the power produced by both TEC1-12706 and TEC1-12710

Key Words: Thermoelectric generators, output power and efficiency, renewable energy source.

Sandviç Tasarımı İçerisindeki Termoelektrik Jeneratörde Elektrik Enerjisinin Analizi

ÖZ: Son zamanlarda enerjinin gittikçe artan öneminden dolayı, araştırmacılar ve sanayi, enerji sisteminin verimliliğini artırarak enerjiyi daha iyi yönetmek istemektedirler. Bu nedenle elektrik enerjisini sağlamak için alternatif enerji kaynaklarına yönelim başlamıştır. Alternatif enerji kaynaklarından ise yenilenebilir enerji kaynaklarına olan ilgi her geçen gün artmaktadır. Güneş, Rüzgâr ve Termal kaynaklar yenilenebilir enerji kaynaklarının öne çıkanlarıdır. Günümüzde termal kaynaklardan seracılık, balık yetiştirme, termal tesisler, şehir ısıtması ve elektrik üretimi gibi birçok alanda faydalanmaktayız. Günümüzde termal suyu kaynağından faydalandığımız yere taşırken, etrafına yaydığı ısıyı elektrik enerjisine dönüştürebileceğimiz bilinmektedir. Bu çalışmada yenilenebilir enerji kaynaklarından termal kaynaklar kullanılarak, elektrik üretiminde termal suyun taşındığı malzemenin türünün ve Termoelektrik Jeneratörün (TEG) yerleşim şeklinin farklı iki Termoelektrik Modülün (TEM) verimi üzerindeki etkisi incelenmiştir. Sıcak ve soğuk su Bakır, Alüminyum ve Pirinç malzemelerinden oluşturduğumuz sandviç bloklardan geçirilerek TEG'de üretilen güç üzerindeki analizi gerçekleştirilmiştir. TEG olarak da TEC1-12706 ve TEC1-12710 malzemeleri kullanılmıştır. Yapılan deneysel çalışmalar sonucunda termal suyun geçtiği malzemenin türünün ve

sıcak/soğuk suyun sandviç plakalardan geçme sırasının hem TEC1-12706'nın hem de TEC1-12710'nun ürettiği güç üzerinde etkili olduğu görülmüştür.

Anahtar Kelimeler: *Termoelektrik jeneratörler, çıkış gücü ve verim, yenilenebilir enerji kaynağı.*

1. INTRODUCTION

Rapid population growth and industrialization in developing countries today cause a surge in demand for energy. Energy production is one of the main factors that reflect the economic and social development potential of a country. Therefore, energy and energy conversion systems that countries have in the world are considered as a measure of development. In order to meet the increasing energy demand with developing technology all over the world, studies are carried out to obtain efficient, cheap and clean energy from alternative energy sources. For this purpose, interest in alternative energy sources, renewable energy sources in particular, is increasing day by day.

In terms of usage, energy sources are divided into renewable and non-renewable energy sources. Non-renewable energy sources are fossil sources, such as coal, oil, natural gas, LPG and wood, which are expected to be consumed in the near future.

Nuclear energy which is again a non-renewable energy source is a type of energy that requires great attention in terms of production and recycling. Renewable energy sources are the resources that can be renewed in the future such as biogas, hydraulic, wind, sun, tidal wave energy, thermal (thermal), geothermal. Although other renewable energy sources are less than geothermal energy, they have negative effects on the environment. In addition, due to reasons such as the efficient use of these resources at specific time intervals, the inadequacy of their technologies and the high cost of their costs, scientists attach more importance to alternative energy sources such as geothermal energy (Champier, 2017;Terzioğlu *et al.*, 2018).

Geothermal energy does not have the potential to compete with non-renewable sources of energy. It is a type of energy that stands out with its pollutant-free, renewable, sustainable, domestic and environmentally friendly features when appropriate technologies are used. In this study, using thermal sources amongst renewable energy sources, the effect of the material conveying thermal water during electricity generation and the placement of Thermoelectric Generator (TEG) on the efficiency of two different TEGs were investigated (He *et al.,* 2017; Ağaçayak *et al.*, 2019; Çimen *et al.*, 2017). Apart from this, many studies have been carried out regarding the use of TEMs as TEGs. Some of these studies are related to obtaining electric energy with TEG at the same time from the heat obtained using solar energy. There are studies conducted about the waste heat is being used again to convert it to electricity while turning solar energy into another energy source. Some of these studies have investigated the design and test results of a combined system of thermosyphon and thermoelectric modules (TTM) to generate electricity from low-grade thermal sources such as a salt-layer solar pool. Thus, it is stated that it is possible to produce a completely passive and simple power supply system for field applications away from power lines using the temperature differences in the solar pool (Singh *et al.*, 2011; La Rocca *et al.*, 2017). In another study using solar energy, a simple arrangement of plane reflectors designed to receive maximum solar energy at noon was used to heat the TEG. Thus, it is determined how many TECs can be used with the energy produced by the models same as TEGs (Khattab and El Shenawy, 2006; Serbülent and Kemal, 2009; Tugay, 2010; Maneewan *et al.*, 2005). In some studies related to solar energy, energy recycle is examined by generating electricity with TEG from the waste heat generated during the production of electricity by PV panels (Champier, 2017; Omer *et al.*, 2017). Some of the solar-powered thermoelectric generator investigations have focused on mathematical modeling and experimental device development (Champier, 2017; Sun *et al.,* 2017). Studies have been carried out on the conversion of exhaust heat energy of vehicles' exhaust gas to electric energy using TEGs (Akçay, 2015; Kushch *et al.,* 2001). In some of these studies, it has been concluded that the output power of the TEG depends on the speed of rotation of the motor (Demir and Dincer, 2017; Kaya, 2010). It is stated that the energies obtained with TEGs can be used in battery charging systems of vehicles (Tie and Tan, 2013; (Kim *et al.*, 2017; Meng *et al.*, 2017). It is suggested

to use the finite time thermodynamics in the technical solution of recovery of waste heat from thermoelectric power generated by exhaust gas. There are also studies that analyze the effect of some key parameters such as exhaust gas inlet temperature, exhaust gas and heat transfer coefficient of the cooling water on the optimal length of the thermoelectric elements (Meng *et al.*, 2017). A TEG system focuses on the structure of the exhaust gas outlet duct in the application of automotive exhaust heat recycle and it has been evaluated the maximum net power output of an object that best suits its size with a sandwich-plate band exhaust exchanger taking into account the effect of exhaust temperature changes on the exhaust heat exchanger (He *et al*, 2017; Kim *et al.*, 2017; Meng *et al.*, 2017). TEGs are used in different systems and will continue to grow.

In the experiments we have done, a design that can be used in the production of electricity by TEM has been created. In the production of electrical energy from TEM, it was seen that the design of the plates in which the thermal water was applied was effective on the electrical energy produced. In the experiment that is carried out, the electric energy is produced by TEMs placed in hot-cold-hot plates and cold-hot-cold plates. Analyzes have been carried out on the power produced in the TEG with the mentioned connection types. At the same time, the effect of thermal water at different pressures on the power produced by TEC was also analyzed. As TEG, TEC1-12706 and TEC1-12710 materials were used. In the article, TEC1-12706 and TEC1-12710 are expressed as TEG-12706 and TEG-12710, respectively. As a result of the experimental studies made, it is seen that the hot-cold-hot connection type is more efficient.

2. THERMOELECTRIC MODULE

A thermoelectric module consists of a ceramic plate on two sides to provide heat conduction and electrical insulation as shown in Figure 1. Between these ceramic plates are P and N type semiconductors which are electrically connected to each other in series and thermally in parallel with copper conductors. While the heat is carried by electrons from the cold environment to the hot environment with the voltage from the direct current source, the transfer of heat from one end of the module to the other end shows the use of the thermoelectric modules as a thermoelectric cooler (TEC) (Terzioğlu and Ağaçayak, 2018; Ağaçayak *et al.,* 2017; Ağaçayak *et al.,* 2018;Terzioğlu, 2020).

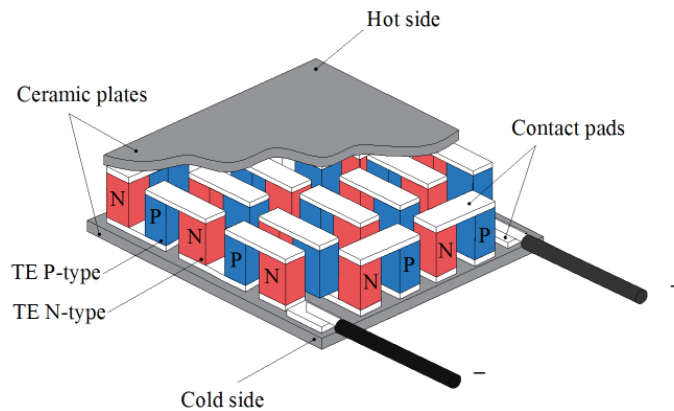**Figure. 1.** Structure of a TEM.

3. THERMOELECTRIC GENERATOR (TEG)

If one of the ceramic surfaces of TEM which is used as TEC by applying DC voltage to its ends is applied cold and the other one is applied hot, the temperature difference between the two surfaces is generated to produce a modular DC current as shown in Figure 2 and thus a thermoelectric power generator is obtained. DC current is generated by thermoelectrically generated electricity, and electrons

move through P and N type semiconductors as a result of heat flow (Demir and Dincer, 2017; Montecucco *et al.*, 2017; Hossam *et al.*, 2017).
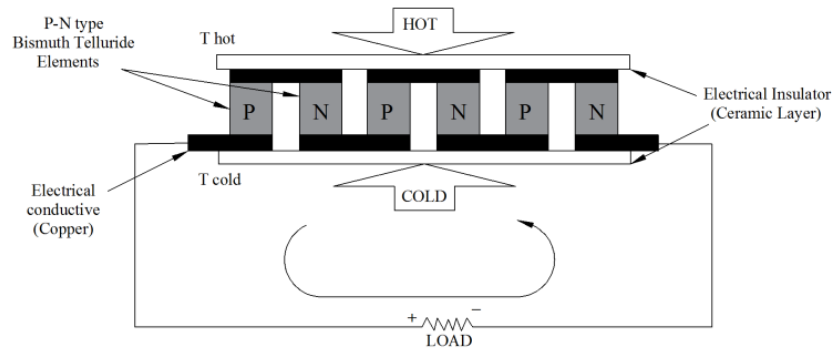

Figure. 2. Thermoelectric generator (TEG)

4. MATERIAL AND METHOD

In this study, a closed hot-cold water circulation system was designed and the TEMs were operated as TEG in the laboratory environment and electrical energy was produced. In the experimental system designed as a closed system, hot-cold water was passed from modules made of copper-aluminum and brass materials. Plates made of copper, aluminum and brass materials have formed sandwich blocks with 3in each. TEMs were placed between the plates in these blocks. Thus, the effect of the material in which the thermal water is conveyed on the power produced by the TEMs is determined. In addition, the effect on different TECs was examined using two different thermoelectric modules, TEG-12706 and TEG-12710, during the experiment.

In this study, thermal water was passed through it using a plate with sizes of 100x100x20 mm. In the designed plates, the distribution of the temperature on the plates was equal and the design characteristics were verified in another study (Yalçin *et al.*, 2016). These plates are made of 3 materials, copper, aluminum and brass. TEG-12706 and TEG-12710 were placed between the formed plates. In addition, as shown in Figure 3, a thermocouple temperature sensor was installed between the TECs placed on the surface of each plate to measure the plate temperature.

In Figure 3 there can be seen the 8 TECs placed between the plates and the shapes of copper sandwich blocks. Four of the 8 TECs used were connected in series to each layer in series. TEC electrical circuit connections were made in 2 groups connected in series by parallel connection. This design has been applied to each material type and TEC type in the whole system.
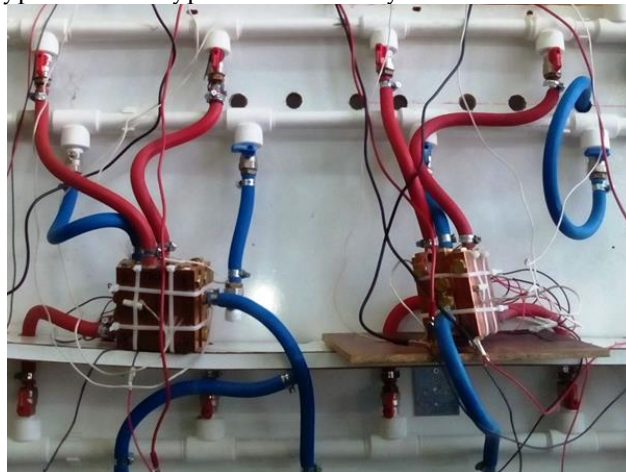

Figure 3. Image of sandwich blocks formed by TEG-12706 and TEG-12710, TEGs placed between copper

5. THE EXPERIMENTAL SETUP

The experimental setup used for the passage of the thermal water from the prepared blocks shown in Figure 4. In the experimental setup shown in Figure 4, two independent closed systems are designed for hot and cold water circulation. The red arrows show a closed system of hot water and the flow direction of the water, and the blue arrows show the closed system of cold water and the flow direction of the water. Hot and cold water circulation is provided by two separate WILO RSL 15 / 5-3 ku model 84W combi engines. In these closed systems, the hot and cold sides are supplied with water from outside and the pressure of the system is set as 1-2,5 and 3,5 bar. Thus, experiments were carried out at different pressure values. In the designed system, the hot and cold water entering the plates and the hot and cold water coming from the plates can be continuously measured with sensors.
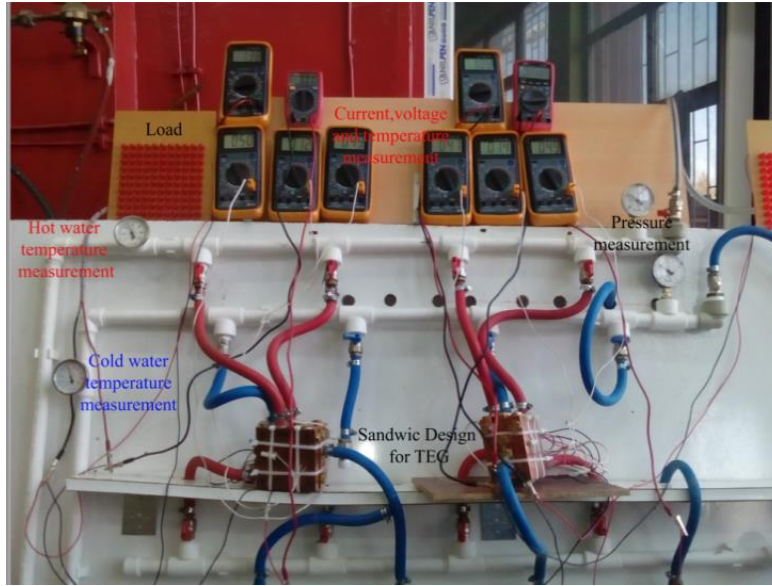
Figure 4. View of the connection of the system designed.

In order to obtain hot water in the designed system, two heat sources were used which are formed by connecting two heat exchangers in series. This allows the hot water in the system to reach the desired value faster. Since the water introduced to the system is influenced by both the plates where hot water is transmitted due to the fineness of the thermoelectric modules as well as from the plates where cold water is conveyed using a propeller heat exchanger to cool the cold water, it is ensured that it is held in a certain cold temperature by air. In the system, two expansion tanks are used separately for cold and hot closed water systems. Thus, the small water escaping from the system is replaced by the additional water from the water tanks and to keep the pressure at the same value for a long time. In the experiments, the temperature values on the plates and the voltage and current values produced by the thermoelectric modules were measured using measuring instruments. The charge obtained by connecting 121 red LEDs of 10mm in parallel to each other is connected to the output of the TECs to see if the system is operating under charge.

6. RUNNING THE EXPERIMENTATION

Experiments were carried out by connecting sandwich copper, brass and aluminum blocks to the system at 3 different motor speeds at 3 different pressures. In each experiment, 2 pieces of sandwich blocks from the same material and TEG-12706 to TEG-12710 were placed between these blocks and the power they produced at the same temperature and pressure were compared. Each sandwich block contains 8 pieces of TEC. Under these conditions, 18 experiments were conducted and the energy and power produced by the TECs were observed. In this study, when the pressures for each material type and TEC

ranges are 1-2,5 and 3,5 bar and the revolving speed motors are in the 1-2-3 level, 20 experiments were carried out on the sandwich blocks, each consisting of 3 plates, passing hot-cold-hot and cold-hot-cold water. Figure 5 shows hot-cold-hot and cold-hot-cold connected blocks. Experiments have been carried out to determine the effect of the type of material conveying thermal water on the power obtained from TEGs.

Figure 5. The image of sandwich blocks in the system with (a) hot-cold-hot (b) cold-hot-cold connection.

Starting from the initiation of the system in the experiments, the voltage (V), current (A) values and time obtained from the (TH) 81odüle hot surface, (TC) 81odüle cold surface and geothermal energy are measured until the hot water reach to 100 ^{0}C. In the experiments performed, the duration of completion of an experiment varies between 30 and 70 min. In experiments, considering that about %88 of geothermal energy in Turkey is low and medium temperature (30-100 ^{0}C), threshold is determined to be 100 ^{0}C.

7. EVALUATION OF EXPERIMENTAL RESULTS

Experiments at various speeds and pressures were carried out on the sandwich blocks formed with 3 plates consisting of 3 different materials in the experiment setup with the hot-cold-hot and cold-hot-cold connection. In the experiments performed, 20 tests were performed for each TEC module. The results of the experiments with the TEG-12706 module are given in Table 1. As shown in Table 1, while the temperature difference (T) between the surfaces is 65 ^{0}C, the passage of thermal water from different materials affects the power change. Table 1 shows that the rate of thermal water movement and the pressure are also effective on the power generated from the sandwich block of TEG-12706 with the hot-cold-hot connection type. As seen in Table 1, the best power in copper was recorded as 0,835 W when the motor speed was at the 3rd level and the pressure was 3,5 bar. It is seen that the best power in aluminum material is produced as 2,485 W when the speed of the motor is in 3rd level and the pressure is 3,5 bar. In case of brass material, it is seen that the best power is produced at 1,755 W when the speed of the motor is at 3rd level and the pressure is 3,5 bar. When Table 1 is examined, the water pressure and speed were influential depending on the material in which the thermal water was conveyed. Under these conditions, the highest power of 3 different materials was obtained with Aluminum at 3,5 bar as 2,485 W.

Table 1. TEG-12706 power(W) values at ΔT = 85 ^{0}C for hot-cold-hot connection.

Motor Speed	Copper Plate		
	1 Bar	**2,5 Bar**	**3,5 Bar**
I	0,495 W	0,599W	0,621W
II	0,465W	0,535W	0,6463 W
III	0,516 W	0,504 W	0,835 W
Motor Speed	**Aluminum Plate**		
	1 Bar	**2,5 Bar**	**3,5 Bar**
I	2,054 W	2,216 W	2,211W
II	2,171 W	2,189 W	2,128 W
III	2,148 W	2,191 W	2,485 W
Motor Speed	**Brass Plate**		
	1 Bar	**2,5 Bar**	**3,5 Bar**
I	1,278 W	1,431 W	1,369 W
II	1,335 W	1,53 W	1,57 W
III	1,472 W	1,53 W	1,755 W

The current-voltage and power graphs of the experiments in which the highest power among the three different materials are obtained in the tests performed in the sandwich block of TEG-12706 with hot-cold-hot connection type are given in Figure 6-8.
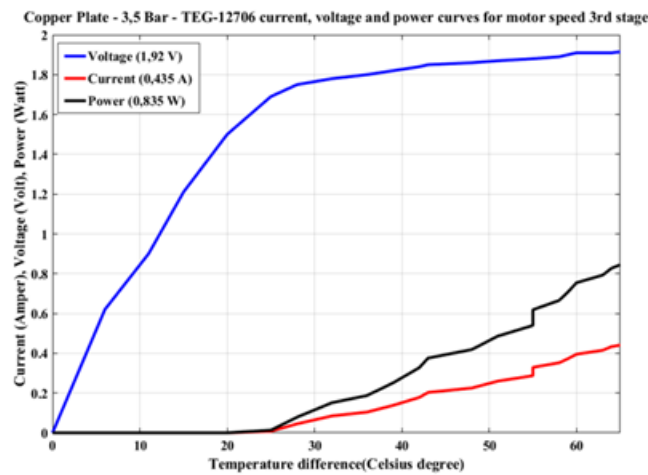
Figure 6. TEG-12706 current, voltage, power curves of Copper Material in Hot-Cold-Hot Sandwich Block Connection Type - 3,5 Bar pressure - Motor Speed at 3rd level.
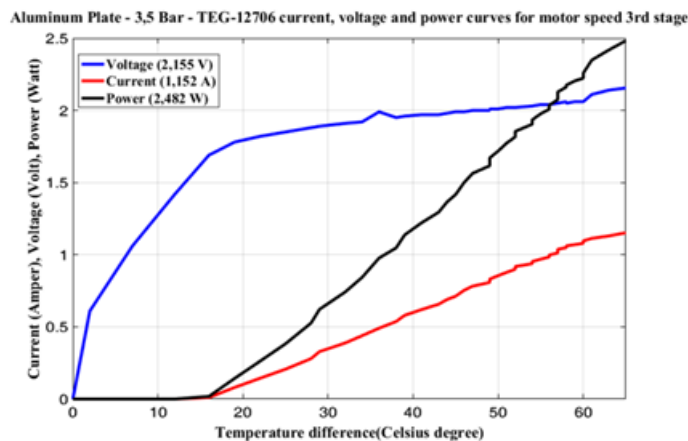
Figure 7. TEG-12706 current, voltage, power curves of Aluminum Material in Hot-Cold-Hot Sandwich Block Connection Type - 3,5 Bar pressure- Motor Speed at 3rd level.
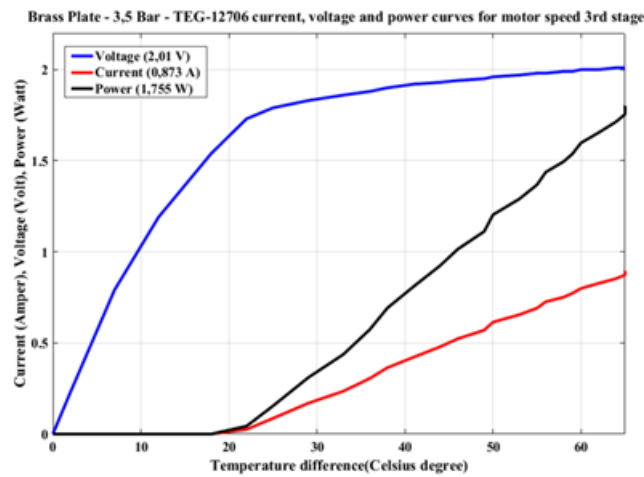
Figure 8. TEG-12706 current, voltage, power curves of Hot-Cold-Hot Sandwich Block Connection Type Brass Material - 3,5 Bar pressure- Motor Speed at 3rd level.

In Figure 9, the highest power values of the tests performed in the type of hot-cold-hot connection of sandwich block TEG-12706 appear as a single graph. As can be seen in Figure 9, the highest power is achieved when thermal water is passed through the Aluminum material. Also, the earliest power value was obtained from the experiment with aluminum when the temperature reached 15 ^{0}C.
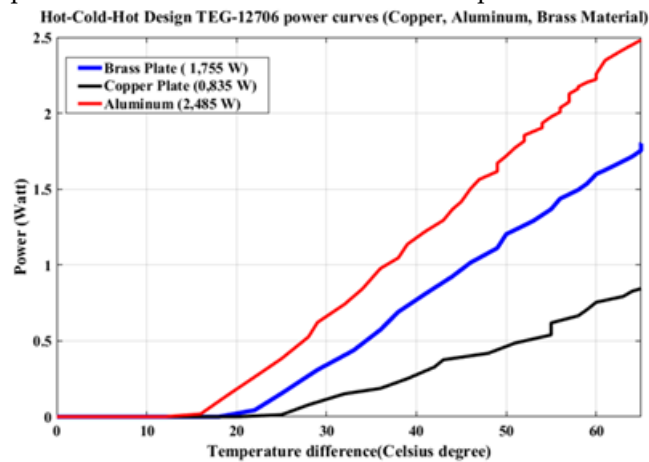
Figure 9. Power curves for TEG-12706 in Hot-Cold-Hot Sandwich Block Connection Type with Copper-Aluminum-Brass Material.

The results of the sandwich block TEG-12706 sandwich block cold-hot-cold connection tests are given in Table 2. In Table 2, it is seen that the best power in copper material is produced as 0,914 W when the speed of the motor is at 1st level and the pressure is 3,5 bar. It is seen that the best power in aluminum material is produced as 2,416 W when the speed of the motor is at 2nd level and pressure is 1 bar. In brass, it is seen that the best power is produced as 2,538 W when the speed of the motor is at 3rd level and the pressure is 1 bar. As seen in Table 2, the highest power was obtained as 2,538 W when the thermal water was passed through Brass, the pressure is 1 bar and motor power is at 3rd level. When these values are compared with the hot-cold-hot connection type given in Table 2, it is seen that the change of the connection type of the sandwich blocks is also influential on the power produced by TEG-12706.

Table 2. TEG-12706 power(W) values at ΔT = 65 ⁰C for cold-hot-cold connection.

Motor Speed	Copper Plate		
	1 Bar	2,5 Bar	3,5 Bar
I	0,914 W	0,514 W	0,532 W
II	0,603 W	0,501 W	0,495 W
III	0,594 W	0,51 W	0,556 W
Motor Speed	Aluminum Plate		
	1 Bar	2,5 Bar	3,5 Bar
I	1,725 W	1,593 W	1,488 W
II	2,416 W	1,654 W	1,532 W
III	1,738 W	1,601 W	1,59 W
Motor Speed	Brass Plate		
	1 Bar	2,5 Bar	3,5 Bar
I	1,65 W	1,599 W	1,502 W
II	1,622 W	1,702 W	1,602 W
III	2,538 W	1,734 W	1,527 W

The current-voltage and power graphs of the experiments in which the highest power is obtained from 3 different materials within the sandwich block of TEG-12706 are shown in Figure 10-12.
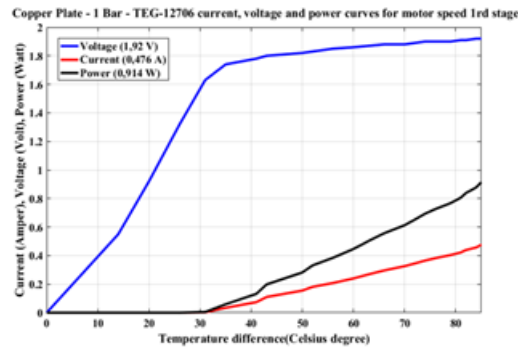
Figure 10. TEG-12706 current, voltage, power curves for Copper Material in Cold-Hot-Cold Sandwich Block Connection Type - 1 Bar pressure- Motor Speed at 1st level
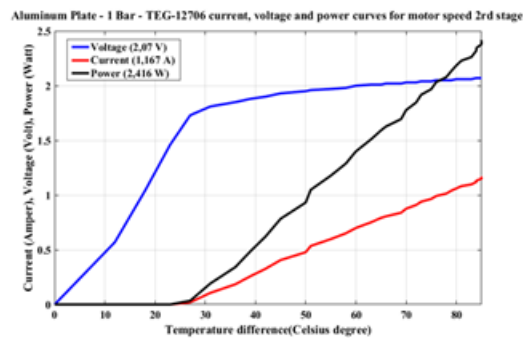
Figure 11. TEG-12706 current, voltage, power curves for Aluminum Material in Cold-Hot-Cold Sandwich Block Connection Type - 1 Bar pressure - Motor Speed at 2nd level
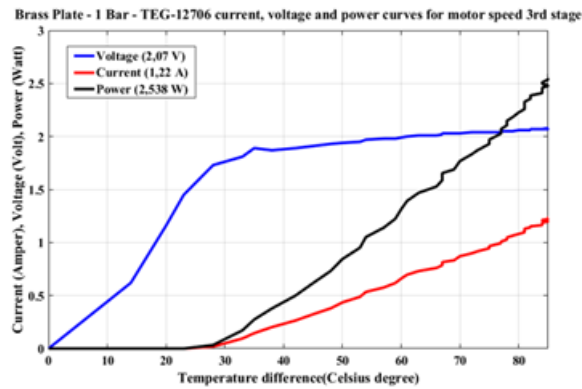
Figure 12. TEG-12706 current, voltage, power curves for Cold-Hot-Cold Sandwich Block Connection Type with Brass Material - 1 Bar pressure - Motor Speed at 3rd level.

In Figure 13, the highest power values of the experiments carried out when the sandwich block consisting of TEG-12706 was cold-hot-cold connection type are seen as a single graph. As seen in Figure 13, the highest power is obtained when the thermal water is passed through the Aluminum material. Also, the earliest power value was obtained from the experiment with rice when the temperature reached at 19 ^{0}C.
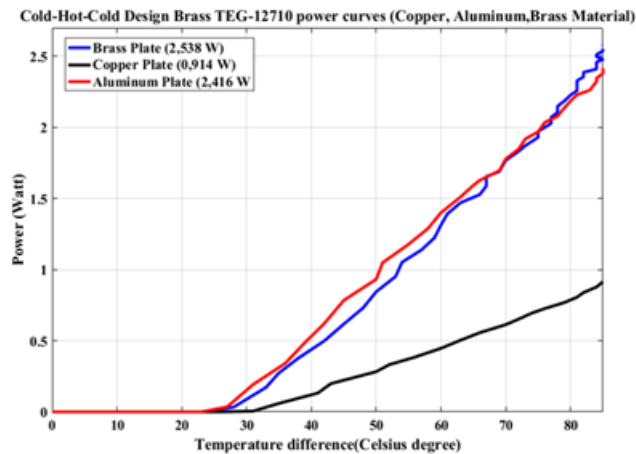

Figure 13. Copper-Aluminum-Brass Material power curves for TEG-12706 with Cold-Hot-Cold Sandwich Block Connection Type.

The results of the experiments made on the sandwich block with hot-cold-hot connection type TEG-12710 are given in Table 3. As shown in Table 3, the best power of 3 material types was obtained when the motor speed was at 3rd level and the pressure was 3,5 bar. It is observed that the maximum power produced were 1,66 W with copper structure, 3,524 W with aluminum structure, and 3,2494 W with the brass structure under these conditions. As shown in Table 3, the highest power was obtained as 3,524 W, at the pressure of 3,5 bar when the thermal water was passed through the Aluminum, and the motor speed was at 3rd level. As shown in Table 3, the highest power rating was obtained at 3,524 W, when the thermal water was passed through Aluminum, the pressure was 2,5 bar and motor speed at 3rd level.

Table 3. TEG-12706 power(W) values at $\Delta T = 85\ ^0C$ for hot-cold-hot connection.

Motor Speed	Copper Plate		
	1 Bar	2,5 Bar	3,5 Bar
I	0,539 W	0,598 W	0,998 W
II	0,558 W	0,676 W	1,036 W
III	0,539 W	0,558 W	1,666 W
Motor Speed	Aluminum Plate		
	1 Bar	2,5 Bar	3,5 Bar
I	3,213 W	3,045 W	3,544 W
II	3,315 W	3,03 W	3,2395 W
III	3,161 W	3,524 W	3,45 W
Motor Speed	Brass Plate		
	1 Bar	2,5 Bar	3,5 Bar
I	1,369 W	1,721 W	1,412 W
II	1,5461 W	1,8 W	1,1376 W
III	1,566 W	1,898 W	2,567 W

The current-voltage and power graphs of the experiments in which the highest power is obtained from three different materials from sandwich blocks made of TEG-12710 in hot-cold-hot connection type are given in Figure 14-16.
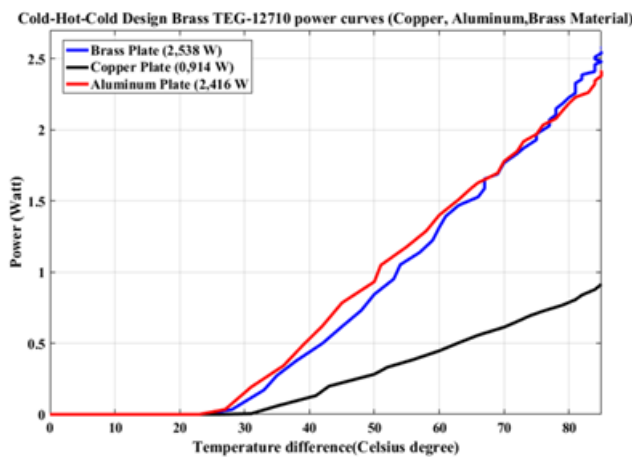
Figure 14. TEG-12710 current, voltage, power curves for Copper Material in Hot-Cold-Hot Sandwich Block Connection Type - 3,5 Bar pressure - Motor Speed at 3rd level.
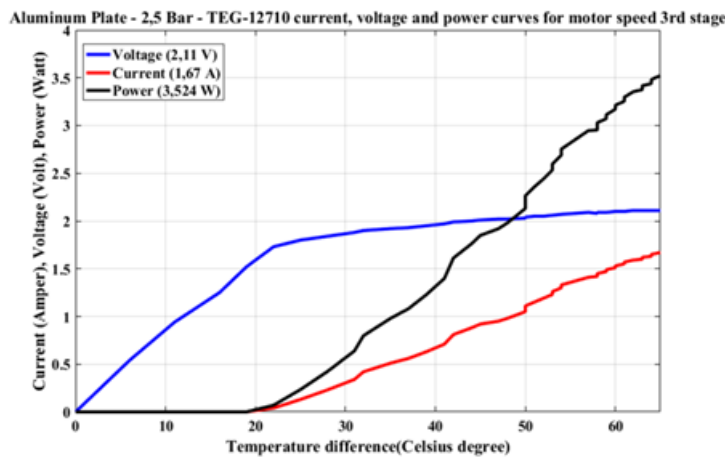
Figure 15. TEG-12710 current, voltage, power curves for Aluminum material in Hot-Cold-Hot Sandwich Block Connection Type - 2,5 Bar pressure - Motor Speed at 3rd level.
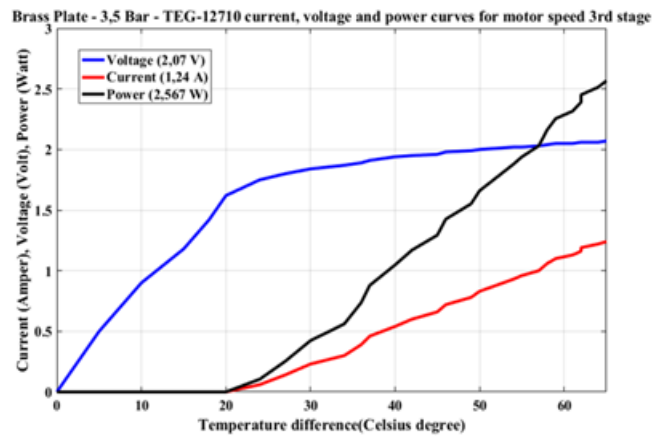
Figure 16. TEG-12710 current, voltage, power curves for Brass Material in Hot-Cold-Hot Sandwich Block Connection Type - 3,5 Bar pressure - Motor Speed at 3rd level.

In Figure 17, the highest power values of experiments performed using TEG-12710 appear as a single graph. As can be seen in Figure 17, the highest power is obtained when the thermal water is passed through the Aluminum material. Aluminum and brass are very close to each other in power generation, but the performance of copper is low compared to them. In addition, the earliest power value was obtained when the temperature reached 21 ^{0}C in the experiments with Aluminum and Brass
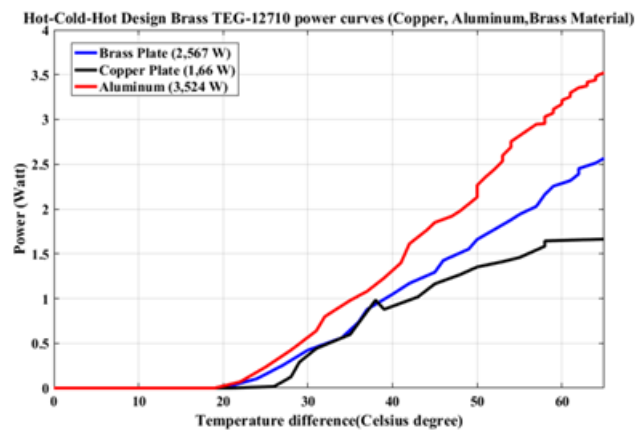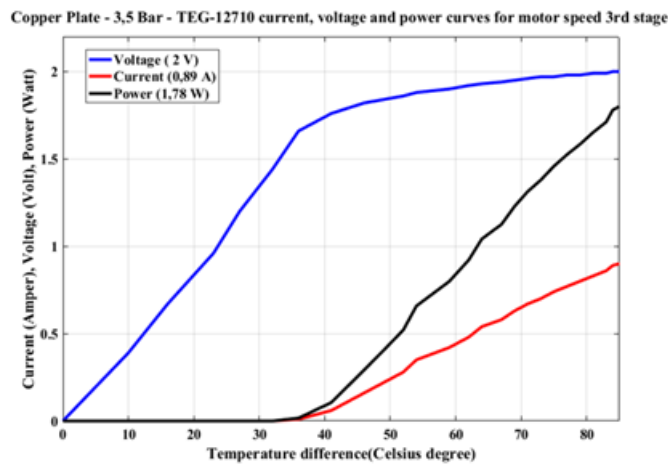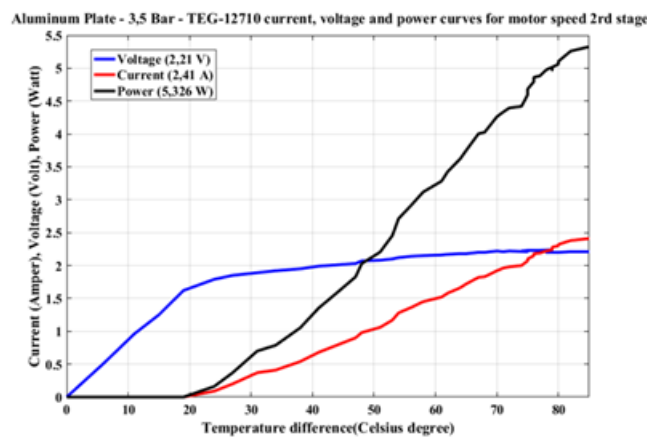

Figure 17. Power curves for TEG-12710 with Copper-Aluminum-Brass Material of Hot-Cold-Hot Sandwich Block Connection Type.

The results of the tests carried out when the sandwich block made with TEG-12710 is of cold-hot-hot connection type are given in Table 4. In Table 4, the best power for copper was produced as 1,78 W when the motor speed was at 3rd level and the pressure was 3,5 bar. The best power in aluminum material was 5,326 W when the engine speed was at 2nd level and the pressure was 3,5 bar. In case of brass material, the best power was produced as 2,863 W while the motor speed was at the 2nd stage and the pressure was 3,5 bar. As seen in Table 4, with TEG-12710, the highest power value was obtained as 5,326 W when the thermal water was passed through Aluminum, the motor speed was at the 2nd level and the pressure was 3,5 bar.

Table 4. TEG-12710 POWER (w) values at $\Delta T = 65\ ^0C$ with cold-hot-cold connection.

Motor Speed	Copper Plate		
	1 Bar	**2,5 Bar**	**3,5 Bar**
I	0,4836 W	1,119 W	0,798 W
II	0,3843 W	0,9359 W	0,722 W
III	0,4026 W	0,4048 W	1,78 W
Motor Speed	**Aluminum Plate**		
	1 Bar	**2,5 Bar**	**3,5 Bar**
I	3,5474 W	3,3072 W	3,483 W
II	3,5145 W	3,7878 W	5,326 W
III	3,7062 W	3,4132 W	3,749 W
Motor Speed	**Brass Plate**		
	1 Bar	**2,5 Bar**	**3,5 Bar**
I	0,9168 W	0,9741 W	1,86 W
II	0,955 W	0,9359 W	2,863 W
III	0,9359 W	0,974 W	0,9359 W

The current-voltage and power graphs of the experiments in which the highest power is obtained with 3 different materials in the sandwich block with TEG-12710 and cold-hot-cold connection type are given in Figure 18-20.

Figure 18. TEG-12710 current, voltage, power curves for Copper Material with Cold-Hot-Cold Sandwich Block Connection Type - 3,5 Bar pressure - Motor Speed 3rd level.

Figure 19. TEG-12710 current, voltage, power curves for Aluminum Material with Cold-Hot-Cold Sandwich Block Connection Type - 3,5 Bar pressure- Motor Speed at 2nd level.
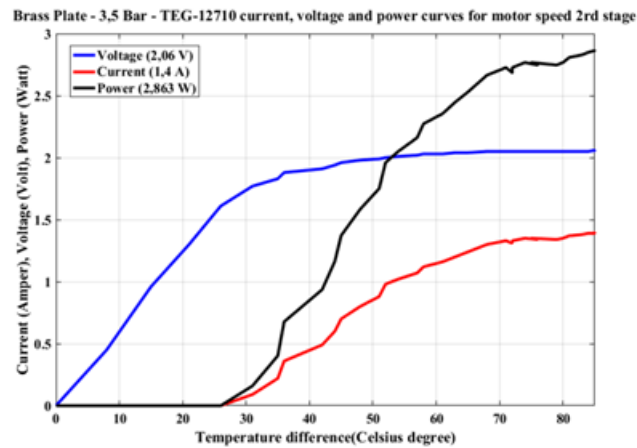
Figure 20. TEG-12710 current, voltage, power curves for Brass Material with a Cold-Hot-Cold Sandwich Block Connection Type - 3,5 Bar pressure - Motor Speed at 2nd level.

In Figure 21, the highest power values of experiments performed using TEG-12710 appear as a single graph. As can be seen in Figure 21, the highest power is obtained when the thermal water is passed through the aluminum material. In addition, the earliest power value was obtained when the temperature reached 20 ^{0}C in the experiment with Aluminum.
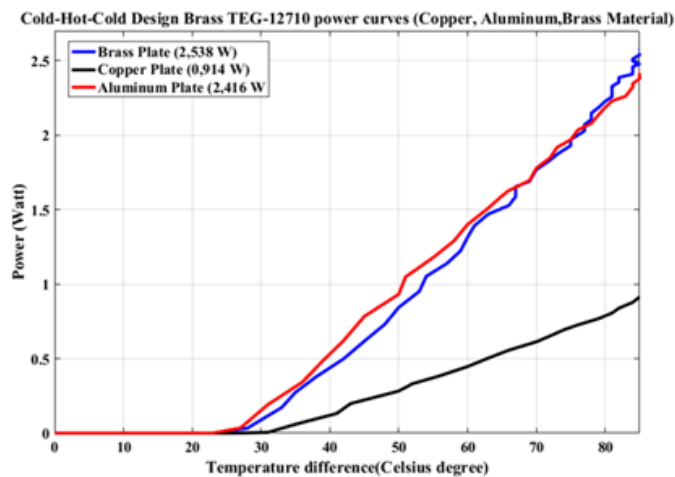

Figure 21. Power Curves for Copper-Aluminum-Brass Material with TEG-12710 and Cold-Hot-Cold Sandwich Block Connection Type.

8. RESULTS AND DISCUSSIONS

In this study, it was determined that the energy obtained by using TEC was affected by the type of material circulated in the thermal water and the speed and pressure of the water. As a result of the experiments carried out, it has been seen that the material through which the thermal water is conveyed, the water pressure and the connection of sandwich blocks to the system have an effect on the energy produced by the TEC.

In this study, TEGs were placed between hot-cold-hot and cold-hot-cold plates. As a result of this work It was observed that the design of the plates carrying thermal water was effective in the amount of electricity generated in TEG.

The temperature difference between the plates in hot-cold-hot operation was 65 ^{0}C, while in cold-hot-cold operation a temperature difference of 85 ^{0}C was formed. This shows that the plates affect each other as temperature.

Highest power value for TEG-12706 in hot-cold-hot sandwich structure. The highest power value for the TEG-12710 in the same sandwich structure was obtained from aluminum plates at 3,524 W at 2,5 bar pressure at level 3.

Highest power value for TEG-12706 in cold-hot-cold sandwich structure. The highest power value for the TEG-12710 in the same sandwich structure was obtained from the aluminum plates at the engine level at a pressure of 3,5 bars at 5,326 W.

The amount of electrical energy produced from TEG placed in cold-hot-cold sandwich design is higher than the hot-cold-hot design.

As a result of the experiments, the best power value from copper, aluminum and brass was obtained from aluminum, while the lowest power value was obtained from copper material.

When the best results of the experiments were evaluated, 5 of the 12 best values were realized with the engine 3. Level water pressure was 3.5 bar. However, if the highest power value is 5,326 W, the engine is at the 2nd level water pressure at 3,5 bar .

REFERENCES

Ağaçayak, A. C., Neşeli, S., & YalçınG, T. H. (2017). The Impact of Different Electric Connection Types in Thermoelectric Generator Modules on Power. *International Journal of Engineering Research & Science (IJOER), 3*, 2395-6992.

Ağaçayak, A. C., Terzioğlu, H., Neşeli, S., & Yalçin, G. (2019). Mathematical Modeling Of Thermoelectric Generator By Regression Analysis. *Selçuk-Teknik Dergisi*, 132-143.

Ağaçayak, A.C., Terzioğlu, Çimen, Neşeli, Yalçın, (2018). "The Effects of Speed and Flow Rate on Power in Thermoelectric Generators", *International Journal of Intelligent Systems and Applications in Engineering*, Vol.6, pp.65-71.

Akçay H. (2015). The conversion of heat lost in the exhaust and cooling system of a spark ignition engine fuelled with LPG to a usable energy via a TEJ module. *M.Sc. Süleyman Demirel University*, Isparta, Turkey.

Champier, D. (2017). Thermoelectric generators: A review of applications. *Energy Conversion and Management, 140*, 167-181.

Çimen, H., Ağaçayak, A. C., Neşeli, S., & Yalçin, G. (2017). *Comparison of Two Different Peltiers Running as Thermoelectric Generator at Different Temperatures.* Paper presented at the 2017 International Renewable and Sustainable Energy Conference (IRSEC).

Demir, M. E., & Dincer, I. (2017). Performance assessment of a thermoelectric generator applied to exhaust waste heat recovery. *Applied Thermal Engineering, 120*, 694-707.

He, W., Wang, S., & Yue, L. (2017). High net power output analysis with changes in exhaust temperature in a thermoelectric generator system. *Applied Energy, 196*, 259-267.

Hossam A.G, C.A.Barry S, Derek S, Cole S, Thomas S, David N, Dominique P, Emmanuel B, (2017). *Evaluation and optimization of thermoelectric generator network for waste heat utilization in nuclear power plants and non-nuclear energy applications*. Annals of Nuclear Energy; 101: 454-464.

Kaya, A. Y. (2010). Experimental research of thermoelectric system that worked by the heat on exhaust gas. *M.Sc. Süleyman Demirel University*, Isparta, Turkey.

Khattab, N., & El Shenawy, E. (2006). Optimal operation of thermoelectric cooler driven by solar thermoelectric generator. *Energy Conversion and Management, 47*(4), 407-426.

Kim, T. Y., Negash, A., & Cho, G. (2017). Direct contact thermoelectric generator (DCTEG): A concept for removing the contact resistance between thermoelectric modules and heat source. *Energy Conversion and Management, 142*, 20-27.

Kushch, A. S., Bass, J. C., Ghamaty, S., & Eisner, N. (2001). *Thermoelectric development at Hi-Z technology.* Paper presented at the Proceedings ICT2001. 20 International Conference on Thermoelectrics (Cat. No. 01TH8589).

La Rocca, V., Morale, M., Peri, G., & Scaccianoce, G. (2017). A solar pond for feeding a thermoelectric generator or an organic Rankine cycle system. *International Journal of Heat and Technology, 35*(1), S435-S441.

Maneewan, S., Hirunlabh, J., Khedari, J., Zeghmati, B., & Teekasap, S. (2005). Heat gain reduction by means of thermoelectric roof solar collector. *Solar Energy, 78*(4), 495-503.

Meng, F., Chen, L., Feng, Y., & Xiong, B. (2017). Thermoelectric generator for industrial gas phase waste heat recovery. *energy, 135*, 83-90.

Montecucco, A., Siviter, J., & Knox, A. (2017). Combined heat and power system for stoves with thermoelectric generators. *Applied Energy, 185*, 1336-1342.

Omer, G., Yavuz, A. H., & Ahiska, R. (2017). Heat pipes thermoelectric solar collectors for energy applications. *International Journal of Hydrogen Energy, 42*(12), 8310-8313.

Serbülent G, Kemal A, (2009). Power generation using concentration solar collectors and thermoelectric generators. *5th International Advanced Technologies Symposium (IATS'09); 13-15 May 2009*; Karabük, Turkey

Singh, R., Tundee, S., & Akbarzadeh, A. (2011). Electric power generation from solar pond using combined thermosyphon and thermoelectric modules. *Solar Energy, 85*(2), 371-378.

Sun, D., Shen, L., Yao, Y., Chen, H., Jin, S., & He, H. (2017). The real-time study of solar thermoelectric generator. *Applied Thermal Engineering, 119*, 347-359.

Terzioğlu, Neşeli &Yalçın, (2018). Termoelektrik Jeneratörler ve Kullanım Alanlarına Genel Bir Bakış. *Mühendislik Alanında Akademik Çalışmalar*, Editör: Prof. Dr. HATİPOĞLU Murat, Dr. Öğr. Üyesi Gündoğan Kadir, Basım sayısı:1, Sayfa Sayısı 160, ISBN:978-605-288-624-3

Terzioğlu, & Ağaçayak, (2018). Analysis of Thermoelectric Cooler Used to Produce Electrical Energy in Terms of Efficiency. *Academic Studies In Engineering*, Editör:Prof. Dr. Hatipoğlu Murat, Dr. Öğr. Üyesi Gündoğan Kadir, Basım sayısı:1, Sayfa Sayısı 134, ISBN:978-605-288-611-3

Terzioğlu H., (2020). Analysis of effect factors on thermoelectric generator using Taguchi method. *Measurement*, 149,1-10

Tie, S. F., & Tan, C. W. (2013). A review of energy sources and energy management system in electric vehicles. *Renewable and sustainable energy reviews, 20*, 82-102.

Tugay M. (2019). Getting optimum level in the generation of electrical energy by means of thermoelectric convertors using parabolic reflector having dinamics structure. *M.Sc. Kırıkkale University*, Kırıkkale, Turkey.

Yalçın, Selek, & Terzioğlu, (2016). "Termoelektrık Jeneratör ile Maksimum Enerji Elde Edilmesi için Levha Tasarımı" *In UMYOS 5th Internatıonal Vocational School Symposium*, Vol.1, pp.909-16. Prizren.

DIJKSTRA ALGORITHM USING UAV PATH PLANNING

¹Elaf Jirjees DHULKEFL ID **, ²Akif DURDU** ID **, ³Hakan TERZİOĞLU** ID

1,2,3Konya Technical University, Faculty of Engineering and Natural Sciences, Department of Electrical-Electronics Engineering, Konya, TURKEY
¹elif.cercis94@gmail.com, ²adurdu@ktun.edu.tr, ³hterzioglu@ktun.edu.tr

ABSTRACT: The use of unmanned aerial vehicles (UAV) is increasing today. UAVs can be divided into two parts, which are remote controlled and can travel automatically due to a certain battery problem. Recent research has also focused on the development and application of new algorithms to autonomously control these vehicles and determine the shortest flight paths. Together with these researches, UAVs are used in many civil activities such as weather forecasts, environmental studies and traffic control. Three-dimensional (3D) path planning is an important issue for autonomously moving UAVs. The shortest path for Unmanned Aerial Vehicles (UAV) is determined by using two-dimensional (2D) path planning algorithms using the obstacles in the environment, and allows UAVs to perform their environmental tasks as soon as possible. The purpose of this study is to determine the shortest path to the target point and avoiding obstacles for UAVs using the Dijkstra algorithm. It was developed to evaluate the arrival time of the UAVs in the path planning algorithm with the simulation performed in the MATLAB program. In this study, the obstacles were defined for the purpose of the building with different heights and different widths and 2D and 3D models were carried out, assuming that the UAV flies at certain heights. In addition, the flight of the UAVs in the route planning determined in the real applications was carried out and the data such as battery consumption, amount of battery spent, speed, amount of travel were examined.

Key Words: UAV, 2D and 3D, path planning, Dijkstra algorithm.

DIJKSTRA ALGORİTMASI KULLANILARAK İHA YOL PLANLAMASI

ÖZ: İnsansız hava araçlarının (İHA) kullanımı günümüzde giderek artmaktadır. İHA'lar uzaktan kumandalı ve belirli bir batarya probleminden dolayı otomatik olarak seyahat edebilen olmak üzere iki kısma ayrılabilirler. Son dönemde gerçekleştirilen araştırmalar, bu araçları otonom bir şekilde kontrol etmek ve en kısa uçuş yollarını belirlemek için yeni algoritmaların geliştirilmesi ve uygulanması konularına da odaklanmışlardır. Bu araştırmalarla birlite kullanım alanı olarak İHA'lar hava tahminleri, çevre çalışmaları ve trafik kontrolü gibi birçok sivil faaliyette kullanılmaktadır. Otonom hareket eden İHA'lar için üç boyutlu (3D) yol planlaması önemli bir konudur. İnsansız Hava Araçları (İHA) için en kısa yol, çevredeki engelleri kullanarak iki boyutlu (2D) yol planlama algoritmaları kullanılarak belirlenir ve İHA'ların çevre görevlerini mümkün olan en kısa sürede yerine getirmelerine olanak tanır. Bu çalışmanın amacı, Dijkstra algoritması kullanılarak İHA'lar için engellerden kaçınarak ve hedef noktasına giden en kısa yolu belirlemektir. MATLAB programında gerçekleştirilen simülasyon ile yol planlama algoritmasında İHA'ların hedefe varış zamanını değerlendirmek için geliştirilmiştir. Bu çalışma farklı yükseklik ve farklı ene sahip olan bina amacıyla engeller tanımlanmış ve İHA'nın belirli yüksekliklerde uçtuğu kabul edilerek 2D ve 3D modellemeleri gerçekleştirilmiştir. Ayrıca İHA'ların gerçek

uygulamalarda belirlenen yol planlamalarında uçuşu gerçekleştirilerek pil tüketimi, harcanan pil miktarı, hızı, alınan yol miktarı gibi verilerde incelenmiştir.

Anahtar Kelimeler: *İnsansız hava araçları (İHA), 2D ve 3D, yol planlama, Dijkstra algoritması.*

1. INTRODUCTION

UAV is an aircraft that is not human, remote and self-controlled. Basic UAV components; the primary body is called the shell, propeller, wing, motor drive, engine, battery, control panel. In addition to these basic components, the UAV also contains electronic sensors, communication electronics, numerous detectors and cameras. The historical development of the UAV began in the mid-19th century, but during the periods of the First and Second World War it was noticeable and continued to develop through increased pilot losses as well as exploration and intelligence during the Cold War era.

The design and quality of drones used for both civil and military purposes has received great attention over the past 10 years. Use UAVs that can operate independently in vibrant and complicated operational environments has become increasingly common. UAVs need to be ready to manage emergencies during the process. Under certain constraints, the usual problem of path planning is to determine between the appropriate locations on an ideal or time-based path. After preparation of the flight plan (unmanned aerial vehicle

Capable of entering enemy threats, performing certain duties in the enemy's air defense zone and ensuring their safety). UAVs have the benefits of low cost, flexibility, high reliability and you don't have to worry about private losses (Yong-Fei *et al.*, 2013). In a complicated environment, UAVs perform their tasks, avoiding obstacles that are necessary. UAV shows two classification methods to overcome obstacles: a traditional algorithm and a smart algorithm. The main element of these autonomous flights is the path preparation. path planning is the main component of these autonomous flights. Preparation of the path shows a variety of factors, such as how to get to a destination to avoid obstacles and shorten the path (Lei *et al.*, 2017).

For UAVs path planning to date, suggested a technique of UAV path planning in complex environments based on genetic algorithms. The showed that the suggested algorithm succeeded in finding a non-optimal, unhindered path in a rapidly changing environment (Gao *et al.*, 2005). An autonomous system for planning the UAV route. Achieved by reviewing the development process and eliminating the caps and restoring old plans that could be missed by contacting a PRM (probabilistic roadmaps) or RRT (rapidly discovered random trees) planner to create new plans right now (Wzorek and Doherty, 2006). This article discusses Portsmouth Harbor, a realistic marine environment to search for the optimal computational time path for a USV between start and end points in a real-time map. In this study, a grid map created from the original was used and the Dijkstra algorithm was used to find the shortest path for a single USV (Singh *et al.*, 2018). Recommended rate if path optimization strategies for unmanned aerial vehicles (UAVs) are based on intelligence. They showed that in case of map coverage, the Ant System algorithm can be used to optimize the UAV system. When comparing another approach, NNS (nearest neighbor search) means that the algorithm is more successful in finding a better route than the nearest neighbor search. (Jevtić *et al.*, 2010). The proposed area height-based Dijkstra algorithm MDA (Modified Dijkstra Algorithm) approach for UAV fixed wing trajectory planning shows that EDA (Elevation Based Dijkstra Algorithm) significantly reduces the computation time (Medeiros and Da Silva, 2010). Approach to FVF based UAV route planning. FVF (Fuzzy Virtual Force) approach for UAV route planning is easy and fast. By comparing the FVF method with the A * search algorithm, the FVF method is superior to online UAV route planning in a complex environment (Zhuoning *et al.*, 2010). An autonomous approach to improving UAV flight plan readiness. We started Q-learning, a kind of reinforcement learning algorithm, to remove obstacles until the UAV reaches the target point. The proposed approach suggests a shorter arrival time (Kim *et al.*, 2017). PSO offered a different approach to formulate and solve problems in 3D path planning. The aim is to reduce fuel consumption and minimize the risk of enemy threats. (Foo *et al.*, 2006). They proposed 3D path algorithms based on 2D frames. They also proposed the Line of

Visibility (VL) method, which can create the shortest path from a starting point to a target point in an area of polygonal barriers. This indicates that it is effective in measurement and suitable for real time applications. (Omar and Gu, 2010). A solution approach has been presented to ensure collaborative scheduling between tool teams. A common control approach was created based on the Voronoi diagram and DPSO. Findings show that the proposed genetic algorithm can be used in time-limited complex group assignments (Tong, 2012).

These feature 3D path planning for low-flying unmanned aerial vehicles (UAVs) in difficult terrain conditions. They proposed an adaptive fluid system (IFDS) with intervention to obtain the optimal 3D orientation for runway length and flight altitude. The proposed solution showed better results (Wang *et al.*, 2015). The mobile robot design was created using the open source simulation software V-REP, and the Dijkstra algorithm was applied to determine the six-optimal and collision-free path. The simulated results showed that the mitigation approach in the created robot path planning environments is effective in terms of time and speed (Fusic *et al.*, 2018). Defined a multi-criteria path planning model for unmanned medium altitude and long aircrafts. Taking environmental dynamics into account, they proposed the A * algorithm for unmanned aerial vehicles in terms of range, time and fuel usage (Arıca *et al.*, 2012). The techniques and algorithms described in this article have been extensively studied, simulated and proposed in low-level applications, as well as high-level decision algorithms and flight optimization processes, as well as UAV motion strategies in unmanned aviation projects. Intelligent techniques used in this study to optimize a UAV mission plan with sensory input (Vladareanu *et al.*, 2016). Quadrotor-type unmanned aerial vehicles (UAVs) also provide path planning to reduce the power consumption of the vehicle, which is required over time to prevent energy waste. It uses the Genetic Algorithm (GA) to determine the shortest way to fly without the need for power and time savings (Galvez *et al.*, 2014). The algorithm used by the modified Dijkstra was used to find an obstacle avoidance path that connects the starting point, the obstacle turning point and the end point. The algorithm used by the modified Dijkstra was used to find the way to avoid obstacles connecting the starting point, the obstacle turning point and the end point. The results show that not only the proposed method is applicable in road planning, but also good results can be achieved (Wu *et al.*, 2017). In this report, for data transmission, civilian UAVs are using existing 3G communication networks. The approach proposed shows that MOGA (Multi-Objective Genetic Algorithm) provides 1.32 and 3.22 times better signal performance than path-greedy and signal-greedy algorithms (Tseng, 2011).

This study is to determine the shortest path to the target point by avoiding obstacles for UAVs using the Dijkstra algorithm. It has been developed to evaluate the arrival time of the UAVs in the path planning algorithm with the simulation performed in the MATLAB program. In this study, obstacles for the purpose of the building with different dimensions were defined and 2D and 3D models were carried out, assuming that the UAV flies at certain heights. When the obtained results were evaluated, it was seen that the Dijkstra algorithm gave good results in the simulation environment. Simulation results of the area used in the actual application were created and flights were carried out with UAV. The main purpose of the route planning in UAVs is to use the battery at the optimum level and reach the target in the shortest way, the electrical parameter values of these flights have been examined and evaluated.

2. PATH PLANNING

Path planning is a strategy by measuring the distance in space between two points to find the best path between them. Research on path planning usually requires multiple input values or parameters: starting position, goal position, and obstacles. In algorithms, some steps are used to discover a 2D path. Algorithms for path planning are used to enter this path at the highest possible price, both from a starting point to a destination point. Some alternative path planning focused on algorithms for road planning. Different techniques assess the most suitable path planning (Cabreira *et al.*, 2019). The aim of path planning, unlike movement planning, which must be taken into account in terms of dynamics, is to find a cinematically optimal route with the least amount of time and to fully model the environment (Dhulkefl and Durdu, 2019; Yang *et al.*, 2016).

3. DIJKSTRA ALGORITHM

A weighted graph is an algorithm that provides the shortest distance between any two nodes with values on a weighted graph. This algorithm was invented by Dutch mathematician and computer scientist Edsger Wybe Dijkstra. Algorithm is used in many areas, especially routing. Dijkstra algorithm Greedy is an algorithm that is greedy.

That is, the dijkstra algorithm chooses the best solution of the current situation when moving from one node to another. The dijkstra algorithm, which is used in computer science and named after the person who introduced the algorithm to the literature, is used to find the shortest path in the graph below. In a series that shows the distance between two nodes, the problem is to find the route with a minimum edge length from the starting node (source node) to a specific end node (target node) (Mozaffari *et al.*, 2016).

This algorithm was developed in 1956 by Edsger W. Dijkstra. The main purpose of this algorithm is to develop a coveted method for implementation, such as shortest path planning. Heavy modification has reduced the complexity of the algorithm. The basis of this algorithm is the relaxation principle. More accurate values gradually change the correct distance approach until finally the optimal solution is reached. The Dijkstra algorithm gets its name from its constructor. The main purpose of the algorithm is to find the shortest path on Graf. Graf can confuse those who first hear the name. We have to keep the data in the computer environment with a certain logic. One of the methods we use most is to keep the data in graph format. Graphs are highly preferred in terms of showing the relations of the nodes on each other (Mozaffari *et al.*, 2016). Sample Dijkstra algorithm nodes as shown in Figure 1.
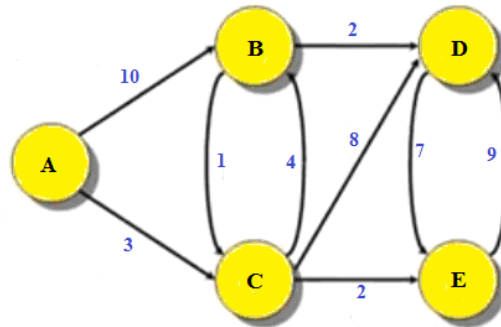

Figure 1. Example nodes for the Dijkstra algorithm

The calculation function used in this algorithm is:

f(n)=g(n)   (1)

As it appears in the equation,
f (n): heuristic function,
g (n): The cost of moving from the starting node to the current node. Flow diagram for Dijkstra algorithm is shown in Figure 2.
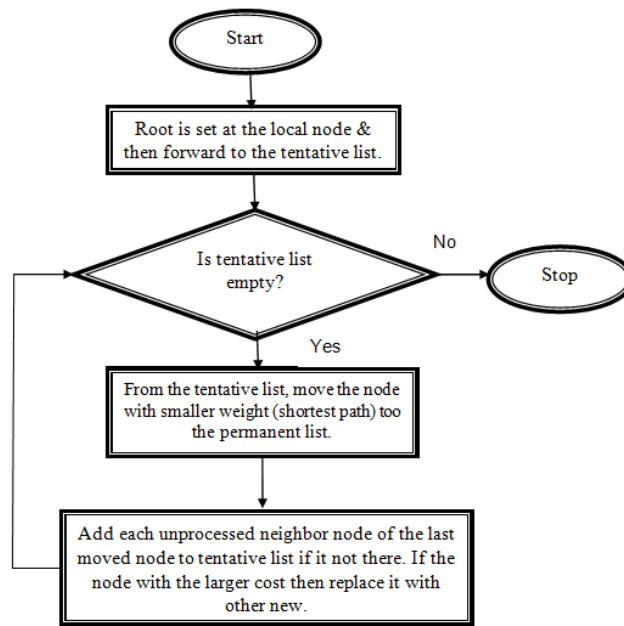
Figure 2. Flow chart for Dijkstra algorithm

3.1. Dijkstra Algorithm Operation

In the Dijkstra algorithm, a starting point is chosen. All remaining nodes should be considered as infinitely far away. We update the distances as we reach the nodes. At each step, Dijkstra looks at neighbors leaving a node, and if a shorter path is found, the distances are updated. And again to the node closest to him. In this way, all nodes on the chart are circulated and the shortest path is found. Dijkstra's Algorithm works by visiting the corners of the graph, starting from the starting point of the object. Then, he repeatedly examines the closest corner that has not been examined and adds the corners to the vertex set to be examined. It expands outward from the starting point until reaching the target. Dijkstra's Algorithm is guaranteed to find the shortest route from the starting point to the destination (Fusic *et al.,* 2018).

The Dijkstra algorithm calculates the shortest paths from one node to all other nodes. The weight value of the edges developed for weighted and directional charts must be zero or greater than zero. If the values of the edges are less than zero, Bellman-Ford can be used in more general algorithms. Because the negative edge consistently produces a better result than the current state, and the algorithm is never stable. In Dijkstra's algorithm, the shortest path from the initially selected node to all other nodes is calculated. Dijkstra's algorithm does not have a target node (Fusic *et al., 2018).*

If a target node is identified as a problem, the Dijkstra algorithm finds the shortest path to all nodes and then selects one of them. So if you use the Dijkstra algorithm, the shortest distance to all nodes is calculated, regardless of whether you have a target or not. If you have a destination, the shortest route to that destination has already been calculated. In Dijkstra, each step is evaluated for a node's neighbors and the distances are updated if a shorter path is found (Fusic *et al.,* 2018).
To use the Dijkstra algorithm:

- Developed for weighted and directional graphs,
- The weight value of the edges must be zero or greater than zero, if the edge values are less than zero, the Bellamn-Ford algorithm can be used,
- Does not work for negative weights.

4. SIMULATION AND APPLICATION

In this article, Matlab is used to create this map. Designing 3D path planning techniques for advanced 2D path planning algorithms for autonomous mobile robots and continuing fast in practice is desirable. Unmanned aerial vehicles ensure, among the barriers created by the simulation environment, that the shortest path is acquired by avoiding obstacles between the starting point and the target and using suggested technique. The method proposed in this article is the Dijkstra algorithm.

A few steps are used in algorithms to discover a 3D path. Next, data is collected from a regional starting point to an endpoint on the heights of obstacles. The maximum height the UAV can fly to is then determined by the height of these obstacles and the shortest path planning. Many alternative path planning focused on 2D path scheduling algorithms based on obstacle heights. the proposed technique finds the shortest path between the starting point and the target point. redline is the outcome of Dijkstra algorithm path planning.

4.1. First 2D Test Medium

As shown in Figures 3, path planning algorithm are used. The proposed algorithm is the Dijkstra algorithm. As shown in the figures, there are three different obstacles, each with a different Length and width. The first and third obstacles are 20 m wide and 60 m long and the second obstacle is 40 m wide and 40 m long.
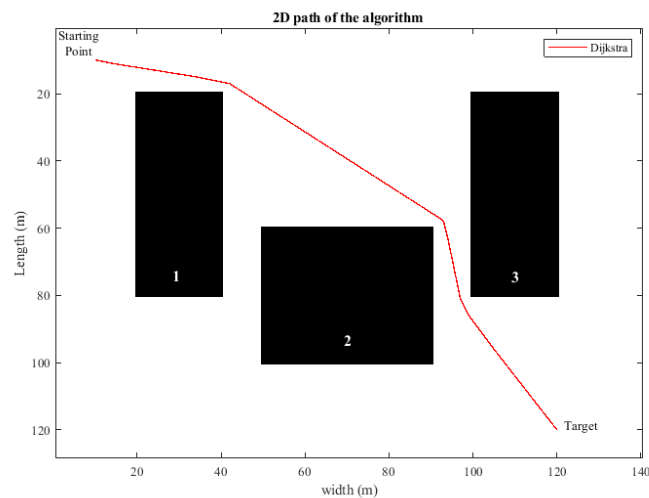

Figure 3. 2D path of the algorithm for the first application

The results of the path in the above figure are as shown in table 1. The path from the starting point to the destination is calculated in 2D. The 154m path is shown to be moving in 1.0410 seconds, according to the Dijkstra algorithm.

4.2. First 3D Test Medium

As shown in Figure 4, the first obstacle is 60 m high after assessing the drone's height and the obstacle, the second obstacle is 40 m high and the third obstacle is 60 m high. The algorithm calculates the path length when the drone's height is 45m, indicating that the second obstacle is higher than the height, thus ignoring the second obstacle and reaching the destination point in a shorter time.
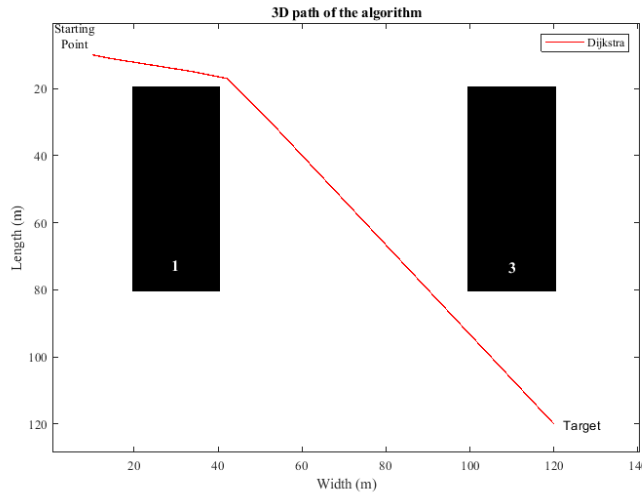
Figure 4. 3D path of the algorithm for the first application

The results of the path in the above figure are as shown in Table 1. The path from the starting point to the destination is calculated in 3D. The 22m path is shown to be moving in 1.2762 seconds, according to the Dijkstra algorithm.

4.3. Second 2D Test Medium

As shown in Figures 5, path planning algorithm are used. The proposed algorithm is the Dijkstra algorithm. As shown in the figures, there are four different obstacles, each with a different Length and width. the first obstacle are 20m wide and 50m long and the second obstacle is 20 m wide, 20m long, the third obstacle is 20m wide and 30m long and the fourth obstacle is 20m wide and 60m long.
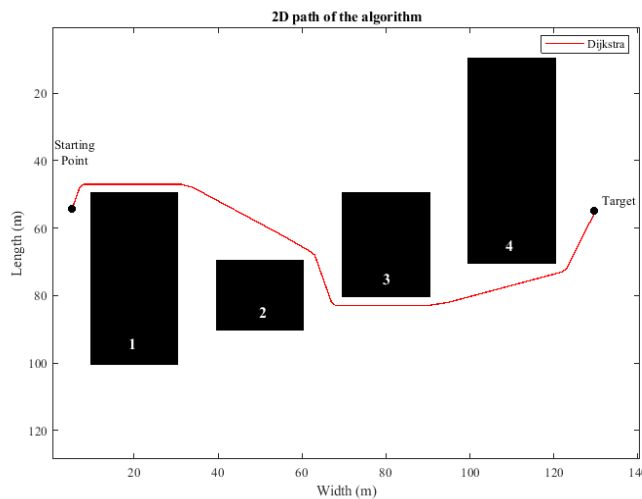

Figure 5. 2D path of the algorithm for the second application

The results of the path in the above figure are as shown in Table 1. The path from the starting point to the destination is calculated in 2D. The 73m path is shown to be moving in 1.1049 seconds, according to the Dijkstra algorithm.

4.4. Second 3D Test Medium

The algorithm calculates the path length when the drone's height is 55 m, indicating that the first, second and third obstacles is higher than the height, thus ignoring the first, second and third obstacle and reaching the destination point in a shorter time.
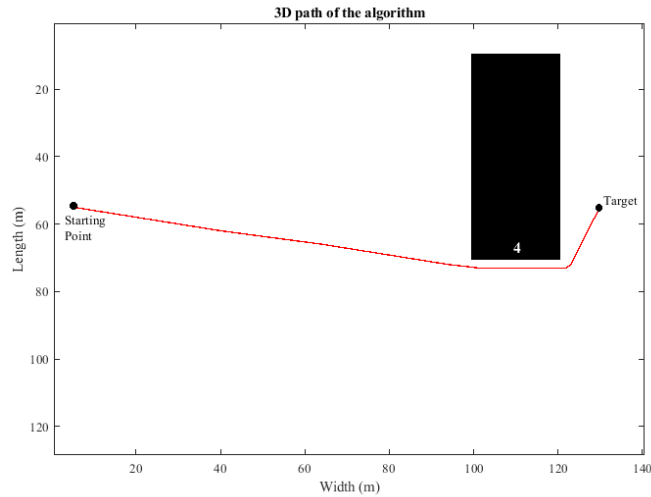

Figure 6. 3D path of the algorithm for the second application

The results of the path in the above figure are as shown in table 1. The path from the starting point to the destination is calculated in 3D. The 43m path is shown to be moving in 1.4835 seconds, according to the Dijkstra algorithm.

Table 1. 2D & 3D path plannıng algorithm performance per second and path planning line length performance

Figure		Dijkstra Algorithm Time (sec)	Dijkstra Algorithm Path Length (m)
First Environment	3	1.0410	154
	4	1.2762	125
Second Environment	5	1.1049	180
	6	1.4835	145

The example of Unmanned aerial vehicle in the real-time test environment is as shown in Figure 7 There are three obstacles, each obstacle has different heights. The first obstacle height is 60m, the second obstacle is 70m and the third obstacle is 80m, paths from the starting point to the destination point are calculated.
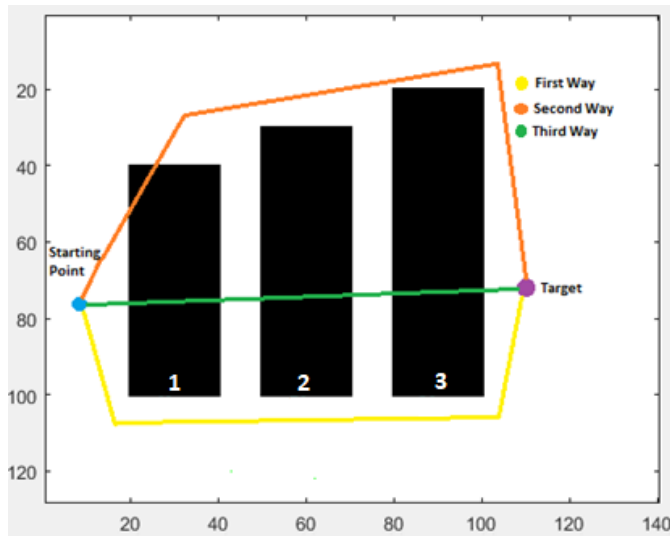
Figure 7. UAV test environment

The results of the UAV test environment are as shown in Table 2. The images on the flight path of unmanned aerial vehicles are as shown in Figure 8, Figure 10 and Figure 12.

Table 2. Energy consumptıon at dıfferent heights

Way	Drone Height (m)	Distance (m)	Drone Speed (m / s)	Battery Expenditure (v)	Battery consumption (%)
First Way	50	385	5	3400	23.43756
Second Way	65	387	5	3400	25.252822
Third Way	85	272	5	3400	22.265682

4.5. Planning of UAV path at different heights

Figure 8. Drone height 50m for first road

As seen in the image below, the drone has a height of 50m. When we try the first path in the simulation

environment, drone height is lower than the height of the obstacles. Therefore, the algorithm passes around obstacles when executed. It shows a path as shown in figure 9.
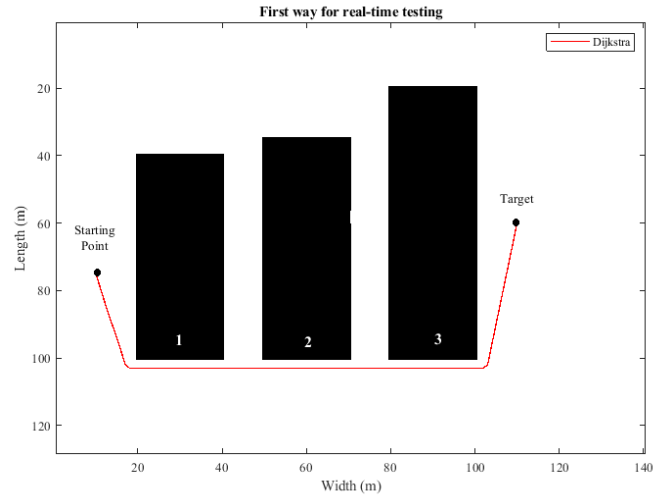

Figure 9. First way for real-time testing

The path from the starting point to the destination is calculated in 3D. The 97m path is shown to be moving in 1.0138 seconds, according to the Dijkstra algorithm.

Figure 10. Drone Height 65m for second way

When the drone height is 65m, we tried the second path in the simulation environment, when the algorithm runs, the first and second obstacles ignores the 60 m, 70 m height because the drone height is higher than the first and second obstacles. The plotted path is as shown in Figure 11 below.
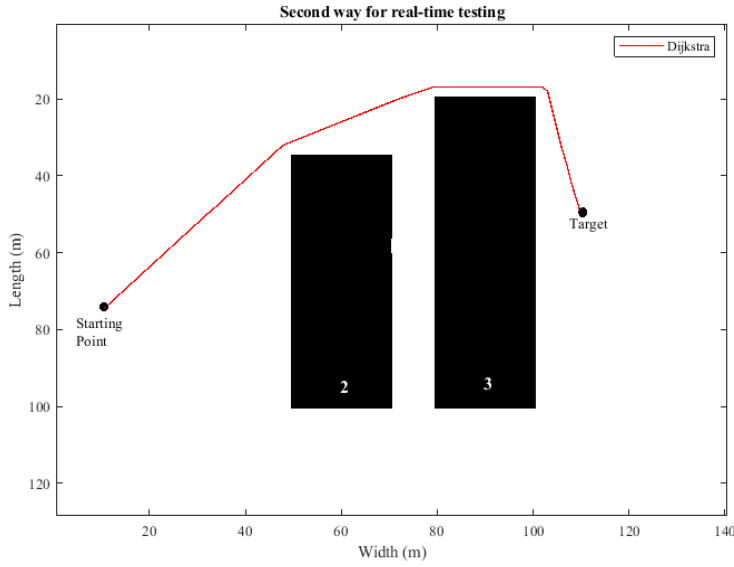
Figure 11. Second way for real-time testing

The path from the starting point to the destination is calculated in 3D. The 61m path is shown to be moving in 1.2142 seconds, according to the Dijkstra algorithm.
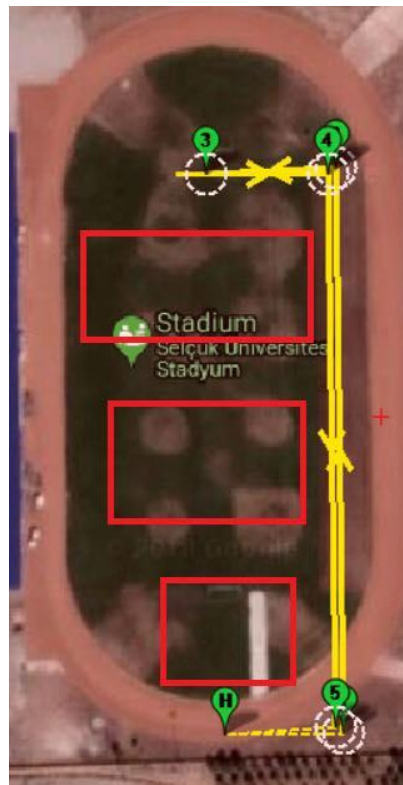

Figure 12. Third way for drone height 85m

When the drone height is 85m, we tried the third way in the simulation environment, since the drone height is more than the height given for three obstacles, it ignores the three obstacles when the algorithm is executed. As a result, it is calculated without any obstacles from the starting point to the destination. The plotted path is as shown in Figure 13 below.
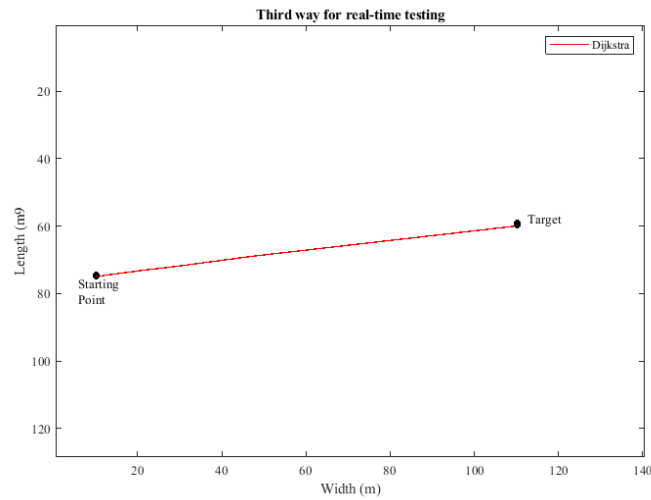
Figure 13. Third way for real-time testing

It is equal to 16.8 V when the battery is full and equal to 13.2 V when the battery is empty. According to the results, the higher the UAV, the more batteries are consumed. The results of the simulation environment are shown in Table 3 below.

Table 3. Three-dimensional simulation result for real-time testing

Three-dimensional simulation result	Dijkstra Algorithm	
	Time (sec)	Optimal path (m)
First way	1.0138	97
Second way	1.2142	61
Third way	1.4389	80

5. RESULTS AND DISCUSSIONS

When we compare the results of Dijkstra algorithm, it gives different results in both experimental environments. By comparing 2D and 3D environments, our algorithm offers better results in 3D environments. As a result, Dijkstra algorithm shows shorter path lengths in three-dimensional environments as a result, unmanned aerial vehicles are used for this purpose comparing simulation and real-time test results as shown in Table 4.

Table 4. Comparison of 2D and 3D real-time test and simulation results per second

Figure		Dijkstra Algorithm (sec)	
		Simulation	Real-Time Testing
First Environment	3	1.0410	0.10
	4	1.2762	0.06
Second Environment	5	1.1049	0.11
	6	1.4835	0.07

REFERENCES

Arıca, N., Cicibaş, H., & Demir, K. A. (2012). İnsansız Hava Araçları için Çok Kriterli Güzergâh Planlama Modeli. Journal of Defense Sciences/Savunma Bilmleri Dergisi, 11(1).

Cabreira, T. M., Brisolara, L. B., & Ferreira Jr, P. R. (2019). Survey on coverage path planning with unmanned aerial vehicles. Drones, 3(1), 4.

Dhulkefl, E. J., & Durdu, A. (2019). Path planning algorithms for unmanned aerial vehicles. International Journal of Trend in Scientific Research and Development (ijtsrd), 359-362.

Foo, J. L., Knutzon, J., Oliver, J., & Winer, E. (2006). Three-dimensional path planning of unmanned aerial vehicles using particle swarm optimization. Paper presented at the 11th AIAA/ISSMO multidisciplinary analysis and optimization conference.

Fusic, S. J., Ramkumar, P., & Hariharan, K. (2018). Path planning of robot using modified dijkstra Algorithm. Paper presented at the 2018 National Power Engineering Conference (NPEC).

Galvez, R. L., Dadios, E. P., & Bandala, A. A. (2014). Path planning for quadrotor UAV using genetic algorithm. Paper presented at the 2014 International Conference on Humanoid, Nanotechnology, Information Technology, Communication and Control, Environment and Management (HNICEM).

Gao, X.-G., Fu, X.-W., & Chen, D.-Q. (2005). A genetic-algorithm-based approach to UAV path planning problem. Paper presented at the Proceedings of the WSEAS International Conference on Simulation, Modeling, and Optimization.

Jevtić, A., Andina, D., Jaimes, A., Gomez, J., & Jamshidi, M. (2010). Unmanned aerial vehicle route optimization using ant system algorithm. Paper presented at the 2010 5th International Conference on System of Systems Engineering.

Kim, I., Shin, S., Wu, J., Kim, S.-D., & Kim, C.-G. (2017). Obstacle avoidance path planning for UAV using reinforcement learning under simulated environment. Paper presented at the IASER 3rd International Conference on Electronics, Electrical Engineering, Computer Science, Okinawa.

Lei, W., LI, B.-j., YIN, Z.-h., Cheng, Z., Xin, Z., & CHU, Y.-n. (2017). An Improved Artificial Potential Field for Unmanned Aerial Vehicles Path Planning. DEStech Transactions on Computer Science and Engineering(cst).

Medeiros, F. L. L., & Da Silva, J. D. S. (2010). A Dijkstra algorithm for fixed-wing UAV motion planning based on terrain elevation. Paper presented at the Brazilian Symposium on Artificial Intelligence.

Mozaffari, M., Saad, W., Bennis, M., & Debbah, M. (2016). Optimal transport theory for power-efficient deployment of unmanned aerial vehicles. Paper presented at the 2016 IEEE international conference on communications (ICC).

Omar, R., & Gu, D. (2010). 3D Path Planning for Unmanned Aerial Vehicles using Visibility Line based Method. Paper presented at the ICINCO (1).

Singh, Y., Sharma, S., Sutton, R., & Hatton, D. (2018). Towards use of dijkstra algorithm for optimal navigation of an unmanned surface vehicle in a real-time marine environment with results from artificial potential field. TransNav, International Journal on Marine Navigation and Safety od Sea Transportation, 12(1).

Tong, H. (2012). Path planning of UAV based on Voronoi diagram and DPSO. Procedia Engineering, 29, 4198-4203.

Tseng, F.-H. (2011). Li-Der Chou, and Han-Chieh Chao.". A survey of black hole attacks in wireless mobile ad hoc networks, 1-16.

Vladareanu, V., Boscoianu, E.-C., Sandru, O.-I., & Boscoianu, M. (2016). Development Of Intelligent Algorithms For Uav Planning And Control. Scientific Research & Education in the Air Force-AFASES, 1, 221-226.

Wang, H., Lyu, W., Yao, P., Liang, X., & Liu, C. (2015). Three-dimensional path planning for unmanned aerial vehicle based on interfered fluid dynamical system. Chinese Journal of Aeronautics, 28(1), 229-239.

Wu, T.-F., Tsai, P.-S., Hu, N.-T., & Chen, J.-Y. (2017). Combining turning point detection and Dijkstra's algorithm to search the shortest path. Advances in Mechanical Engineering, 9(2), 1687814016683353.

Wzorek, M., & Doherty, P. (2006). Reconfigurable path planning for an autonomous unmanned aerial vehicle. Paper presented at the 2006 International Conference on Hybrid Information Technology.

Yang, L., Qi, J., Song, D., Xiao, J., Han, J., & Xia, Y. (2016). Survey of robot 3D path planning algorithms. Journal of Control Science and Engineering, 2016.

Yong-Fei, M., Luo, Z., & Luo-Sheng, X. (2013). Application of improved sparse A* algorithm in UAV path planning. Information Technology Journal, 12(17), 4058.

Zhuoning, D., Rulin, Z., Zongji, C., & Rui, Z. (2010). Study on UAV path planning approach based on fuzzy virtual force. Chinese Journal of Aeronautics, 23(3), 341-350.